

UNCLASSIFIED

AD NUMBER
AD915423
NEW LIMITATION CHANGE
TO Approved for public release, distribution unlimited
FROM Distribution authorized to U.S. Gov't. agencies only; Test and Evaluation; AUG 1973. Other requests shall be referred to Air Force Armament Laboratory, Attn: DLYA, Eglin AFB, FL.
AUTHORITY
AFATL ltr, 6 Jun 1977

THIS PAGE IS UNCLASSIFIED

AFATL-TR-73-160

VOLUME II

AD915423

**CALCULATION OF SHAPED-CHARGE JETS
USING ENGINEERING APPROXIMATIONS AND
FINITE DIFFERENCE COMPUTER CODES
VOLUME II. MODIFICATION AND UTILIZATION
OF A TWO-DIMENSIONAL FINITE DIFFERENCE
CONTINUUM MECHANICS CODE TO
CALCULATE THE JET FORMATION PARAMETERS
FOR ANY GENERALIZED AXISYMMETRIC
SHAPED CHARGE**

PHYSICS INTERNATIONAL COMPANY

TECHNICAL REPORT AFATL-TR-73-160, VOLUME II

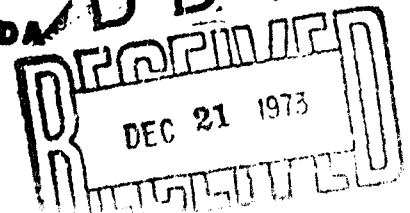
AUGUST 1973

Distribution limited to U. S. Government agencies only;
this report documents test and evaluation; distribution
limitation applied August 1973 . Other requests for
this document must be referred to the Air Force Armament
Laboratory (DLYA), Eglin Air Force Base, Florida 32542.

AIR FORCE ARMAMENT LABORATORY

AIR FORCE SYSTEMS COMMAND • UNITED STATES AIR FORCE

EGLIN AIR FORCE BASE, FLORIDA



**Calculation Of Shaped-Charge Jets Using Engineering
Approximations And Finite Difference Computer Codes**

**Volume II. Modification And Utilization Of A
Two-Dimensional Finite Difference Continuum Mechanics
Code To Calculate The Jet Formation Parameters For
Any Generalized Axisymmetric Shaped Charge**

L. Behrmann

N. Birnbaum

Distribution limited to U. S. Government agencies only;
this report documents test and evaluation; distribution
limitation applied August 1973 . Other requests for
this document must be referred to the Air Force Armament
Laboratory (DLYA), Eglin Air Force Base, Florida 32542.

FOREWORD

This report was prepared by Physics International Company, 2700 Merced Street, San Leandro, California 94577, under Contract No. F08635-72-C-0229 with the Air Force Armament Laboratory, Eglin Air Force Base, Florida. Mr. Lovonia J. Theriot (DLYA) managed the program for the Armament Laboratory. This effort was conducted during the period from June 1972 to August 1973.

The contractor report number assigned is PIFR-430.

This report is divided into two volumes. Volume I presents the generalized analytical approach to shaped-charge warhead design. Volume II describes the modification and utilization of a two-dimensional finite difference continuum mechanics code utilizing the Lagrangian coordinate system to calculate the complete jet formation parameters for any generalized axisymmetric shaped charge. This is Volume II.

This technical report has been reviewed and is approved.

Robert W. Dillon
ROBERT W. DILLON, Colonel, USAF
Chief, Weapon Systems Analysis Division

ABSTRACT

This report describes a technique to optimize the current shaped-charge design procedure as follows. Starting with the desired target to be defeated, a determination of the desired penetration characteristics of the jet would be made. Existing jet penetration theory would then be used to estimate the ideal characteristics of the jet to defeat the given target. A shaped charge launcher would then be designed to give these ideal jet characteristics. However, a suitable design procedure requires (1) a viable analytical or empirical design approach to obtain a first cut shaped charge design, (2) a better understanding than now exists of the detailed mechanisms of jet formation, and (3) a better understanding of the phenomenon of jet penetration. This report, which is contained in two volumes, addresses the first two of these requirements. Volume I describes the use of the existing non-steady state theory of jet formation with experimental data and one-dimensional finite difference continuum mechanics calculations to obtain the linear collapse velocity for generalized axisymmetric shaped charges. The results of this work are then used to obtain non-unique shaped charge designs which give the required idealized jet parameters. Volume II describes the modification and utilization of a two-dimensional finite difference continuum mechanics code utilizing the Lagrangian coordinate system to calculate the complete jet formation parameters for any generalized axisymmetric shaped charge. The utilization of this code allows a more detailed study of such phenomena as jet stability, bifurcation on the axis, shear gradients, viscosity, shocks, incipient vaporization, surface tension, and possible other effects. The combined use of both the engineering formulations along with the sophisticated two-dimensional code calculation allows design engineers the versatility to design the most optimum shaped charge for their particular application.

Distribution limited to U. S. Government agencies only; this report documents test and evaluation; distribution limitation applied August 1973 . Other requests for this document must be referred to the Air Force Armament Laboratory (DLYA), Eglin Air Force Base, Florida 32542.

TABLE OF CONTENTS

<u>Section</u>	<u>Page</u>
I INTRODUCTION	1
II TECHNICAL DISCUSSION	3
1. General	3
2. Zoning of the Grid	3
3. New Detonation Logic	5
4. Equation of State for Copper	20
5. Slideline Calculation	21
6. Rezoning	23
7. Anti-Hourglassing Options	25
8. Imp Option	26
9. Tracer Points	26
III CALCULATIONAL PROCEDURE	29
IV RESULTS	33
V CONCLUSIONS	37
REFERENCES	39
APPENDIX A COORDINATE AND VELOCITY VECTOR PLOTS	
APPENDIX B GENERALIZED BOUNDARY POINT MOTION	
APPENDIX C AUTOMATIC REZONER	

LIST OF FIGURES

Figure	Title	Page
1	Peak Pressure in Each Zone for Standard Detonation in Composition B	7
2	Stress Versus Time at Zone Number 6 (Original Position = 0.260 cm) for Standard Detonation in Composition B	8
3	Stress Versus Time at Zone Number 11 (Original Position = 0.518 cm) for Standard Detonation in Composition B	9
4	Stress Versus Time at Zone Number 16 (Original Position = 0.760 cm) for Standard Detonation in Composition B	10
5	Stress Versus Time at Zone Number 21 (Original Position = 1.01 cm) for Standard Detonation in Composition B	11
6	Stress Versus Time at Zone Number 41 (Original Position = 2.01 cm) for Standard Detonation in Composition B	12
7	Stress Versus Time at Zone Number 61 (Original Position = 3.01 cm) for Standard Detonation in Composition B	13
8	Peak Pressure in Each Zone for Special Detonation in Composition B	14
9	Stress Versus Time at Zone Number 6 (Original Position = 0.26 cm) for Special Detonation in Composition B	15
10	Stress Versus Time at Zone Number 11 (Original Position = 0.510 cm) for Special Detonation in Composition B	16

LIST OF FIGURES (CONCLUDED)

<u>Figure</u>	<u>Page</u>
11 Two-Dimensional Geometry Used to Test Detonation Ignition Logic	18
12 Slideli:	22

SECTION I

INTRODUCTION

The design of advanced shaped-charge warheads requires a detailed understanding of the mechanisms of both jet formation and jet penetration. Much of the previous research on shaped charges has been devoted to characterization testing of existing designs rather than to development of optimal designs with maximized effectiveness against a given target or class of targets. The tools for developing such designs exist: advanced multi-dimensional, finite difference, continuum mechanics (hydro) computer program. Prior to the effort funded under this contract, an Eulerian code (References 1 and 2) developed by Systems, Science, and Software for Ballistic Research Laboratories, known as BRLSC (Ballistic Research Laboratory Shaped Charge), was the principal code used to calculate the formation of shaped-charge jets. This code has certain inherent limitations:

- (a) The HE burn cannot be calculated accurately without either excessive computer time or cumbersome pressure boundary condition patches.
- (b) The code is limited to a constant thickness/constant slope liner.
- (c) The details of jet formation are not well described.

In order to design more effective shaped charges it is necessary to understand the physics of jet formation, thus a Lagrange formulation of the problem is required. The objectives of this program were (a) to adapt the existing PISCES 2DL code provide a new Lagrangian shaped-charge code capable of calculating jet formation from variable thickness, axially symmetric shaped charges, and (b) to develop a generalized analytical theory to provide approximate geometrical designs for specific-application shaped-charge warheads.

The generalized analytical approach to shaped-charge warhead design is presented in Volume I of this report. This volume describes the modifications of the PISCES 2DL code developed to meet the objectives discussed above and presents the results of a computer simulation of the formation of an axial jet from the 105 mm BRL precision shaped charge.

Section II of this report discusses the general calculational problems associated with the numerical simulation of a shaped-charge jet and the modifications to the standard PISCES 2DL code that were made to address these problems. Section III presents the calculational procedure, and Section IV presents results, conclusions, and suggestions for further study.

The calculation was performed on a CDC 7600 with 170 K octal words. There is no particular limitation on the size (number of zones) for a problem because of the basic design of PISCES 2DL. The modifications detailed in Section II were straightforward additions or extensions to the structure of the code.

SECTION II

TECHNICAL DISCUSSION

1. GENERAL

The numerical simulation of a shaped-charge jet is challenging. A numerical study must account for the following phenomena: (a) detonation of an explosive, (b) interaction on an explosive-metal interface, and (c) formation of a jet and stagnation region due to the collapsing metal liner. The detonation logic employed must result in a detonation wave of the correct velocity and magnitude. The interaction of the explosive and the metal liner may result in instabilities that are numerical and/or physical. The material properties, including the material strength of the metal liner, may be very sensitive in the jet formation and in the possible growth of instabilities. Zonal resolution in the numerical simulation will have a large effect on the jet formation and potential instabilities. The large distortions experienced by the metal liner induce calculational problems. Rezoning techniques can be employed in a Lagrange code to handle the distortions without sacrificing a description of the material flow. The following section discusses the various program modifications made to address the above problems.

2. ZONING OF THE GRID

The initial zoning used to describe the geometry of the 105 mm BRL precision shaped charge was selected with the following considerations in mind:

(a) A slideline, a computational slip surface, should exist at the copper-explosive interface, the copper liner being the master material and the explosive being the slave material. The motion of the master material is governed by its internal stress gradients and by the external pressure exerted on it by the slave material. The motion of the slave material is governed by its internal pressure gradients and is constrained to slide along the boundary of the master material.

(b) The copper liner should contain at least six columns across its thickness and should contain enough rows so that no rectangular zone has a length-to-width ratio greater than two.

(c) The zones in the explosive should be as square as possible so that the detonation phenomena will be described correctly.

(d) To avoid excessive tangling of the explosive slave-points as they slide along the copper liner (masterline), the rows connecting the gridpoints on the column adjacent to the column of slavepoints (slideline+1) to the slave-points should intersect the masterline at approximately right angles.

Several modifications had to be made to the standard PISCES 2DL file to allow for the above considerations.

(a) The maximum number of rows that a problem could have was increased from 60 to 145.

(b) The restriction that the column of slavepoints and the slideline+1 column have the same number of rows was removed.

(c) Non-standard coordinate-generating subroutines, called GENLIN, EQPZON, and TRIZON, were used to generate the coordinates of grid points in the copper liner and the explosive.

The initial grid configuration is reproduced in Appendix A.

3. NEW DETONATION LOGIC

A new method to simulate the ignition of the shaped-charge explosive is described in this section. PISCES 1DL and 2DL runs are presented to show the features of the new method. In the one-dimensional case, the new method has an advantage over the standard method in that the correct detonation velocity and shape of the detonation front are established in a fewer number of zones. The advantage of the new method in the two-dimensional case is even more pronounced.

In PISCES 2DL, the standard high-explosive burn logic is not accurate for certain applications. Typically, in the standard two-dimensional logic, the detonation velocity is correct but the shape of the wavefront does not agree well with the shape predicted by theory or by one-dimensional calculations. In particular, the magnitude of the peak pressure at the detonation front is typically only one-half to two-thirds of the Chapman-Jouguet pressure (p_{CJ}) for a reasonable number of zones. In contrast, the peak pressure at the detonation front in the new method is equal to the Chapman-Jouguet pressure, even when the front is just passing over zones which are adjacent to the zones being detonated.

a. Standard PISCES 1DL Detonation Logic. The standard method of describing an explosive detonation in PISCES 1DL is presented in Appendix A of Reference 3. To begin a detonation in an explosive material, a particular zone is specified by input to be "ignited." Ignition is achieved by setting the zone's burn fraction initially to unity. This allows the zone's chemical energy to be converted to pressure through the zone's equation of state. This pressure propagates into neighboring zones,

compressing them. Explosive neighbors then will subsequently detonate if compression reaches the Chapman-Jouguet volume. A detonation in an explosive material will usually proceed for 15 to 20 zones in the explosive material before the detonation front is correctly established.

A problem illustrating this latter point is shown. The problem consists of a 5-cm slab of Composition B explosive which is divided into 100 equally spaced zones. Both surfaces of the slab are specified to be free and the point of ignition is specified to be in the leftmost zone. The explosive is assumed to be properly described by a JWL equation of state (Reference 3) with the following coefficients:

$$\begin{array}{lll} A = 5.24 \text{ (Mbar)} & R1 = 4.2 & \omega = 0.34 \\ B = 0.0768 \text{ (Mbar)} & R2 = 1.1 & \end{array}$$

The results of the illustrative problem are summarized in Figures 1 through 7. Figure 1 shows the peak pressure in each zone. It is seen that the pressure initially increases with zone number and then asymptotically approaches a value equal to the Chapman-Jouguet pressure of the explosive. This value is essentially reached after the explosive has burned through 20 or 30 zones. Figures 2 through 7 are pressure-time histories at several locations (zones) in the explosive. Again, it is observed that the maximum pressure obtained in a zone increases with zone number.

b. Special P7SCES 1DL Detonation Logic. Figures 8 through 10 show output from a calculation similar to the one described in paragraph a (although it was not carried as far in time) using a special detonation ignition logic. As can be observed from

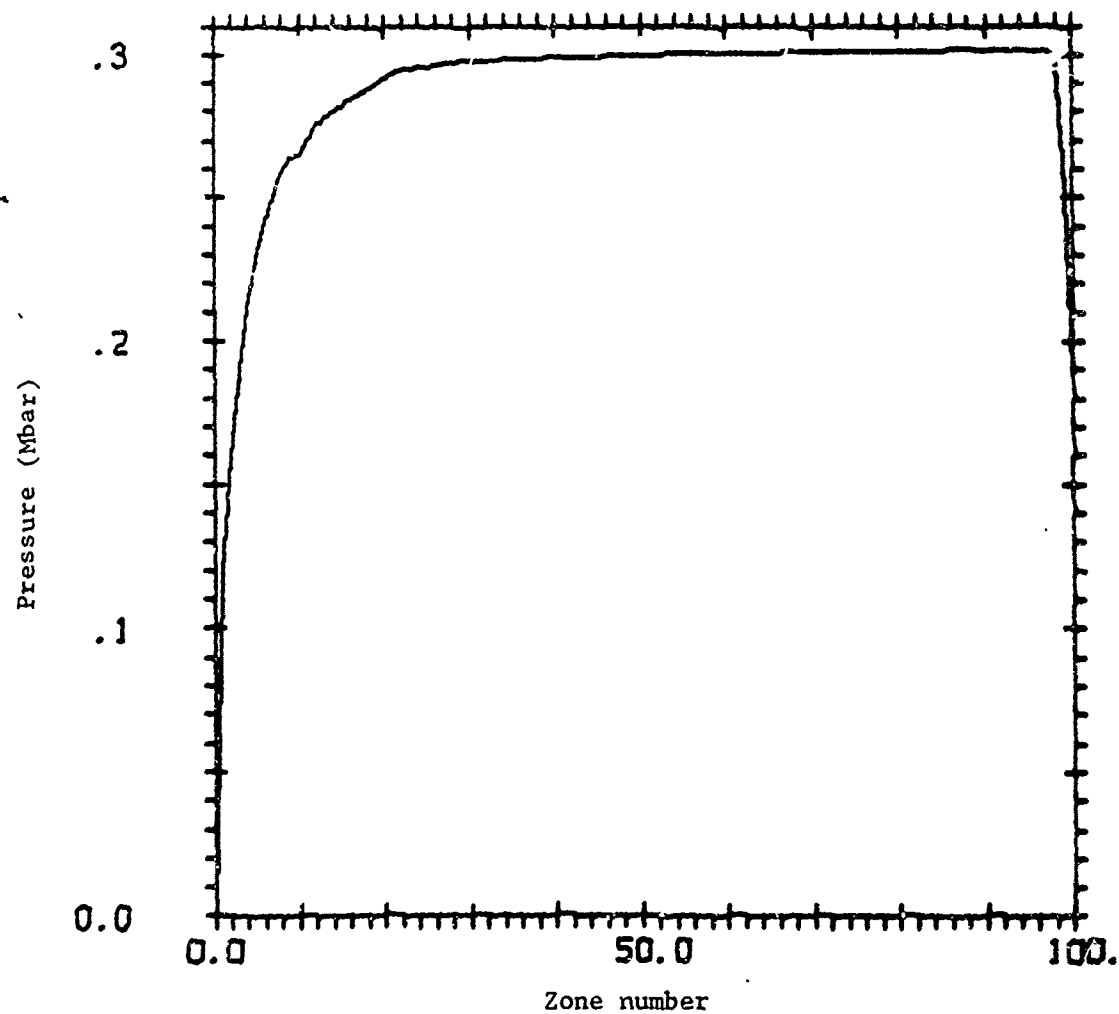


Figure 1. Peak Pressure in Each Zone for Standard Detonation in Composition B

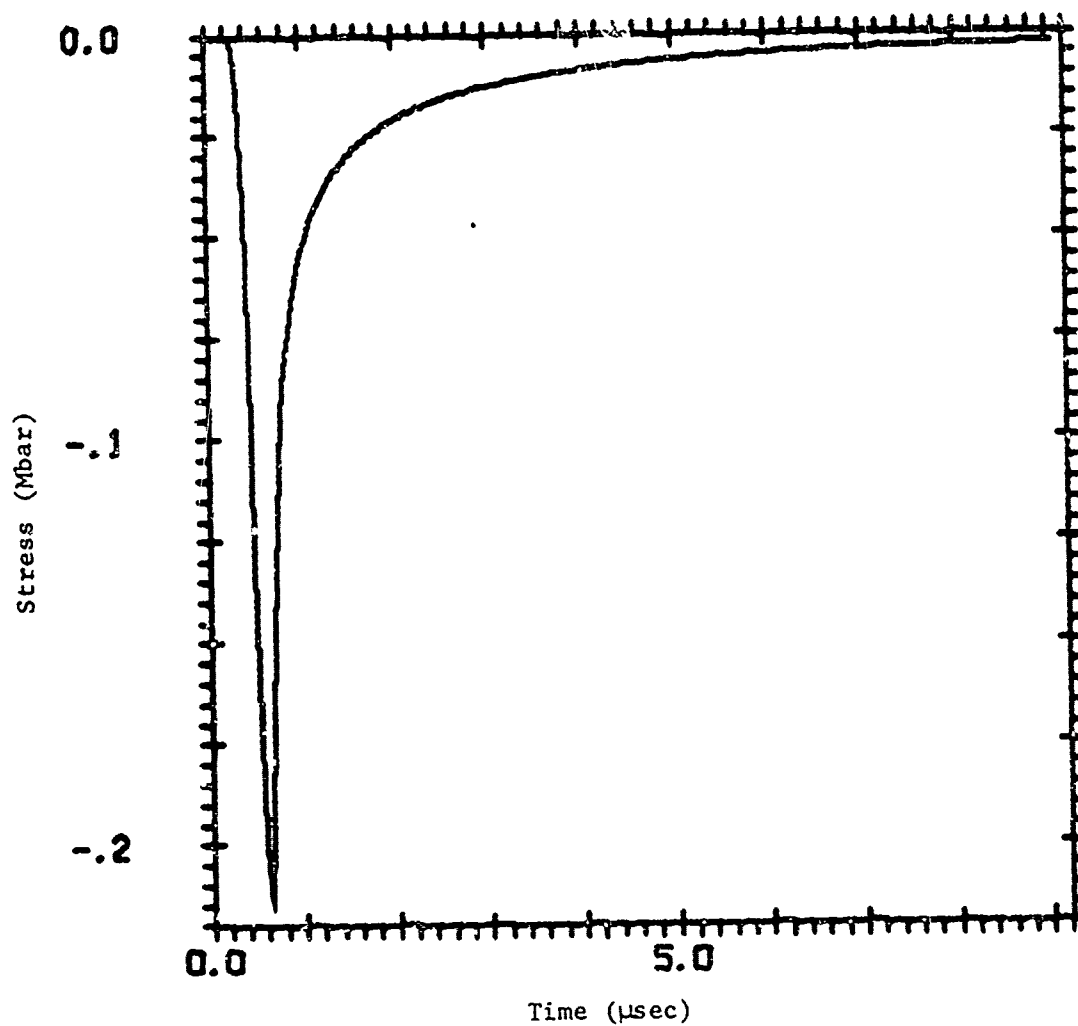


Figure 2. Stress Versus Time at Zone Number 6 (Original Position = 0.260 cm) for Standard Detonation in Composition B

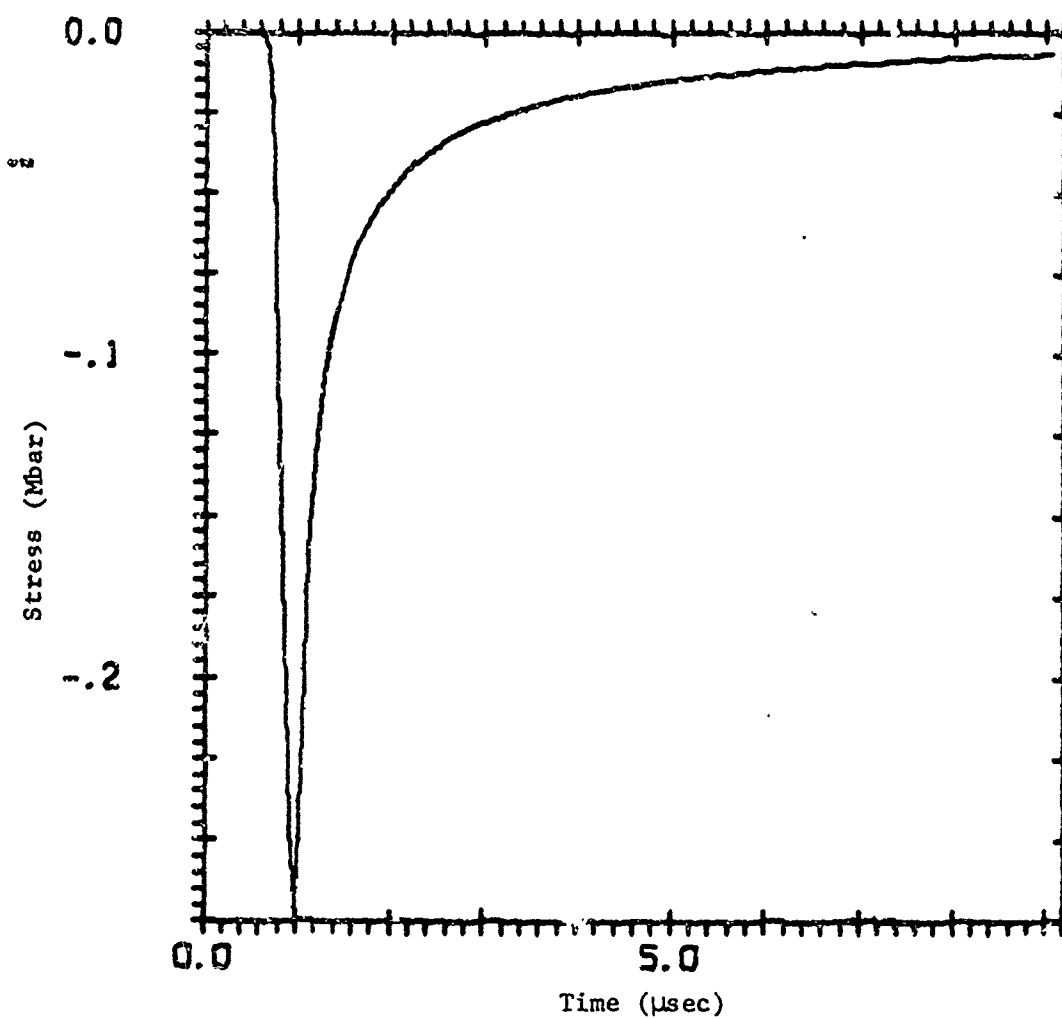


Figure 3. Stress Versus Time at Zone Number 11 (Original Position = 0.518 cm) for Standard Detonation in Composition B

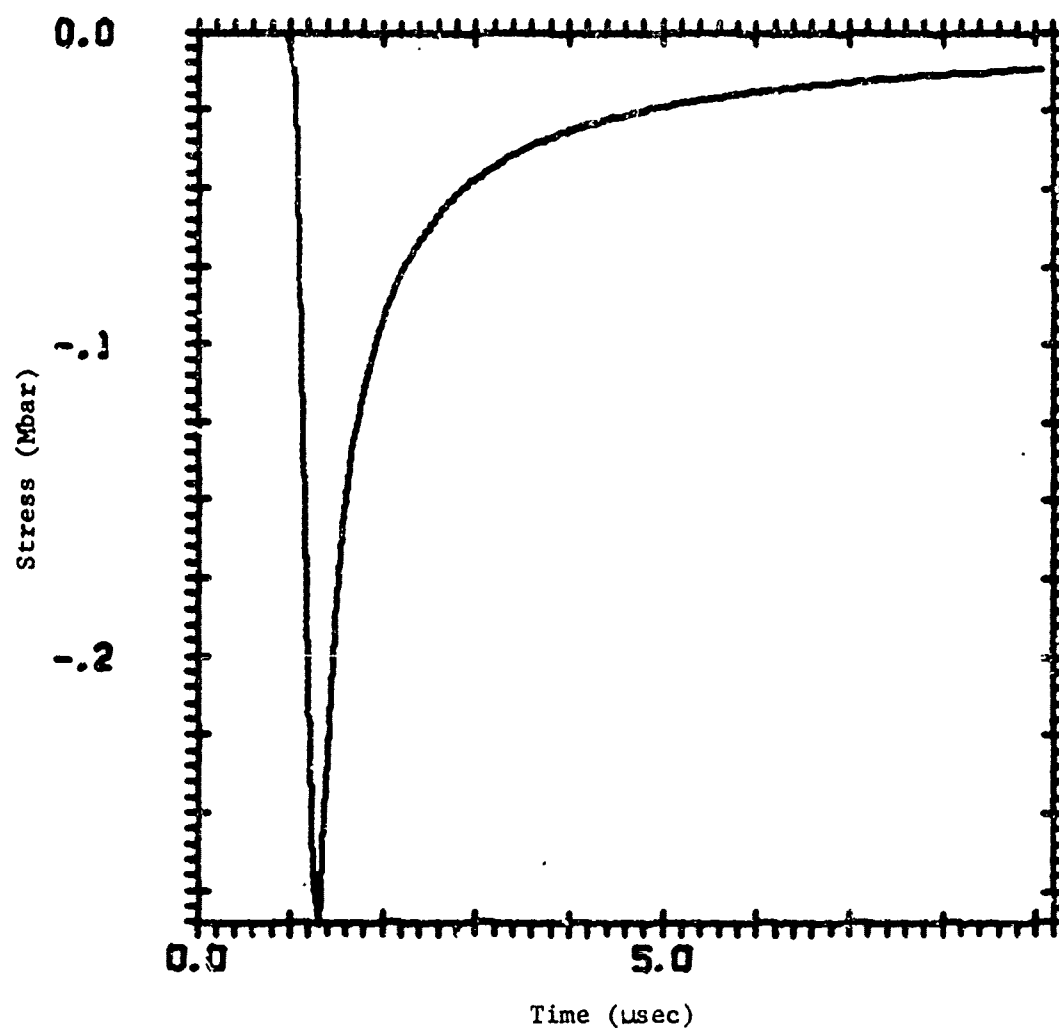


Figure 4. Stress Versus Time at Zone Number 16 (Original Position = 0.760 cm) for Standard Detonation in Composition B

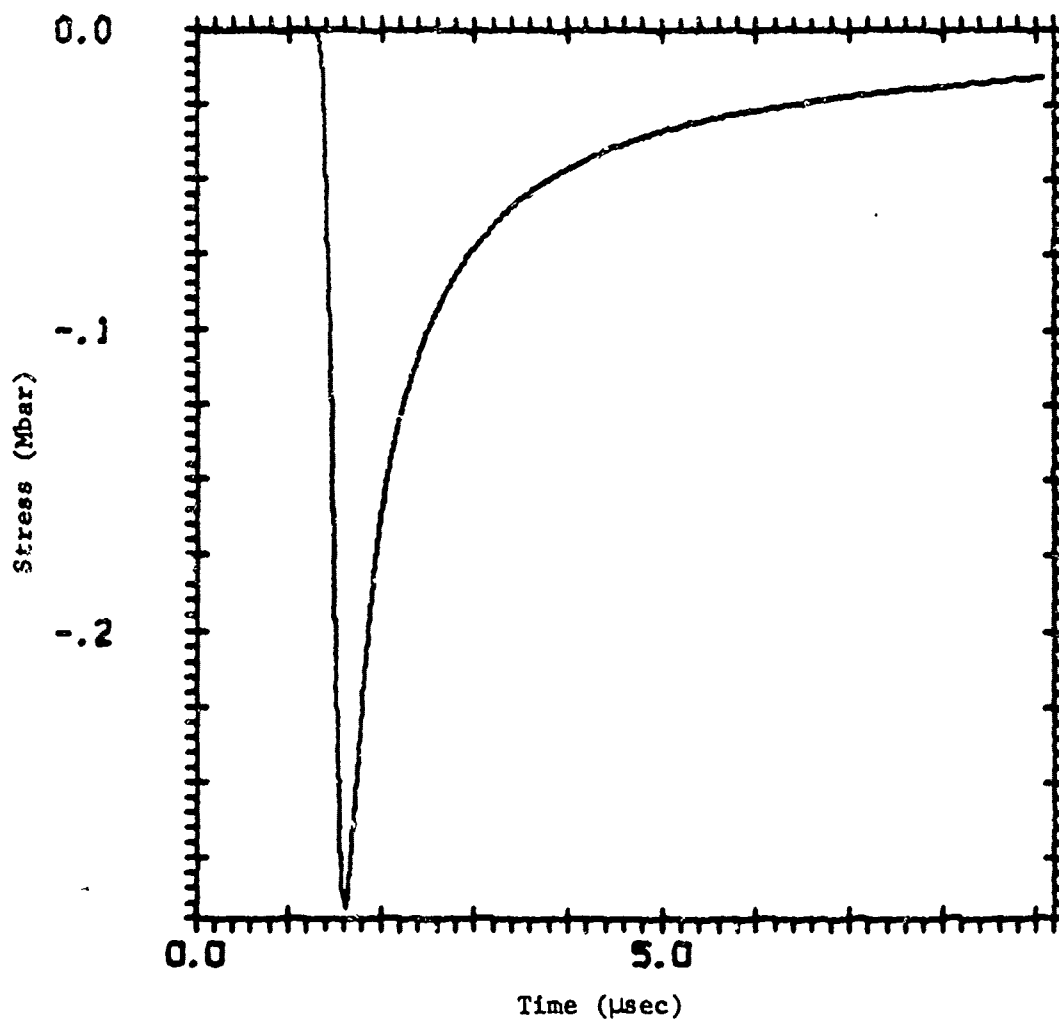


Figure 5. Stress Versus Time at Zone Number 21 (Original Position = 1.01 cm) for Standard Detonation in Composition B

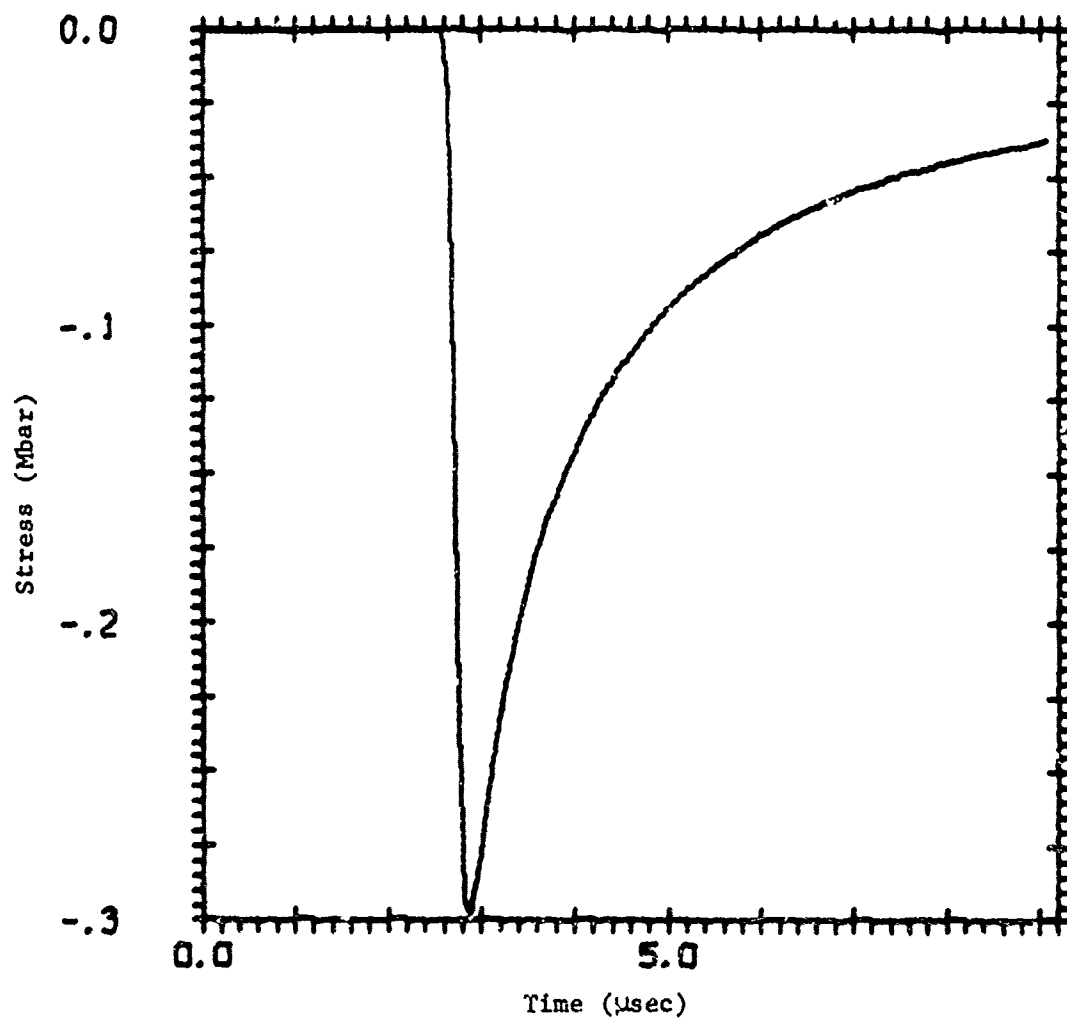


Figure 6. Stress Versus Time at Zone Number 41 (Original Position = 2.01 cm) for Standard Detonation in Composition B

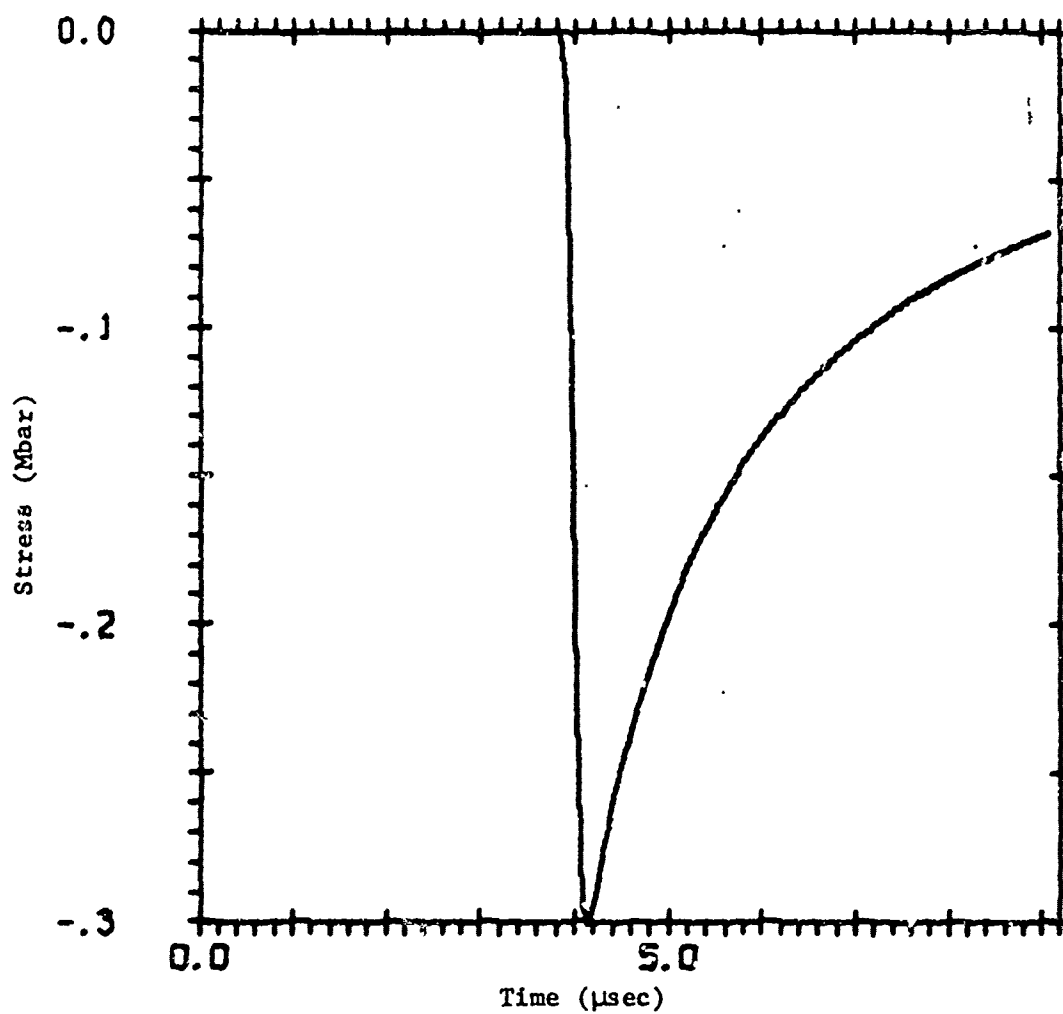


Figure 7. Stress Versus Time at Zone Number 61 (Original Position = 3.01 cm) for Standard Detonation in Composition B

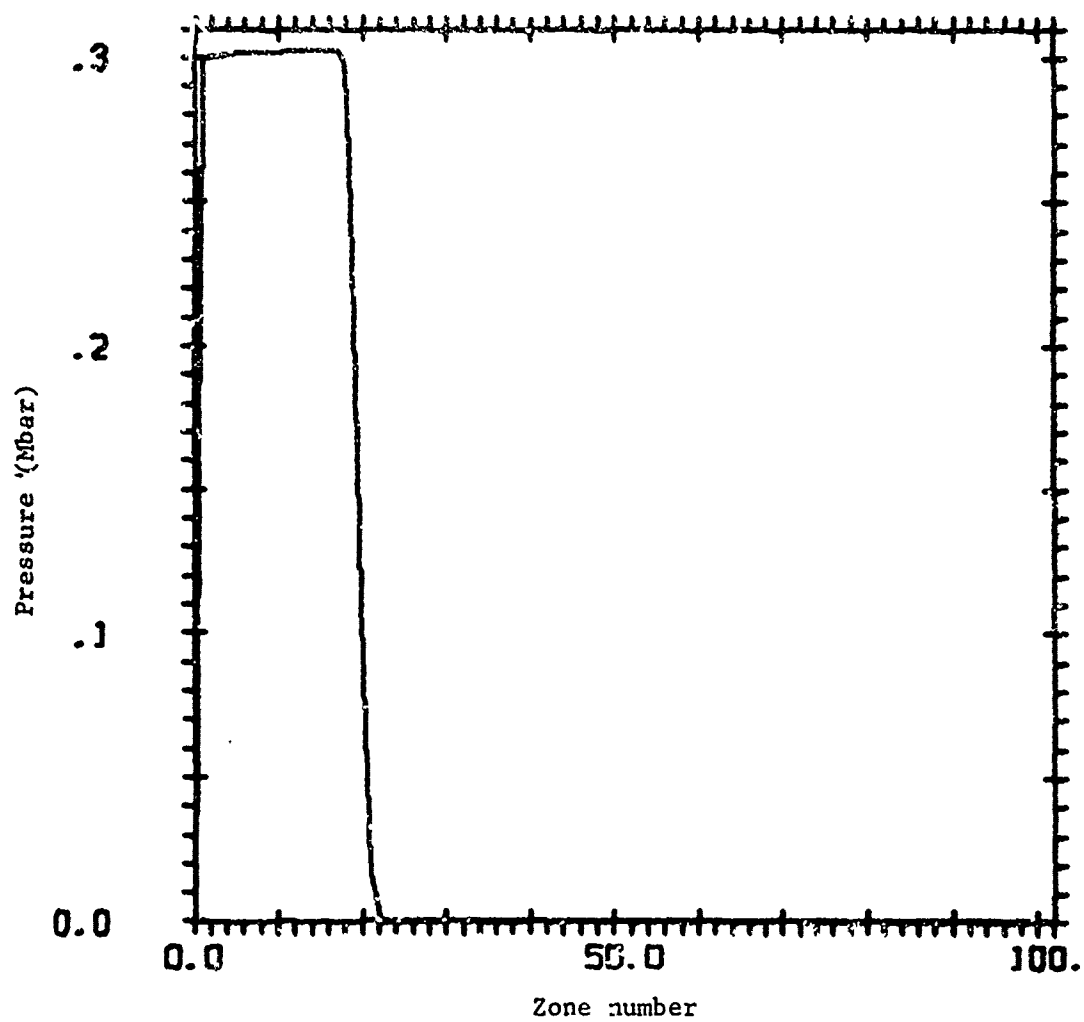


Figure 8. Peak Pressure in Each Zone for
Special Detonation in Composition B

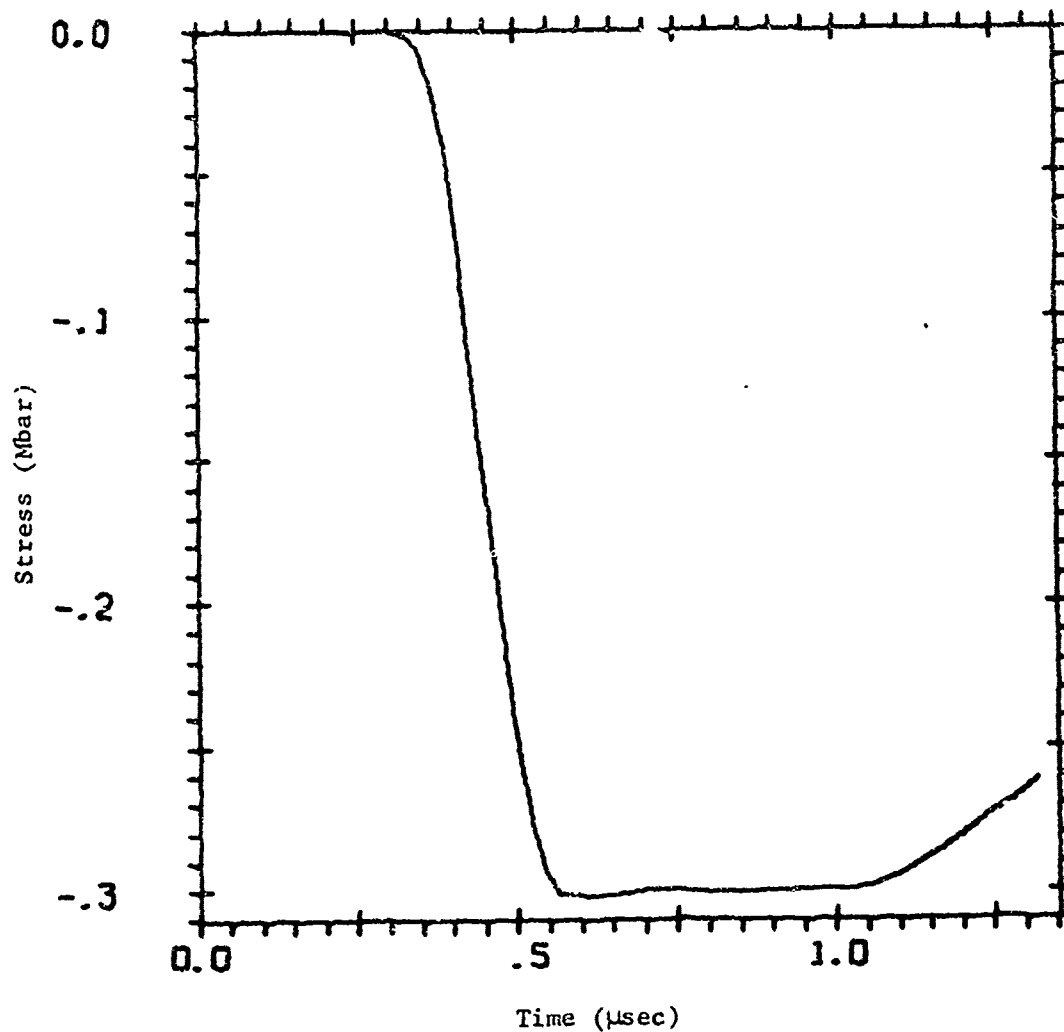


Figure 9. Stress Versus Time at Zone Number 6 (Original Position = 0.26 cm) for Special Detonation in Composition B

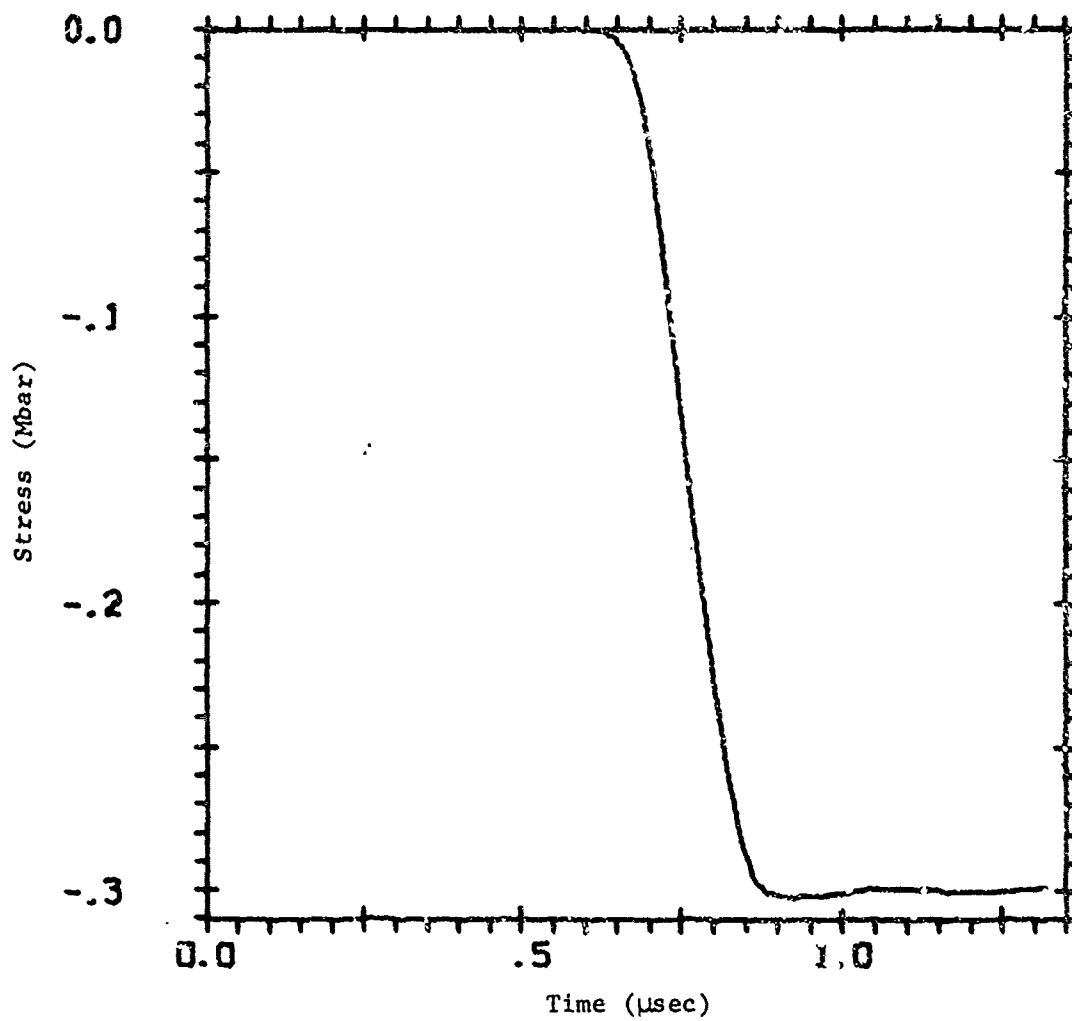


Figure 10, Stress Versus Time at Zone Number 11 (Original Position = 0.510 cm) for Special Detonation in Composition B

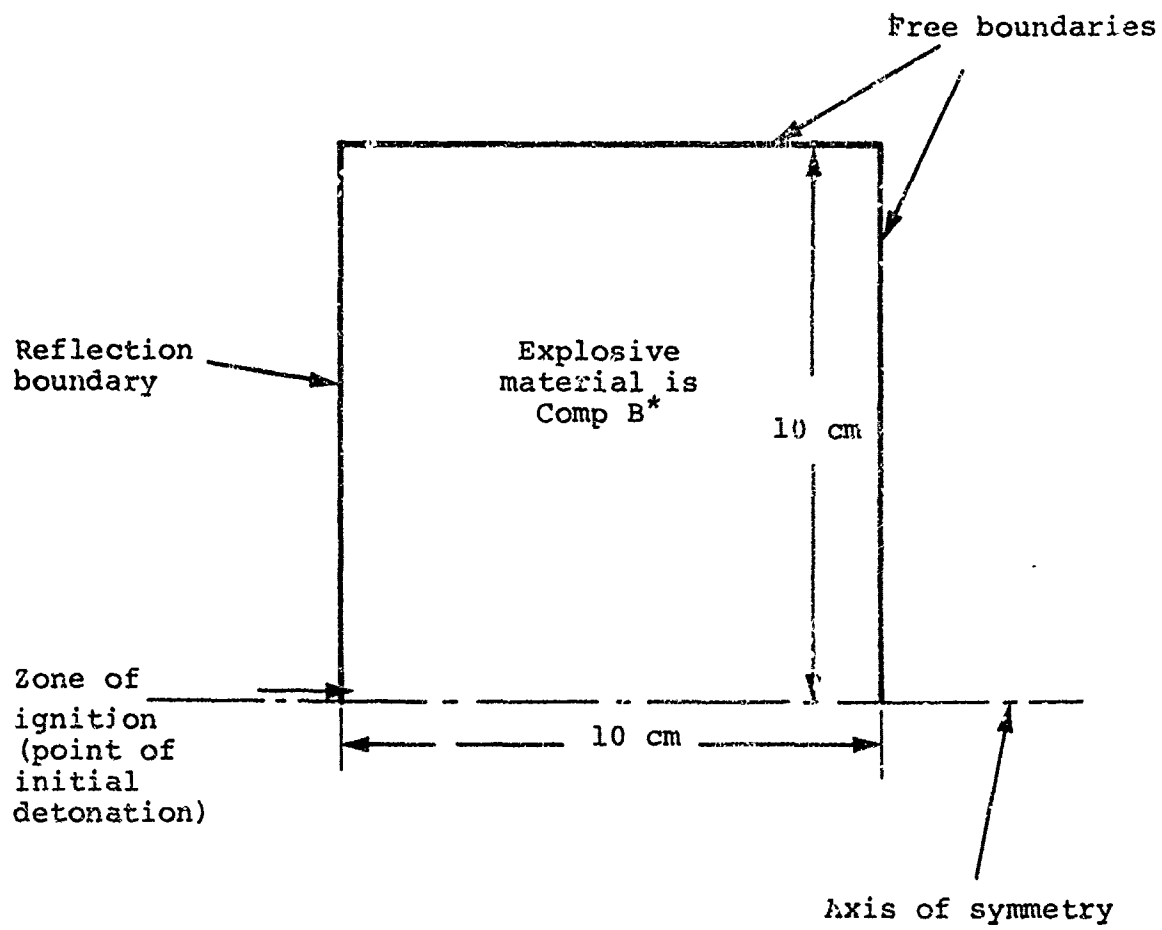
Figures 8, 9, and 10, the new logic no longer requires 20 or more zones for the detonation front to build up to the Chapman-Jouguet pressure.

The explanation for the difference lies in the manner in which the two calculations are ignited. In the first case, the ignition is accomplished by giving a zone an initial burn fraction equal to 1.0 and the detonation automatically propagates according to the burn logic described in Appendix A of Reference 3.

In the second case, the zone to be ignited is assigned a special equation of state which determines the pressure in that zone as a pre-programmed function of time. The pressure in that zone is forced artificially to rise from $p = 0$ to $p = p_{CJ}$ in a time, τ , equal to the time that it would take for a fully established detonation wave to pass over that zone.

Except for this difference in ignition, the detonation mechanisms are identical in the two sample calculations. Each uses the same burn logic and the same material description for the explosive.

c. Two-Dimensional Detonations. Two calculations were performed on PISCES 2DL, contrasting the standard two-dimensional detonation logic, described in Appendix B (case A), in Reference 3, and a special two-dimensional detonation logic (case B). The results of these calculations are summarized in Appendixes C and D, respectively, of Reference 3. (Figures C-1 through C-16 for case A are parallel in origin to Figures D-1 through D-16 for case B.) The geometry for the two calculations is shown in Figure 11.



* Same equation of state used for one-dimensional calculations.

Figure 11. Two-Dimensional Geometry Used To Test Detonation Ignition Logic

The burn logic used in case B (special two-dimensional detonation) is very similar to the standard form and involves only slight modifications of the standard burn description. In particular:

- (1) As in the one-dimensional case described earlier, the zone to be ignited is assigned a special equation of state. This equation of state forces the pressure in that zone from 0 to P_{CJ} in the characteristic zone burn time, τ .
- (2) The burn fraction computations in the remainder of the explosive zones do not require a pre-specified propagation velocity. In other words, the burn fraction calculation for the special two-dimensional calculation is the same as that described in paragraph b for the one-dimensional calculations.

A comparison of the two calculations presented in Appendixes C and D of Reference 3 shows significant differences in the two detonation descriptions. The major distinctions between the two solutions are that case A appears to be smoother than case B and the peak velocities at the detonation front of case A are lower (by a factor of 1/2 to 2/3) than those of case B. In addition, a well defined detonation "front" does not exist in case A but does exist in case B. Finally, the shape and magnitude of the front in case B appear to agree quite well with theoretical predictions while the waveform in case A is only approximately correct.

In summary, the results of these calculations indicate that the special detonation description has a sharper and stronger detonation front which agrees more closely with the Chapman-Jouguet theory of detonations.

4. EQUATION OF STATE FOR COPPER

Using data from Reference 3, the equation of state for copper is of the form

$$p = (C\mu + D\mu^2 + S\mu^3) \times (1 - \frac{\Gamma}{2} \mu) + \Gamma \rho E$$

where the coefficients have the following values:

$$C = 1.37 \text{ (Mbar)}$$

$$D = 1.75 \text{ (Mbar)}$$

$$S = 5.6 \text{ (Mbar)}$$

$$\Gamma = 1.96$$

This equation of state in PISCES is just a form of the polynomial equation of state with

$$A1 = C = 1.37 \text{ (Mbar)}$$

$$A2 = (D - \frac{\Gamma}{2} C) = 1.75 - 1.34 = 0.41 \text{ (Mbar)}$$

$$A3 = (S - \frac{\Gamma}{2} D) = 5.6 - 1.7 = 3.9 \text{ (Mbar)}$$

$$B0 = B1 = \Gamma = 1.96$$

To describe the strength of the copper, a constant yield stress, von Mises model is used. The yield stress in uniaxial tension is 0.00219 Mbar and the shear modulus is 0.458 Mbar. The density of copper is 8.93 gm/cm³. A spall limit of -0.0007 Mbar was applied to the mean stress (pressure).

5. SLIDELINE CALCULATION

A more general scheme than that presented in the preliminary report has been developed for the slideline calculation. Computational problems can occur in the motion of the slavepoints as the explosive slides along the metal liner. A generalization of the sliding logic allows for possible voiding, transmission of a shear stress as well as a normal stress across a slideline if desired, and an improved motion calculation for the slavepoints and the masterpoints.

The goal in the calculation of the motion of gridpoints along a slideline is to treat the calculation not in some special manner but in the same way that regular points are calculated.

A slideline is composed of a masterline and a slaveline--two separate adjacent columns in the Lagrange grid (Figure 12). Formerly, PISCES 2DL treated the motion of the points on the masterline (masterpoints) and the points on the slaveline (slavepoints) in a special and different way from other points in the grid. However, the masterline is a geometric boundary for the slavepoints while the slavepoints simply provide an external force to the masterline. A slavepoint behaves precisely as any other point that exists on a geometric boundary and a masterpoint behaves exactly as a gridpoint subject to an external stress. The logic used to move a slavepoint or a masterpoint is, in theory, identical to that used for any boundary point under a particular constraint. Appendix B contains a description of a generalized boundary motion scheme that incorporates masterpoints and slavepoints.

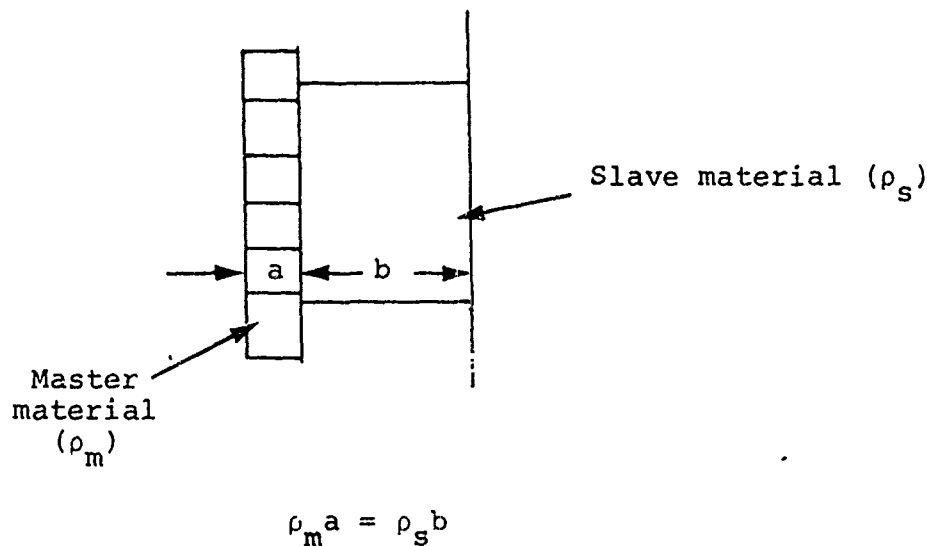


Figure 12. Slideline

As a result of the generalized boundary, the weighting of the external force of the slave material on the master material is done identically to the way stress contributions around an internal gridpoint (Reference 4) contribute to its motion. Thus, rules regarding mass matching apply to the Lagrange-Lagrange interface. The mass weighting of stresses does not employ a true mass density times zonal volume, ρV , but rather an areal density, ρA , density times zonal area. In planar symmetry there is no difference between ρA and ρV weighting. In axial symmetry the radial coordinate of adjacent zones is taken to be the same. This is highly desirable across a slideline where a mismatch of zonal size with non-square zones in conjunction with the radial divergence of mass renders strict mass weighting, ρV , undesirable as well as incorrect.

On a slideline interface where different size zones of different materials may exist, it is not important to have exact mass matching. What is more important is to mass match in a normal direction to the interface. This is identical to the mass matching criterion of a one-dimensional code.

The code performs a masterpoint calculation as an interior point calculation with the properly weighted surrounding stress contributions. As described in the preliminary report, a linear weighted average of the slavepoint force contributions is utilized for the force on any particular masterpoint. It should be noted, mass weighting considerations aside, that a sufficient number of slavepoints must be defined along the slideline in a tangential direction to adequately describe the stress contribution to the master material. This is analogous to stating that sufficient points must be used in the piecewise linear approximation of a continuous function or, more obviously stated, that the spatial resolution of the stress profile is dependent on the number of slave zones.

6. REZONING

Rezoning techniques are defined as methods whereby a distorted Lagrange grid is mapped onto a new, smoother Lagrange grid. This mapping may be applied to grid coordinates and the associated zonal quantities of mass, energy, and stress, as well as to grid point velocities. Rezoning allows a two-dimensional Lagrange calculation to be extended beyond a point where the grid has become distorted to the extent that time step inefficiencies and computational inaccuracies have occurred. Rezoning is applied at periodic intervals so that a grid remains relatively smooth. It is important that rezoning not obscure (diffuse) the solution and yet allow a long running time. The guiding precepts in the use of rezoning techniques are: (1) use a rezoner as infrequently as possible and (2) when using the rezoner apply as small a perturbation to the solution as possible.

Two basic types of rezoning techniques are available at the contractor facility for use in conjunction with the PISCES 2DL code. The first rezoner is known as a manual snapshot rezoner while the second is an automatic (continuous) rezoner. The snapshot rezoner is used as follows. The user selects a restart edit on a restart tape to be rezoned. On special rezoner input cards the coordinates of the new grid are defined. New grid points can be generated by an equipotential method, point by point, or by any grid point generation technique. The rezoner reads the restart edit, generates the new grid, and then maps the state of the old grid onto the new grid. A restart edit of the new grid and rezoned variables is written on a new restart tape. PISCES 2DL reads the new restart tape and the calculation proceeds using the new (rezoned) grid. The snapshot rezoner is integral to the PISCES 2DL program, and the rezone and restart of a problem can be run as a single job.

For a two-dimensional problem that frequently gets into calculational difficulties due to a grid distortion, the repeated application of the snapshot rezoner could become quite tedious and time consuming. The automatic rezoner, however, does not require that a 2DL problem be stopped and restarted at rezone time. The automatic rezoner performs its rezoning functions simultaneously as needed with the normal calculational sweep through the grid. The user specifies (a) what region he wishes to be rezoned, (b) what calculational cycle to start rezoning, (c) what cycle to stop rezoning, (d) the frequency of cycles to be rezoned, and (e) the rezoning options desired. Following the general precepts of rezoning, the frequency of rezone cycles is kept to a minimum and the rezone options specified perform a small perturbation to the solution. It should be noted that the magnitude of the perturbation to the solution as a result of the application of either rezoner is largely empirical and can only be judged from previous tests and from the quality of the solution.

The use of one of the two rezoners does not preclude the use of the other. In fact, the rezoners may be used together and do not interfere with each other. A more detailed description of the snapshot rezoner is contained in Reference 5. Appendix C contains a description of the automatic rezoner.

7. ANTI-HOURLGLASSING OPTIONS

Two-dimensional Lagrangian codes that use quadrilateral zones are susceptible to a grid instability known as hourglassing. The anomalous hourglass shaped grid distortion results in incorrect computed displacements and eventually more serious problems.

PISCES 2DL has the option of employing a triangle viscosity to damp the anomalous motion of the grid points. The triangle logic utilizes a Navier-Stokes type viscosity defined for triangular zones surrounding each grid point. The viscosity coefficient varies for particular materials and with the amount of numerical damping to be imposed on the solution. Reference 7 gives a further explanation of this technique.

Another approach to eliminating hourglass instability, known as hourglass subtraction, has been developed by the contractor. The idea is to subtract the hourglass motion from the grid at each cycle. The hourglass component of the velocity field of a mesh of quadrilaterals is defined, the hourglass component having zero net momentum. Subtracting this hourglass component from the velocity field at each cycle maintains a mesh of parallelograms and results in a continuous velocity smoothing which is similar to the velocity smoothing option of the continuous rezoner (Reference 7).

8. IMP OPTION

Occasionally in a calculation, a zone far from the region of interest may distort to the point where it controls the time step of the entire problem. An example of this occurs on the free surface of the unconfined explosive in the shaped charge under study. The explosive blows off radially and its turbulent nature causes the Lagrange grid at the free surface in some areas to get into time-step difficulty or to tangle into a zero or negative volume. Rather than simply applying the rezoner to this region, it is much easier to simply ignore these zones. This is possible when these zones have released all their chemical potential energy and in fact can no longer influence the motion of the liner. Removal of these zones from the problem requires that they be isolated from the rest of the grid. A logic called IMP, Isolated Mass Point, is used. The procedure consists of replacing the zone with a free boundary condition and not allowing the zone to be calculated any more, but rather maintaining the values it possesses at the time it is removed from the grid.

9. TRACER POINTS

Implicit in the idea of Lagrange rezoning is the fact that original zones and their associated values will lose their identity through rezoning. As rezoning is performed, it becomes more and more difficult to tell where mass originated. This is a common problem for Eulerian codes where mass units never exist. Eulerian codes often use Lagrange tracer points to define material interfaces and allow general mapping of the fluid motion. These tracer points are moved through the grid according to the average velocity of the surrounding material.

A scheme has been devised whereby tracer points could be used in a Lagrangian code in conjunction with a rezoner. It should be obvious that tracer points are not necessary in a Lagrange code if no rezoning is performed. Tracer points in 2DL are different than Eulerian tracer points in that their motion is described completely by the motion of the Lagrangian cell in which they reside. A Lagrangian tracer point stays with a Lagrangian zone and moves as the zone moves, maintaining its same relative position within the zone. At rezone time the tracer point may find itself in a new relative position inside the zone or in fact may now reside within a different zone. The tracer point only has to be updated at rezone times rather than every cycle as in an Eulerian code. The tracer point positions and velocities are derived from two numbers defining the relative position inside the zone and the zone's coordinates and velocities. It is only necessary to derive the tracer positions and velocities at output times for printout and plotting. This scheme, although designed, was not implemented into the PISCES 2DL code for these calculations.

SECTION III

CALCULATIONAL PROCEDURE

The shaped-charge calculation proceeded as follows:

(1) The grid was generated, plotted, and checked.

(2) Calculation was begun at time zero with initiation of the explosive and run to a point just before the detonation wave hit the copper liner ($\sim 5.6 \mu\text{sec}$). This duplicates exactly the previous solution (Reference 3).

(3) At this time, on the basis of the preliminary calculation, it was decided to employ the automatic rezoner in the apex area of the copper liner. The following automatic rezone options were employed:

Three rezone areas were defined.

Region 1--columns 2 to 6, rows 120 to 146

Region 2--column 1, rows 120 to 146

Region 3--columns 2 to 7, rows 120 to 146. (Column 1 is the inside surface of the liner while column 7 is the liner surface in contact with the explosive.)

The options for each rezone region were as follows (see Appendix C):

Region 1 NSTART = 199
 NEND = 10000
 NFREQ = 10
 N5OPT = 14200

Region 2 NSTART = 198
 NEND = 10000
 NFREQ = 10
 N5OPT = 12200

Region 3 NSTART = 198
 NEND = 10000
 NFREQ = 10
 N5OPT = 12250

The automatic rezoning schedule is as follows: At cycle 198 ($\sim 6.8 \mu\text{sec}$), column 1, the inside surface of the liner has a coordinate rezone of $NXY = 2$ (Appendix C). This helps keep the points on this column from crossing over each other as they form the jet. No velocity rezoning or momentum conservation is performed. The velocity distribution along the inner surface is quite important so that, rather than the true phenomenon being obscured, no velocity rezoning is performed.

At cycle 198, region 3 has a coordinate rezone of $NXY = 2$. This will help keep zones from tangling by trying to maintain parallelogram zones. A velocity rezone of $NVEL = 5$ is performed to smooth slightly the velocity distribution in the interior of the liner and the explosive interface. This small amount of smoothing is done in order to damp out the ripples previously experienced at the explosive liner interface.

At cycle 199, the next cycle, region 1 has a coordinate rezone of $NXY = 4$. This allows the columns within the liner to remain equidistant in order to keep adequate resolution near the expanding jet. No velocity rezoning is performed.

The sequence of automatic rezoning will then occur every ten cycles thereafter until the user respecifies the options.

In general, a coordinate rezone of $NXY = 4$ should be used only after a coordinate rezone of $NXY = 2$, because the centroid method ($NXY = 3, 4$) will not work properly on a tangled zone. The operational rule is to use $NXY = 1$ or 2 to untangle the grid and to use $NXY = 3$ or 4 to more evenly space zones. The centroid method ($NXY = 3, 4$) was used in the case of expanding zones to maintain good resolution. In the case of compressing zones, $NXY = 3$ or 4 will keep a zone from crushing with a resultant small time step.

Note that in the three rezone regions specified, care was taken in the selection of rezone parameters to avoid overly constraining the solution. Coordinate rezonings used the lesser constraint of $NXY = 2$ or 4 versus $NXY = 1$ or 3 . Velocity rezoning was only performed in the interior of the copper liner and on the back surface. The value of $NVEL = 5$ is an intermediate value and does not force a large constraint on the solution to the problem. Also, it is important to note that the rezoning does not destroy the various gradients that exist in the problem. Radial or axial velocities are not forced to behave in some monotonic manner. This is highly important if the actual jet formation process is to be characterized.

(4) Snapshot rezoning of slavepoints was performed to allow for better resolution of the stress profile along the liner. The slavepoints were moving in a more reasonable manner due to the new motion logic; however, due to the relatively coarse explosive zoning, these snapshot rezones were necessary.

(5) The calculation was carried to 10 microseconds. At this point a large snapshot rezoner would have to be performed in the liner. This would move the columns toward the front of the jet to allow for more resolution in the jetting area and would result in the stagnation region having relatively coarser zoning. This is allowable since significant gradients do not exist in this region.

SECTION IV

RESULTS

The shaped-charge jet calculation is presented in coordinate and velocity vector plots in Appendix A. The results from the preliminary calculations are also presented in Appendix A for comparison. A comparison of the previous and current calculation at about 8 μ sec shows that the explosive-metal interface is experiencing instabilities near the liner apex in both calculations. In the first calculation, these instabilities continued to grow and it was necessary to use the snapshot rezones to eliminate them from the problem. Since the cause of these instabilities was uncertain, it was decided to let the automatic rezoner try to damp them out. As seen, the automatic rezoning did not get rid of the instabilities completely but did retard their growth.

There are two possible sources of these instabilities. The first may be a characteristic of the slavepoint position, and the ~~second may be a Taylor instability.~~ The position of the slavepoint with respect to the master material would give characteristic wavelengths of the instabilities dependent upon the slavepoint position. If this is the cause of the instabilities, then finer zoning in the explosive along the liner would remedy it. It should also be noted that, prior to the use of a linear interpolation scheme for the slave zones, very large amplitude instabilities were produced on the interface.

The rippling on the explosive-metal interface may, in fact, be due to a classic Taylor-like instability. The calculation at the interface involves the relatively constant pushing of a heavy material, copper, by a light material, Composition B, which is a condition ripe for a Taylor instability. The ripples, if they are a Taylor instability, should be worse in areas where there is a shorter radius of curvature. The observation is made that the ripples occur near the apex of the cone and are not particularly evidenced in the linear part of the liner.

If the ripples on the back surface of the liner are Taylor instabilities, the amplitude of the perturbation will decay exponentially with distance. For the given width of the liner the amplitude at the back surface will have decayed to about 5 percent of its value when it reaches the inside surface. However, the automatic rezoner through successive rezones will couple the motions on the back and front of the liner and therefore help transmit any perturbation that occurs. It is therefore desirable to keep the ripples to a minimum in the numerical simulation. It should be noted that the Taylor-like instabilities may also occur physically and be highly sensitive to machining tolerances.

Independent of the cause of these instabilities there are means that could be employed to keep them from growing. The first is to use the triangle viscosity described in Section III, and the second is to increase the copper yield strength. Since copper is strain-rate dependent, it is probable that the 2.19-kbar value is too low for the high strain rates of this problem (Reference 8).

At 8.7 μ sec on the current calculation, a perturbation is noted on the liner that was not associated with the previous instabilities. It is believed that this perturbation is the result of an adjustment in the automatic rezoner near this time. Further calculations would be needed to clarify this assumption.

The sequence of plots illustrates the nature of jet break-out. At early times it is noted that the jet does not have a monotonic character. The first few zones just off the axis initially lag the rest of the liner motion. This appears to be the result of the instabilities affecting the inside of the liner. As the solution progresses, the jet can be seen to form in a smooth manner. The automatic rezoner helps allow for the smooth nature of the solution. The application of the automatic rezoner has shown itself to be a highly useful tool. Further study and experimentation are necessary to develop its potential fully. Additional algorithms for coordinate and velocity rezoning are being developed to increase its capabilities.

Unfortunately, the scope of this contract did not permit running the final calculation long enough for complete comparison with experimental data and further comparison with the preliminary calculation was not possible. However, one interesting result of the preliminary calculation was the formation and growth of the jet tip instability followed by a stable jet. This same jet tip instability has been observed experimentally with X-ray photography.* The jet velocity increases from about 0.6 cm/ μ sec to 0.78 cm/ μ sec from the tip through the instability at a time of 13 μ sec.

*Personal communication between Dr. C. Godfrey and L. Behrmann with R. Vitelli of BRL.

SECTION V

CONCLUSIONS

The calculation of a shaped-charge jet with a finite difference, Lagrangian coordinate continuum mechanics code has been demonstrated. Although the final calculation was not carried out as far as the preliminary calculation, a sufficient jet length was obtained to arrive at the above conclusion. The fact that the jet tip showed a mass⁶ buildup and instability similar to experiments could result only if the jet radial velocities were not arbitrarily fixed to allow the problem to run.

The code modifications that were made assured that the physics of the problem was correctly calculated. Two of those modifications are worth reviewing. The first is the automatic rezoner. This rezoner was designed with considerable flexibility so that the engineer could adjust both the magnitude and frequency of the rezone within a specified space. With this and the snapshot rezoner, Lagrange calculations will be more versatile where large grid distortions occur. The second modification of importance is the availability of multiple column slidelines with the option of void open and closure on each slideline. This modification will allow, for example, the study of possible bifurcation of the jet. Further modification of the automatic rezoner to include tracer prints would be desirable but was beyond the scope of this contract. When rezoning is performed, correlation with the jet parameter theory developed in Volume I of this report would be tedious unless tracer points are used.

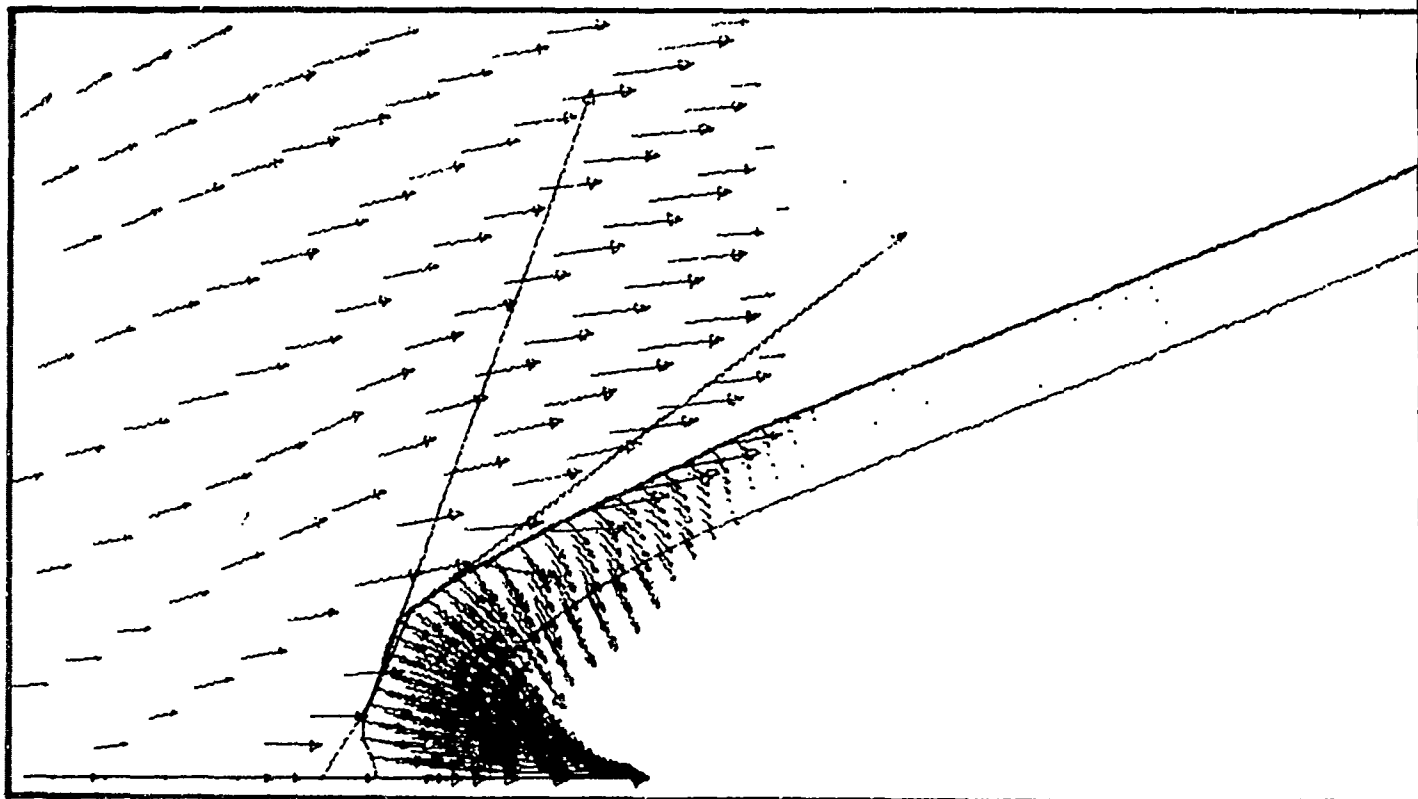
In summary, this calculation addressed the solution of the complete shaped-charge jet formation problem. A full explosive detonation was calculated for the loading on the metal liner. The code is not restricted by the shaped-charge geometry as long as an axis of symmetry is present, i.e., variable thickness liner, curved liner, multi-material liner, and explosive case shaping are all acceptable geometries. The code can also use a forcing function to simulate the explosive loading on the copper liner. The forcing function could be an external pressure or velocity constraint. The velocity condition would not allow for any Taylor-like instabilities to appear on the back surface of the liner.

REFERENCES

1. M. L. Gittings, R. I. Sedgwick, and J. M. Walsh, Numerical Analysis of Jet Formation from Lined Shaped Charges, Contract Report No. 51, 3SR-641, Ballistic Research Laboratory, August 1971.
2. L. I. Walsh, D. E. Wilkins, and R. T. Sedgwick, User's Manual for an Eulerian Shaped Charge Computer Program, Air Force Armament Laboratory Technical Report AFATL-TR-73-24, February 1973.
3. R. Hofmann, N. Birnbaum, and S. Jardin, Preliminary Calculation of Jet Formation from the 105-mm BRL Precision Shaped Charge, TCAM Technical Memo 72-21, Physics International Company, November 1972.
4. PISCES 2DL, Manual A, General Description and Finite-Difference Equations, Revision 1, Physics International Company, San Leandro, California, 1972.
5. S. L. Hancock, A Lagrange Rezonar, TCAM Technical Memo 73-1, Physics International Company, San Leandro, California, February 1973.
6. E. D. Giroux, HEMP User's Manual, UCRL-51079, Lawrence Livermore Laboratory, June 1971.
7. S. L. Hancock, An Hourglass Subtraction Procedure, TCAM Technical Memo 73-6, Physics International Company, San Leandro, California, May 1973.
8. E. L. Lee, H. C. Hornig, and J. W. Kury, Adiabatic Expansion of High Explosive Detonation Products, UCRL-50422, Lawrence Radiation Laboratory, Livermore, California, May 2, 1968.

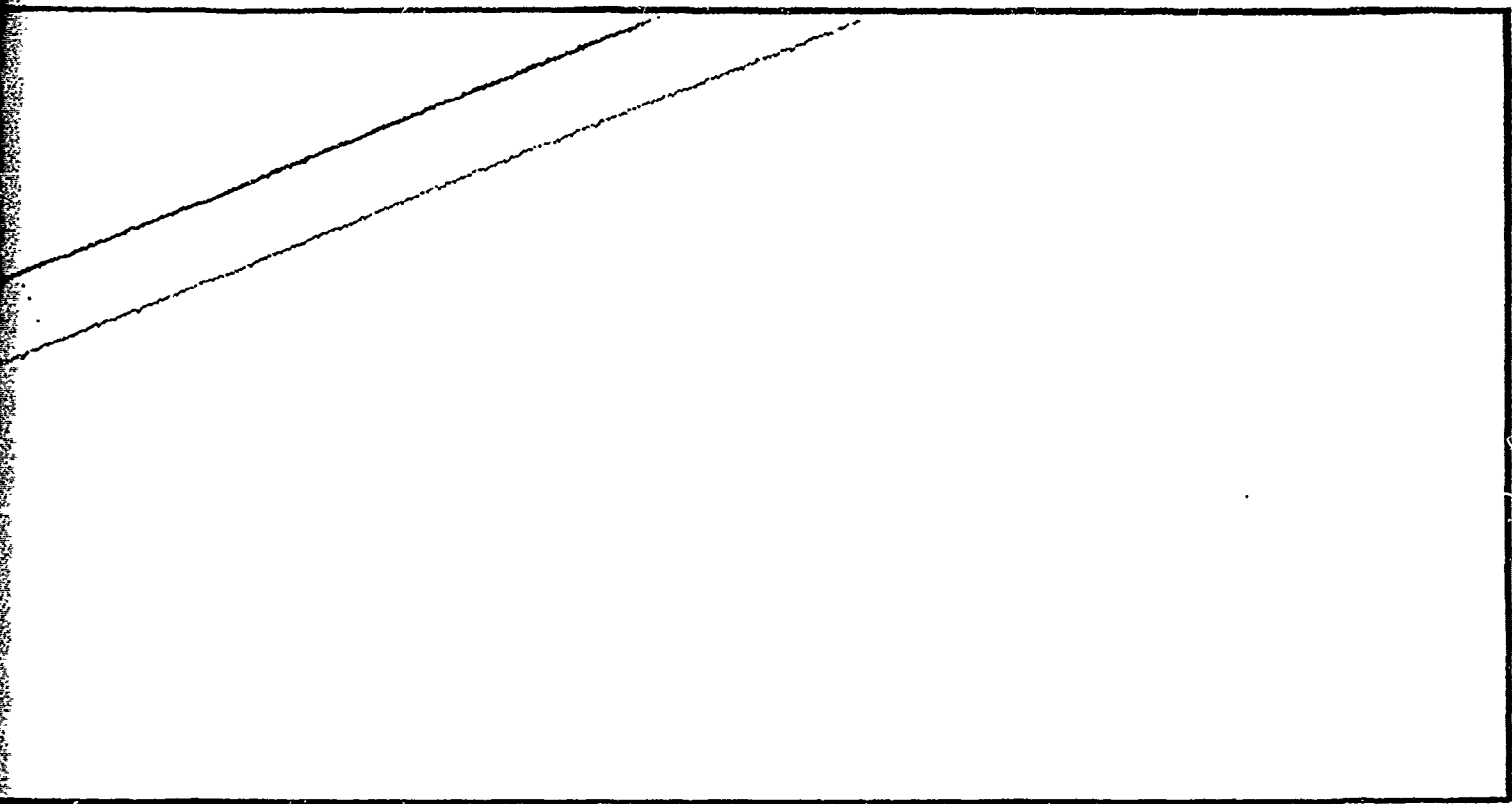
APPENDIX A
COORDINATE AND VELOCITY
VECTOR PLOTS

Figures A-1 through A-12 are coordinate and velocity vector plots of the preliminary shaped-charge jet calculations. Figures A-13 through A-33 represent the current calculations.



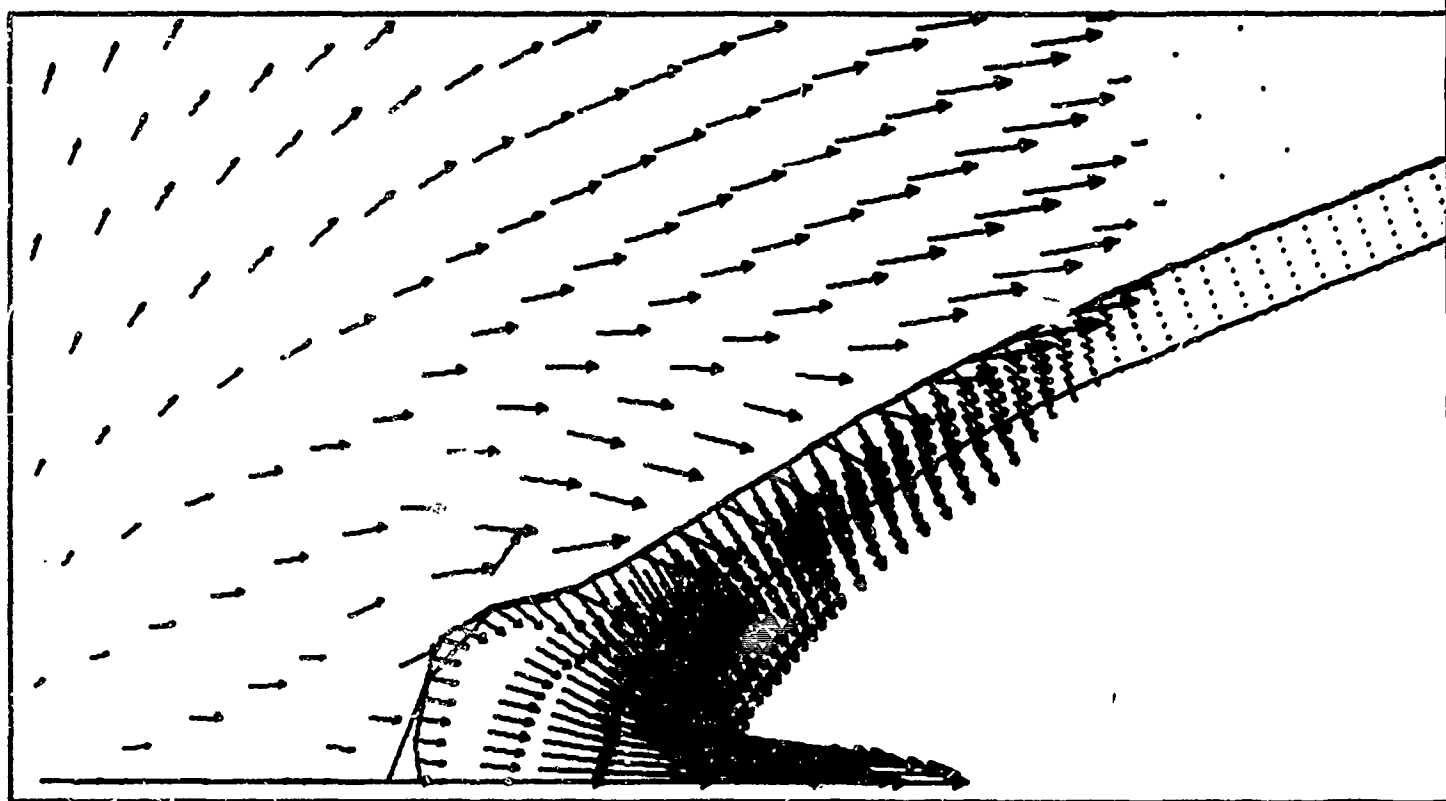
Scale: 1 inch (plotter un
1 inch (plotter un

2

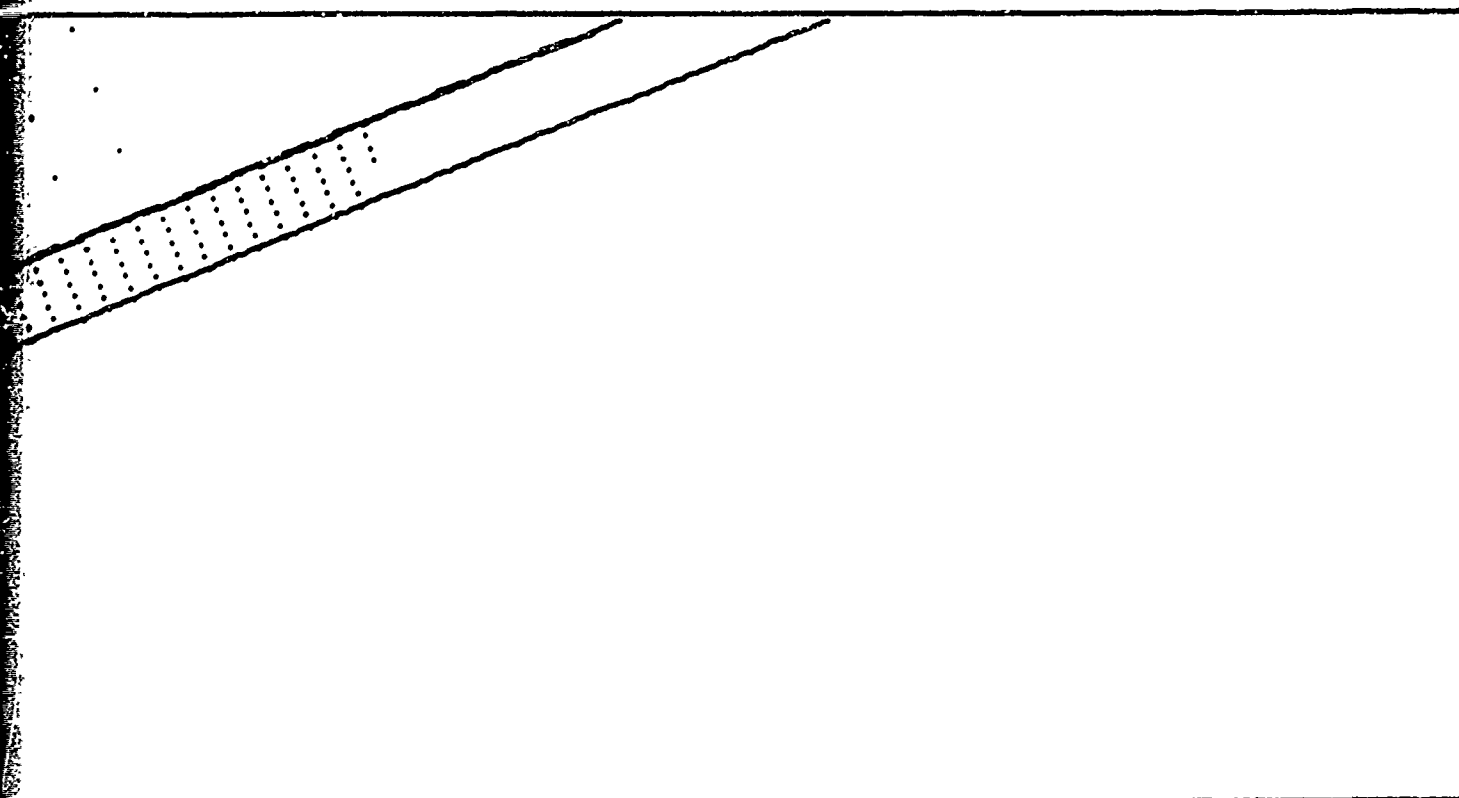


inch (plotter units) = 0.5 cm
inch (plotter units) = 0.5 cm/ μ sec

Figure A-1. Snapshot Velocity Vector Plot
Plot at Time = 8.01 μ sec

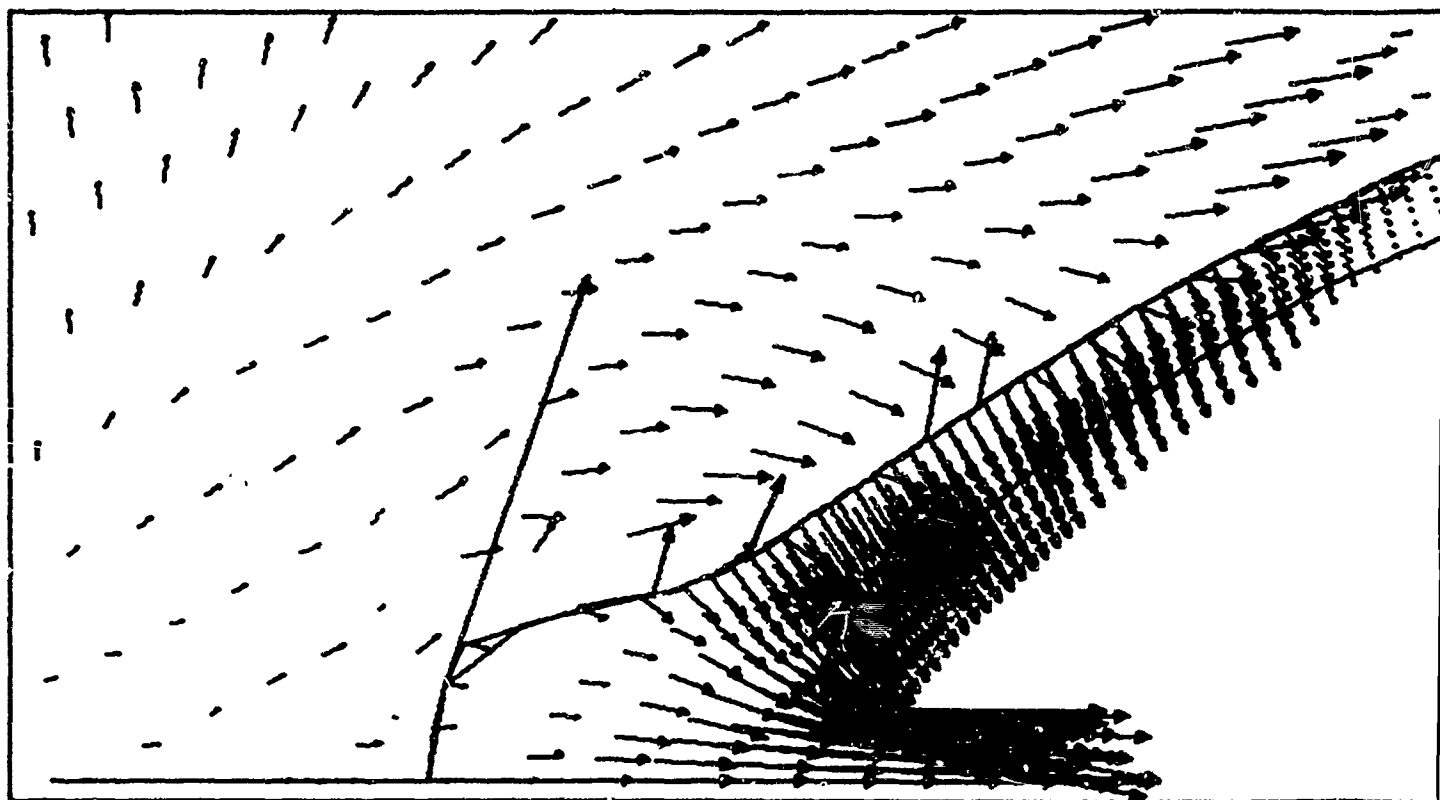


Scale: 1 inch (plotter unit)
1 inch (plotter unit)



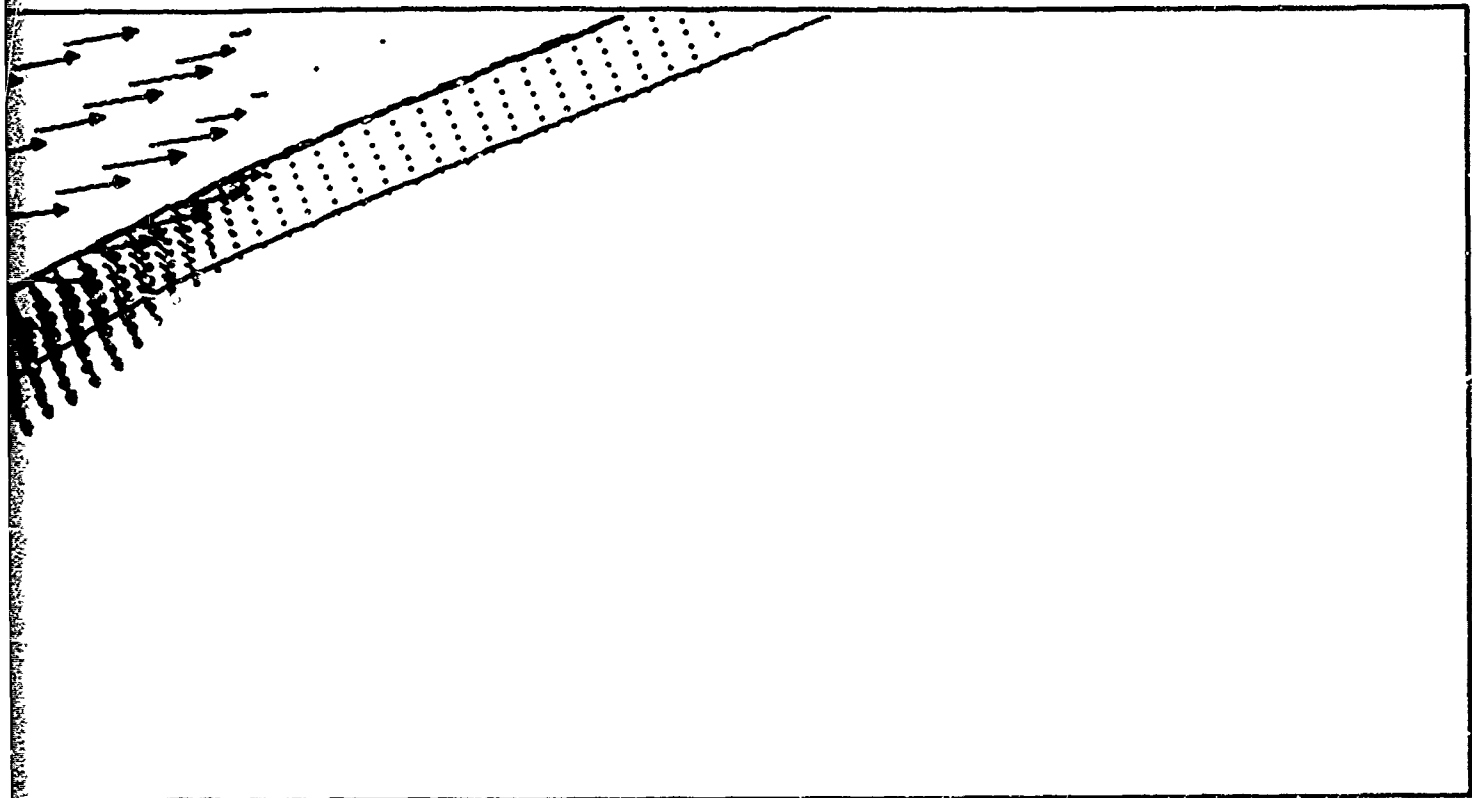
inch (plotter units) = 0.5 cm
inch (plotter units) = 0.5 cm/ μ sec

Figure A-2. Snapshot Velocity Vector Plot
at Time = 9.3 μ sec



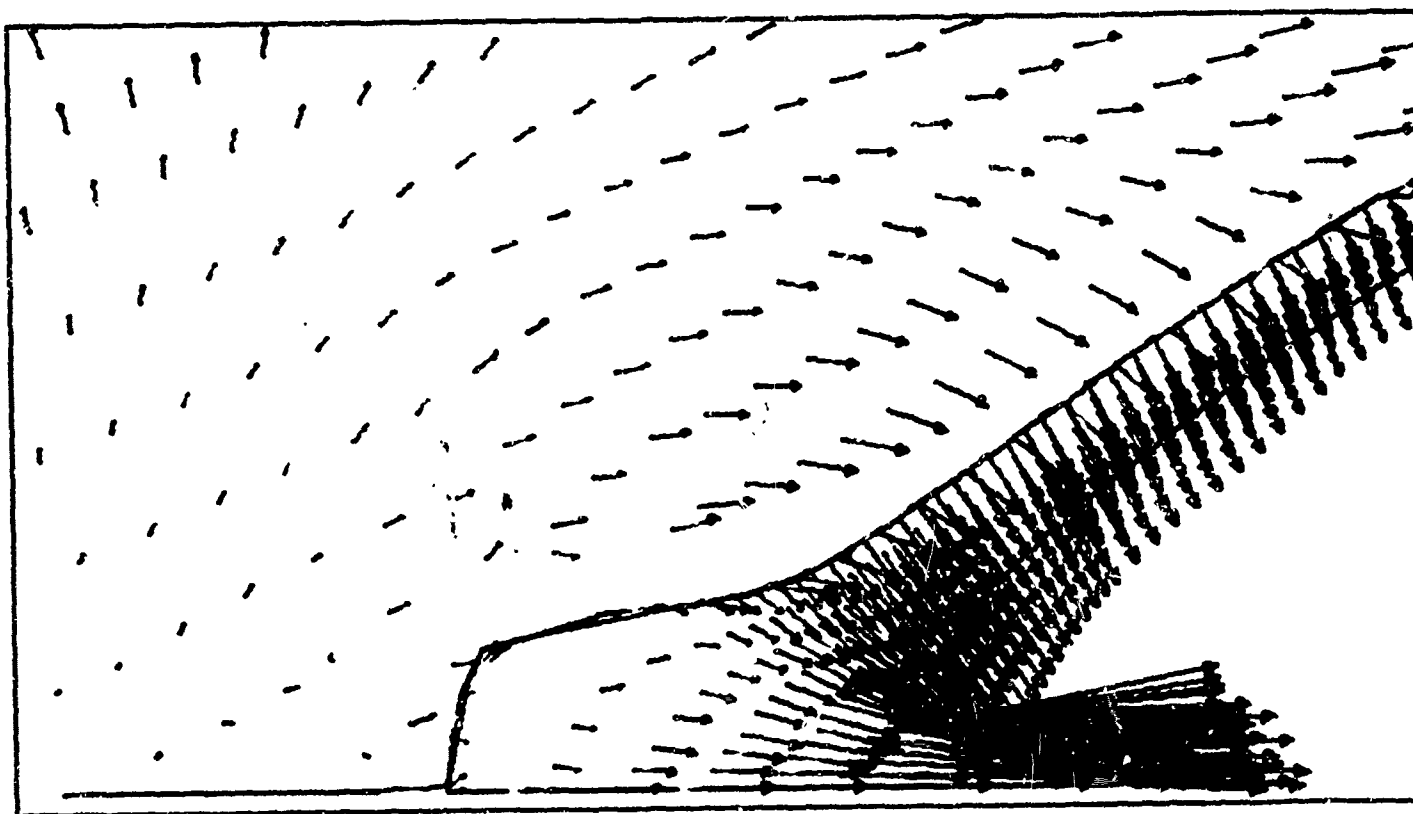
Scale: 1 inch (plotter u
1 inch (plotter u

2



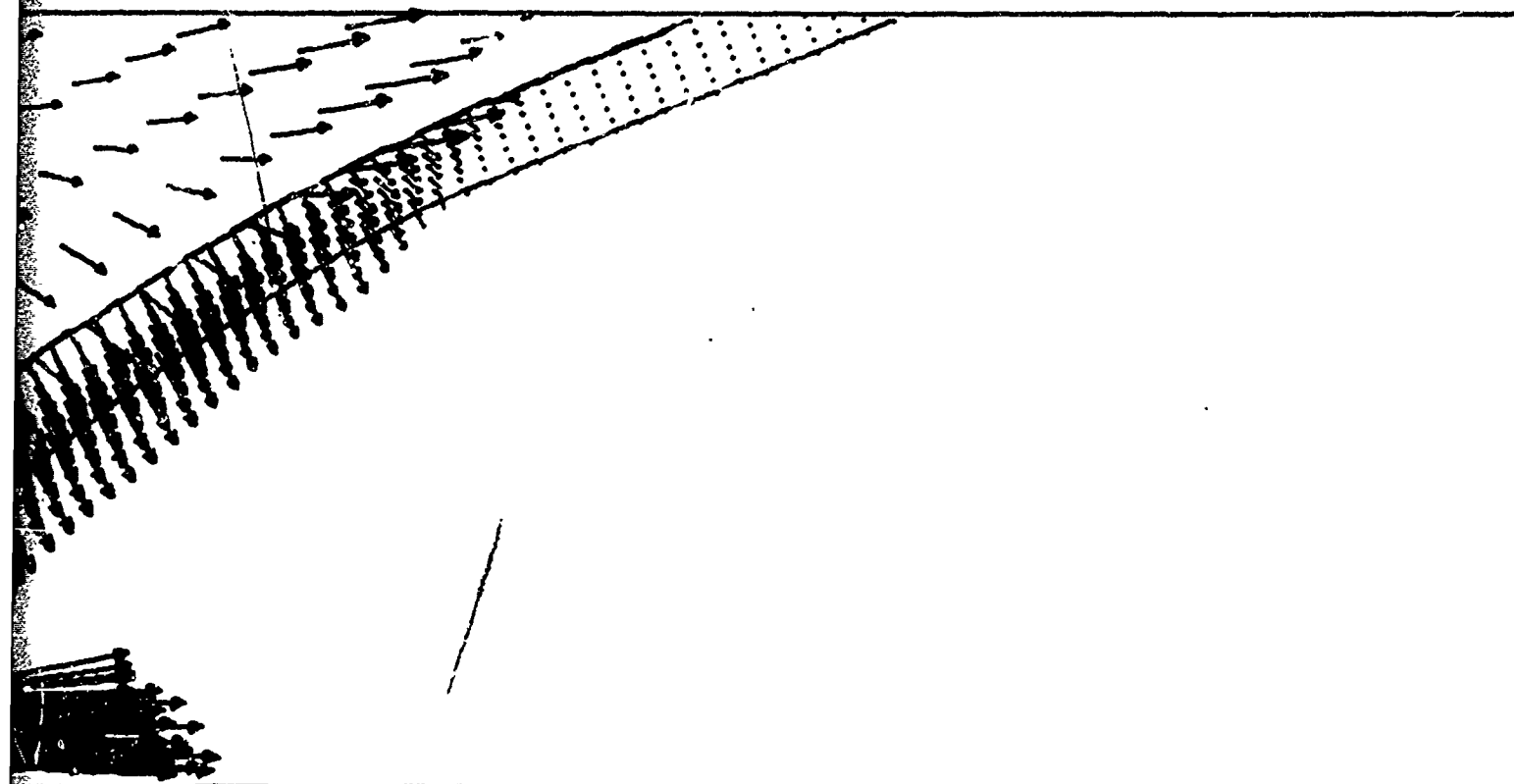
inch (plotter units) = 0.5 cm
inch (plotter units) = 0.5 cm/ μ sec

Figure A-3. Snapshot Velocity Vector Plot
at Time = 10.3 μ sec



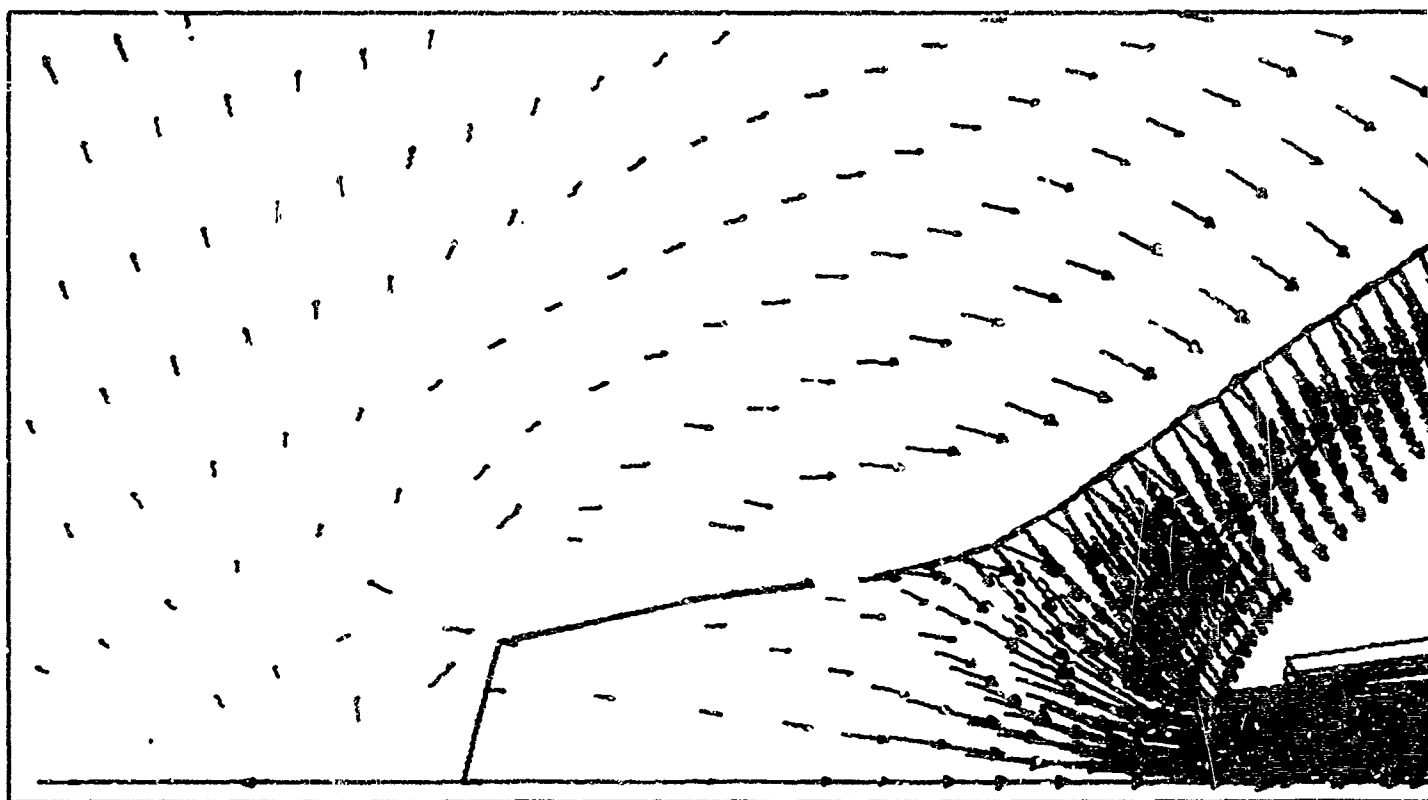
Scale: 1 inch (plotter u
1 inch (plotter u

2

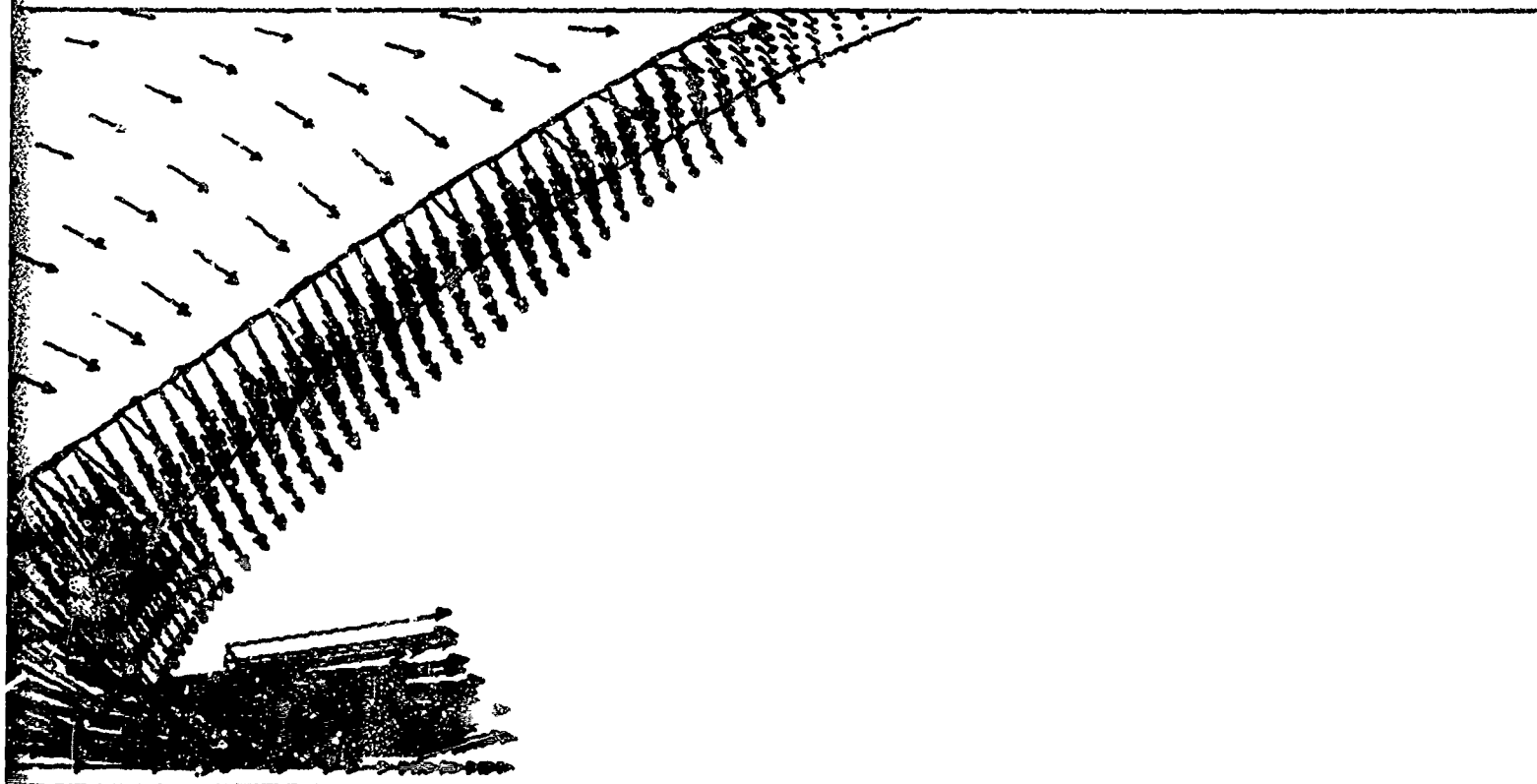


1 inch (plotter units) = 0.5 cm
1 inch (plotter units) = 0.5 cm/μsec

Figure A-4. Snapshot Velocity Vector Plot
at Time = 11.0 μsec

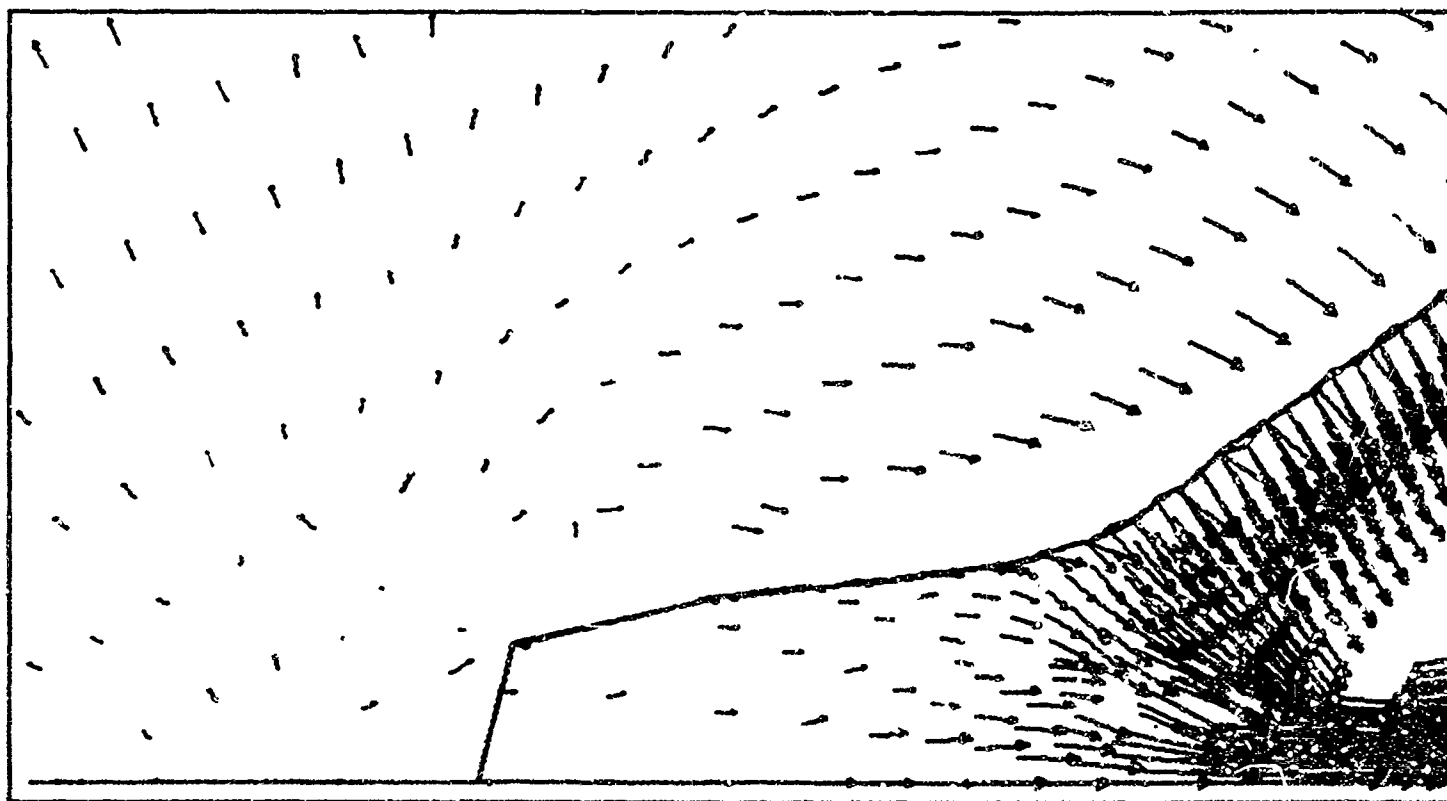


Scale: 1 inch (plotter ur
1 inch (plotter ur

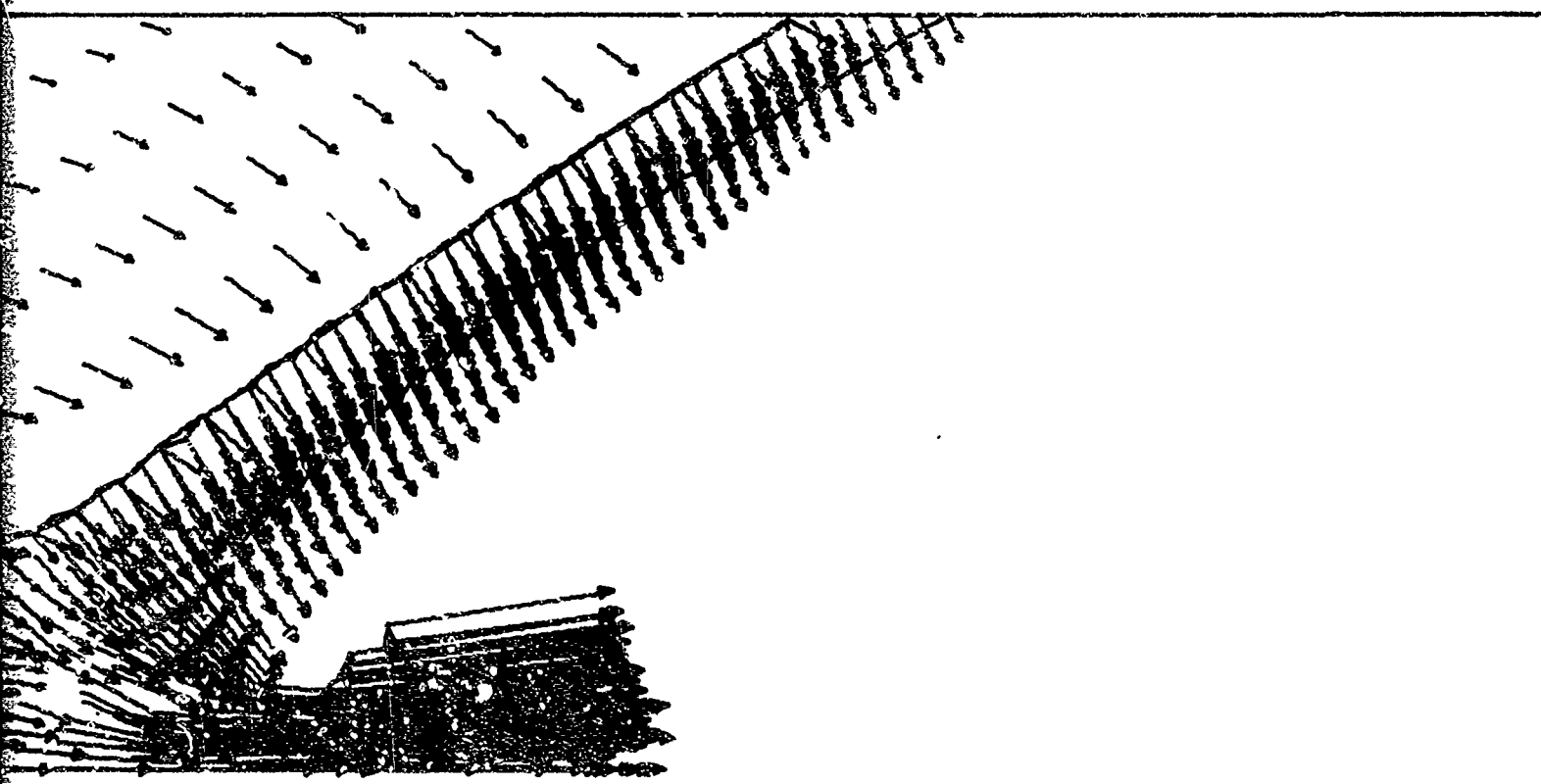


1 inch (plotter units) = 0.5 cm
1 inch (plotter units) = 0.5 cm/μsec

Figure A-5. Snapshot Velocity Vector Plot
at Time = 12.3 μsec

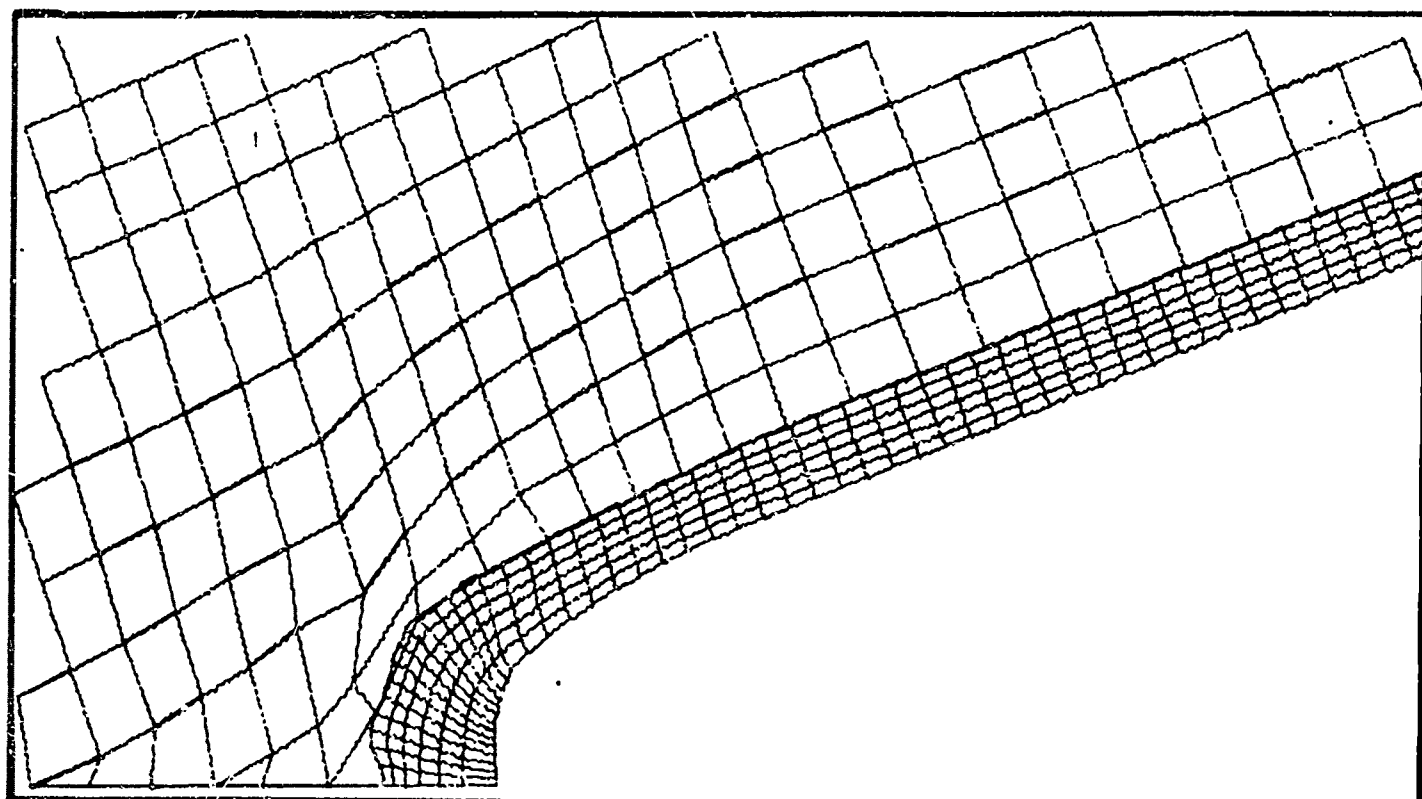


Scale: 1 inch (plotted)
1 inch (plotted)

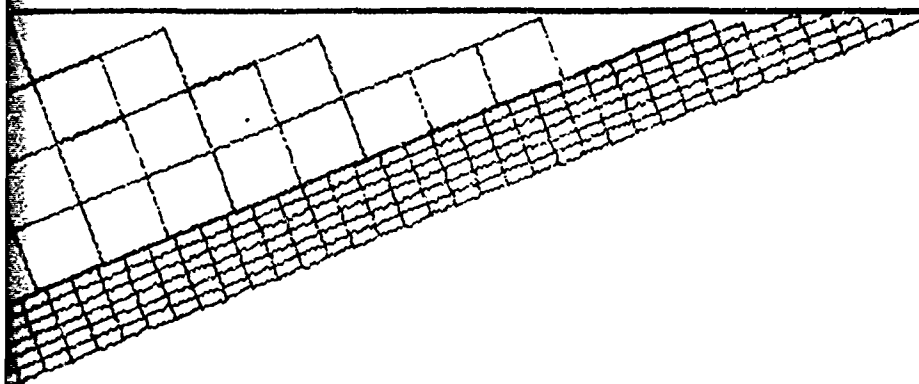


Scale: 1 inch (plotter units) = 0.5 cm
1 inch (plotter units) = 0.5 cm/μsec

Figure A-6. Snapshot Velocity Vector Plot
at Time = 13.6 μsec

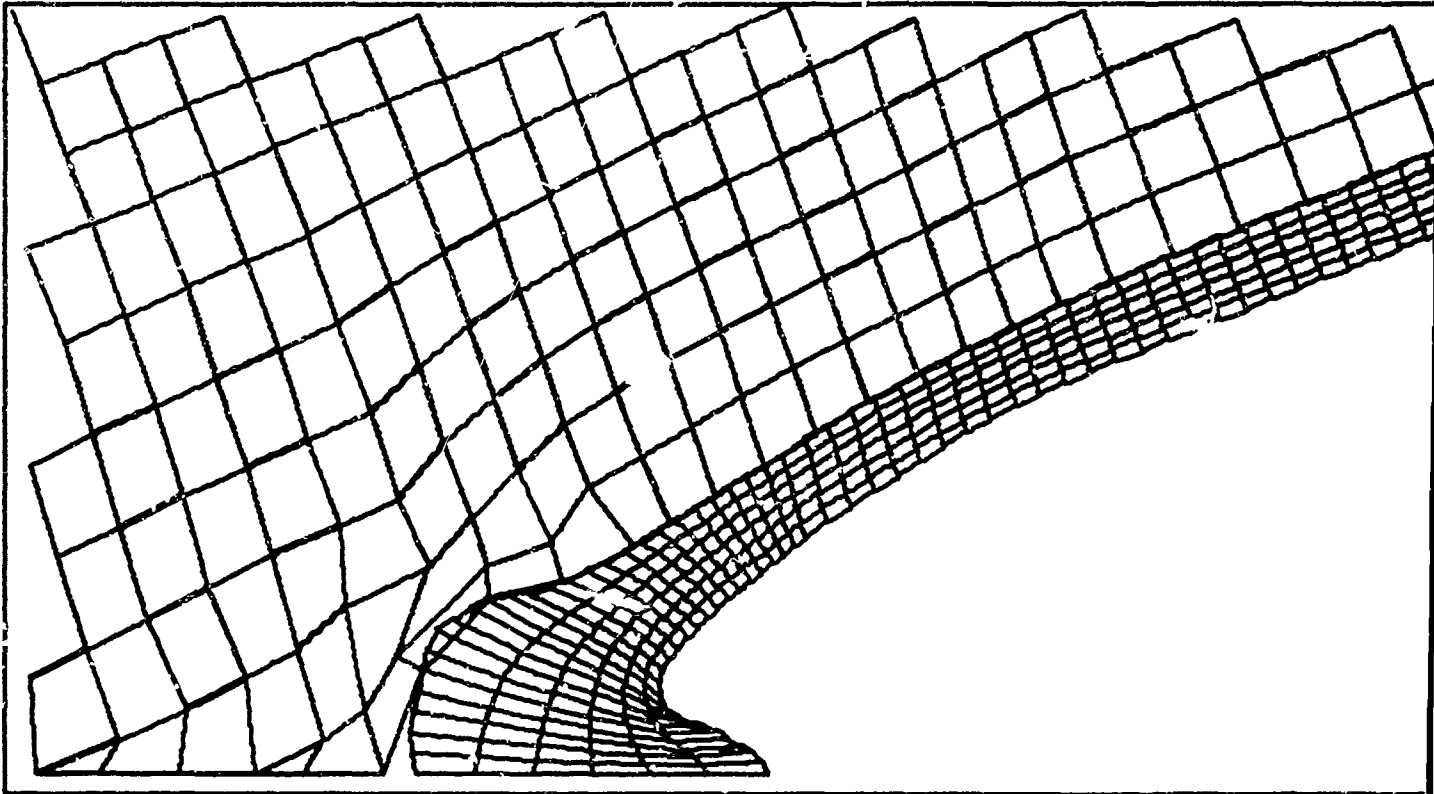


Scale: 1 inch (plotter

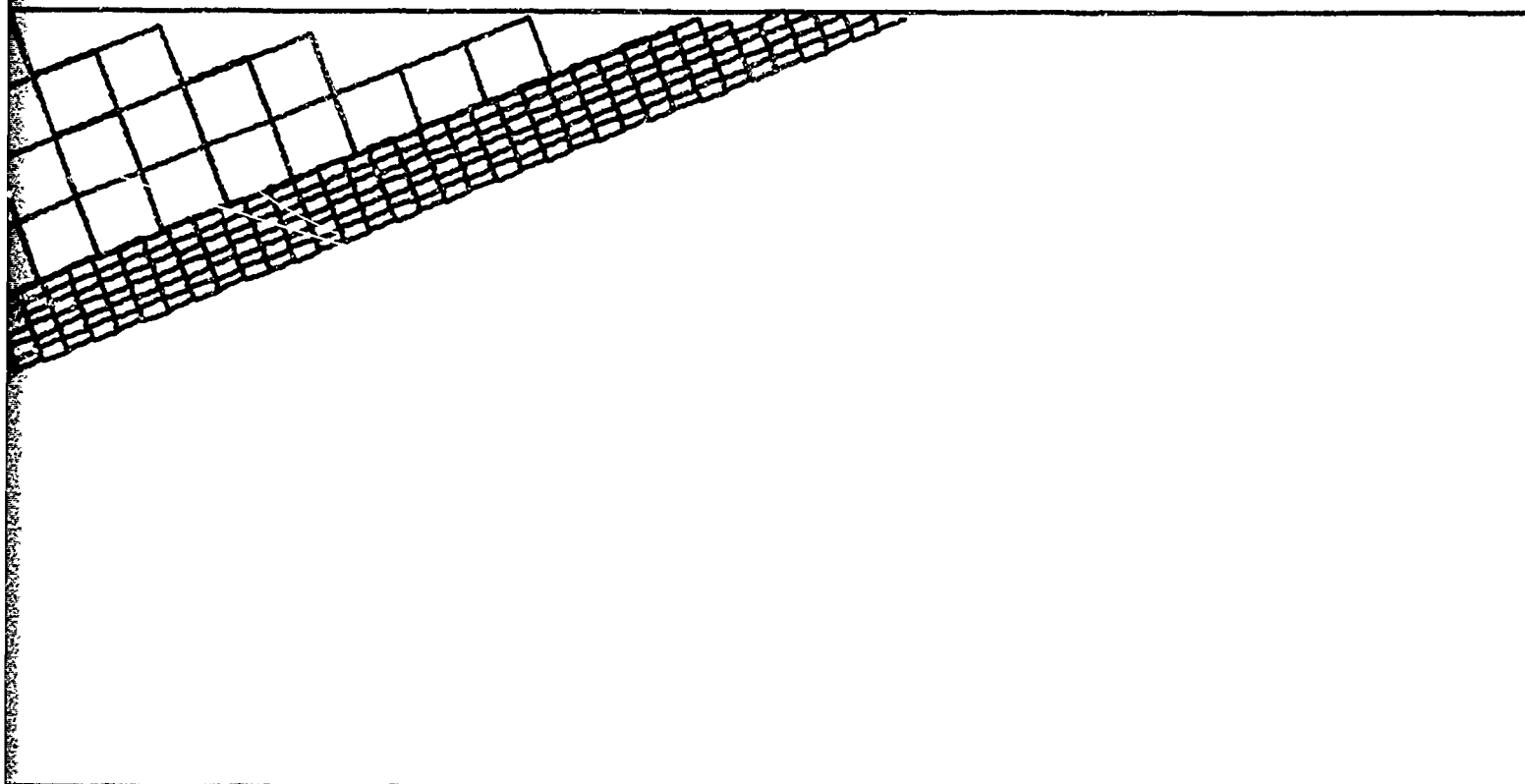


1 inch (plotter units) = 0.5 cm

Figure A-7. Snapshot Velocity Vector Plot
at Time = 8.01 μ sec

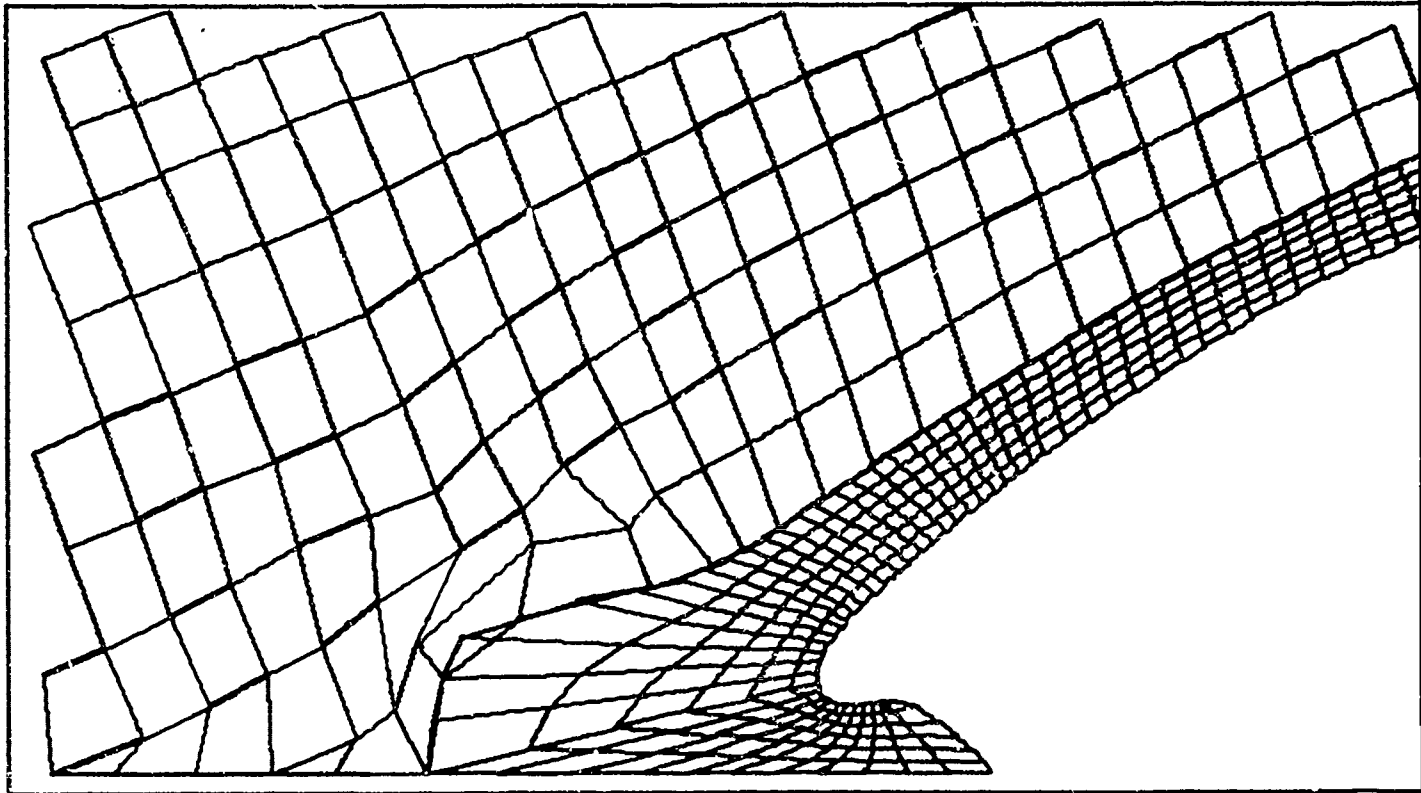


Scale: 1 inch (plotter



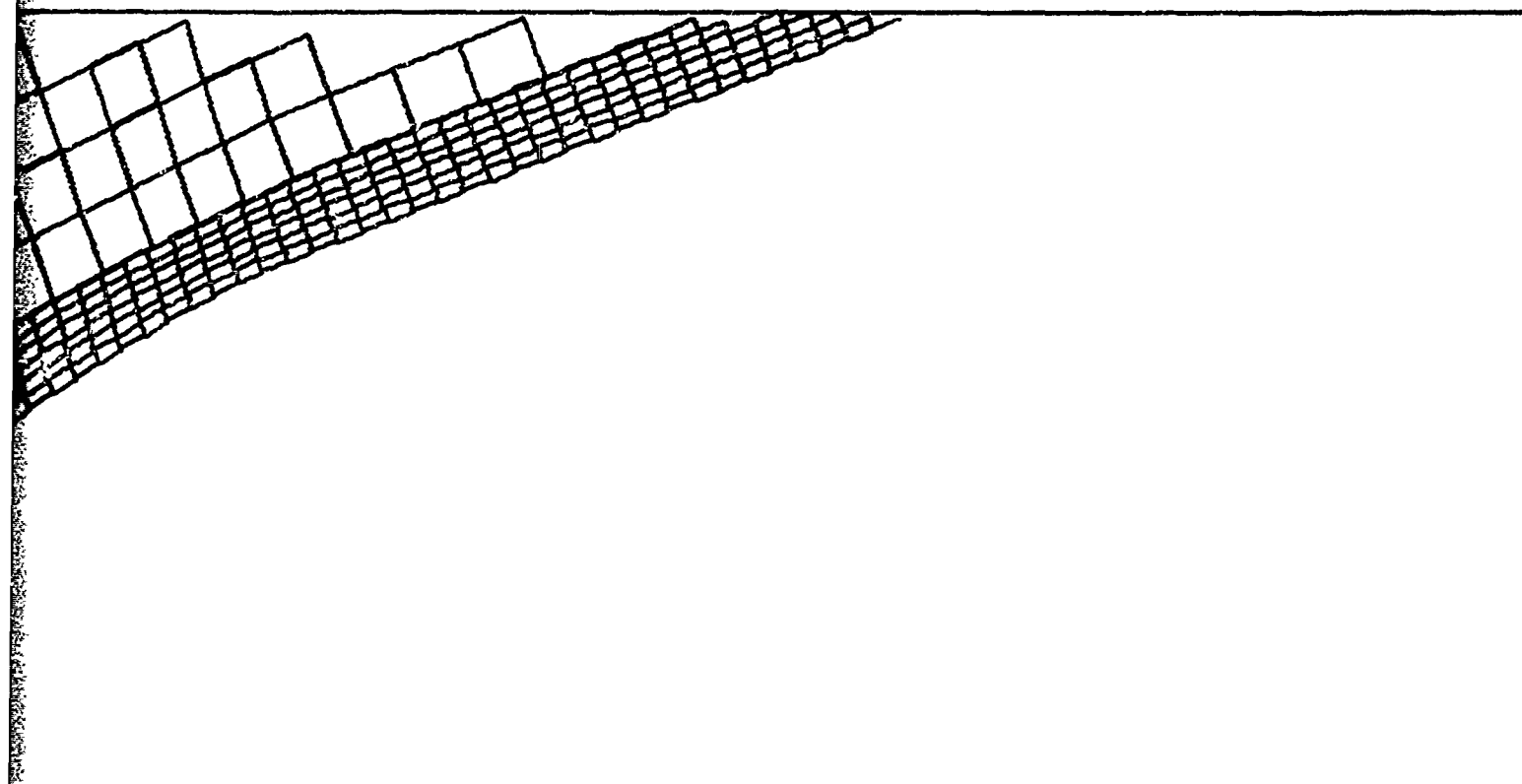
1 inch (plotter units) = 0.5 cm

Figure A-8. Snapshot Velocity Vector Plot
at Time = 9.3 μ sec



Scale: 1 inch (plotted)

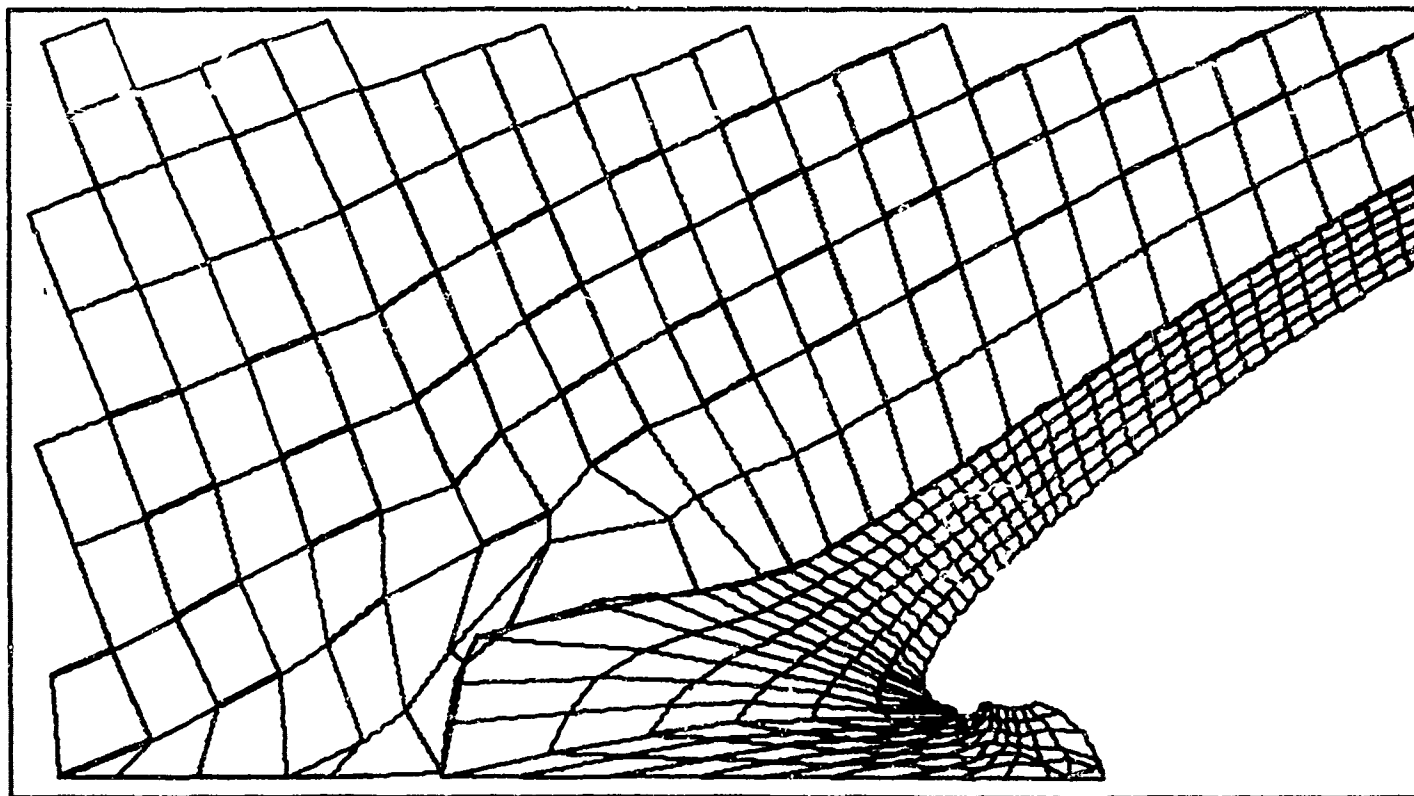
2



e: 1 inch (plotter units) = 0.5 cm

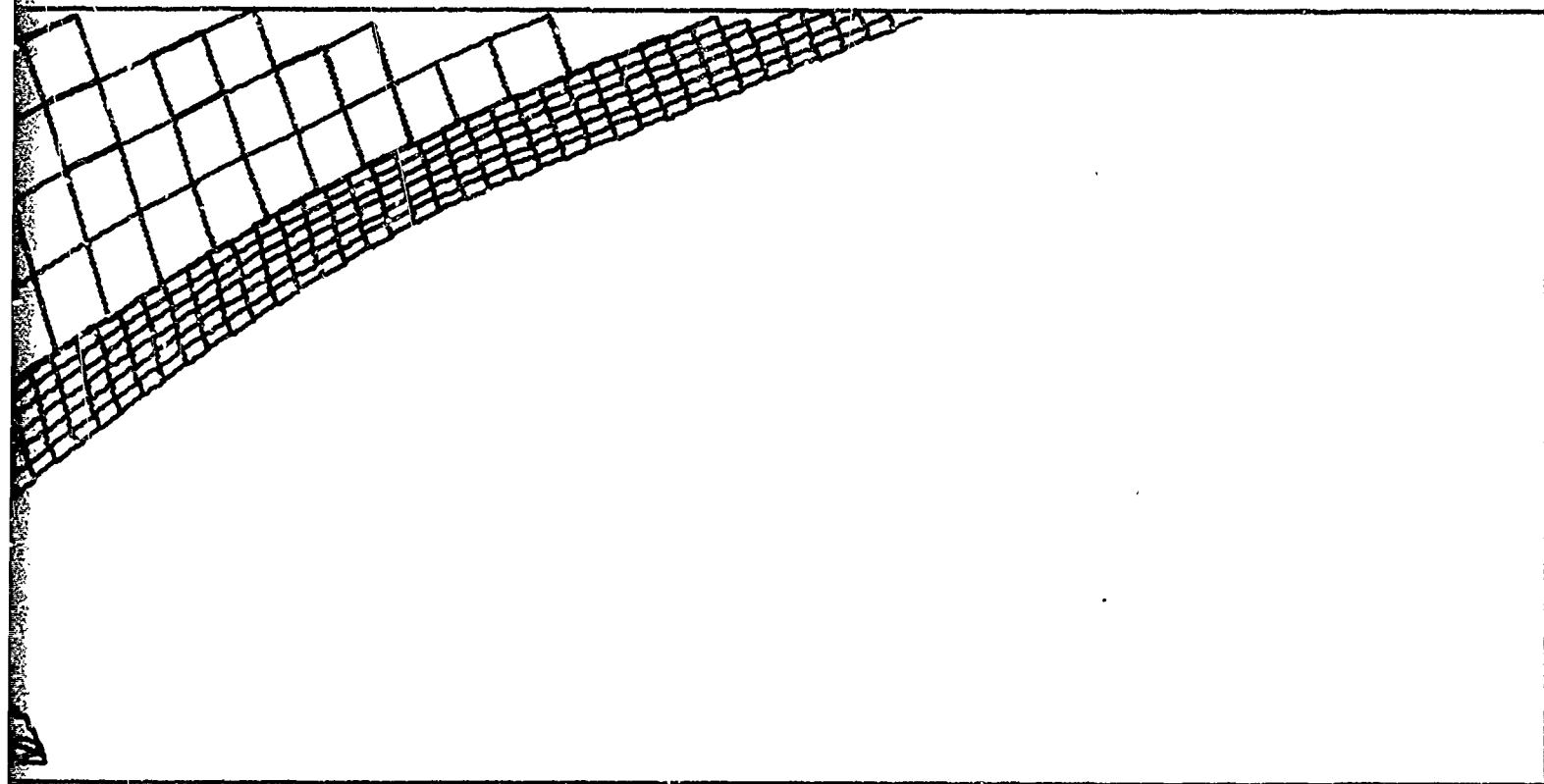
Figure A-9. Snapshot Velocity Vector Plot
at Time = 10.3 μ sec

1



Scale: 1 inch (plotter)

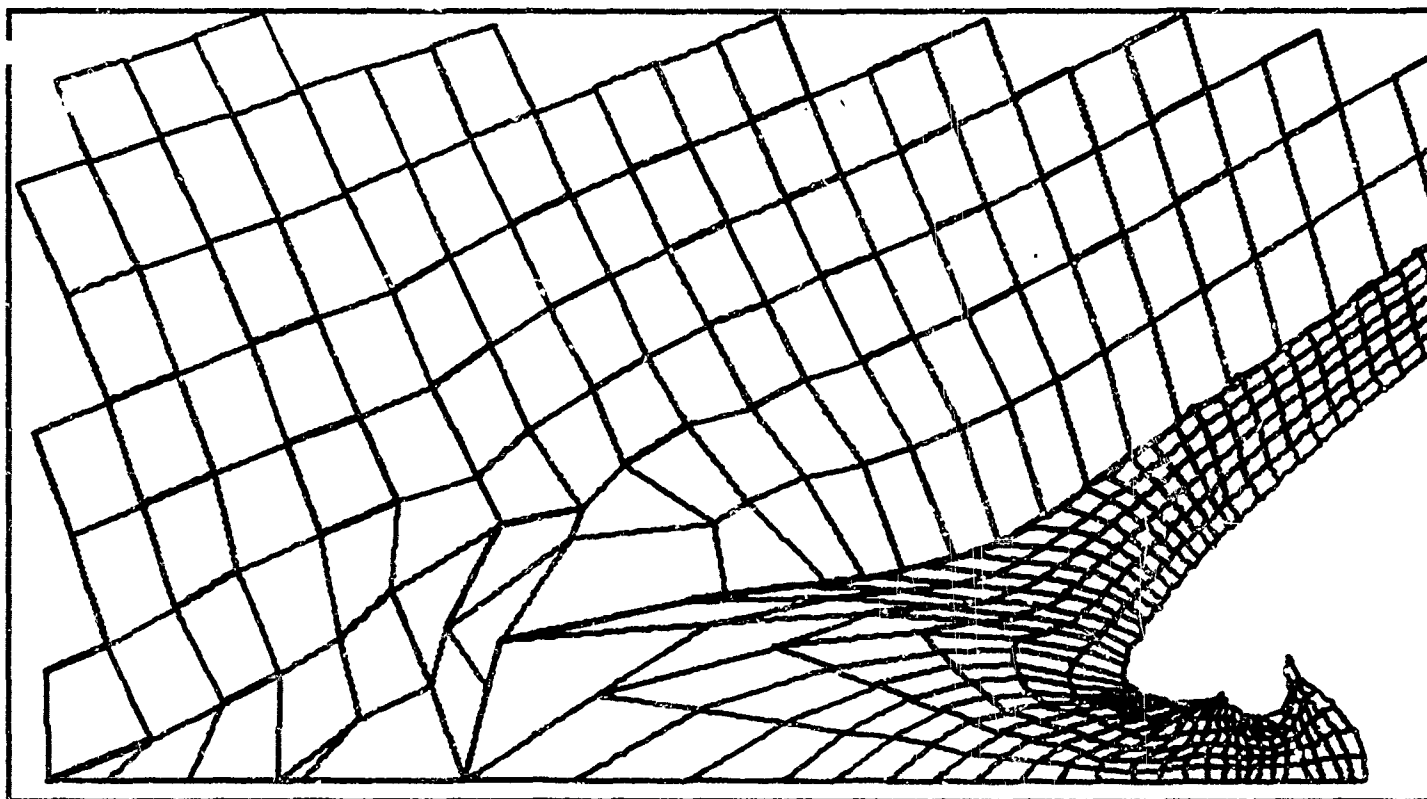
2



1 inch (plotter units) = 0.5 cm

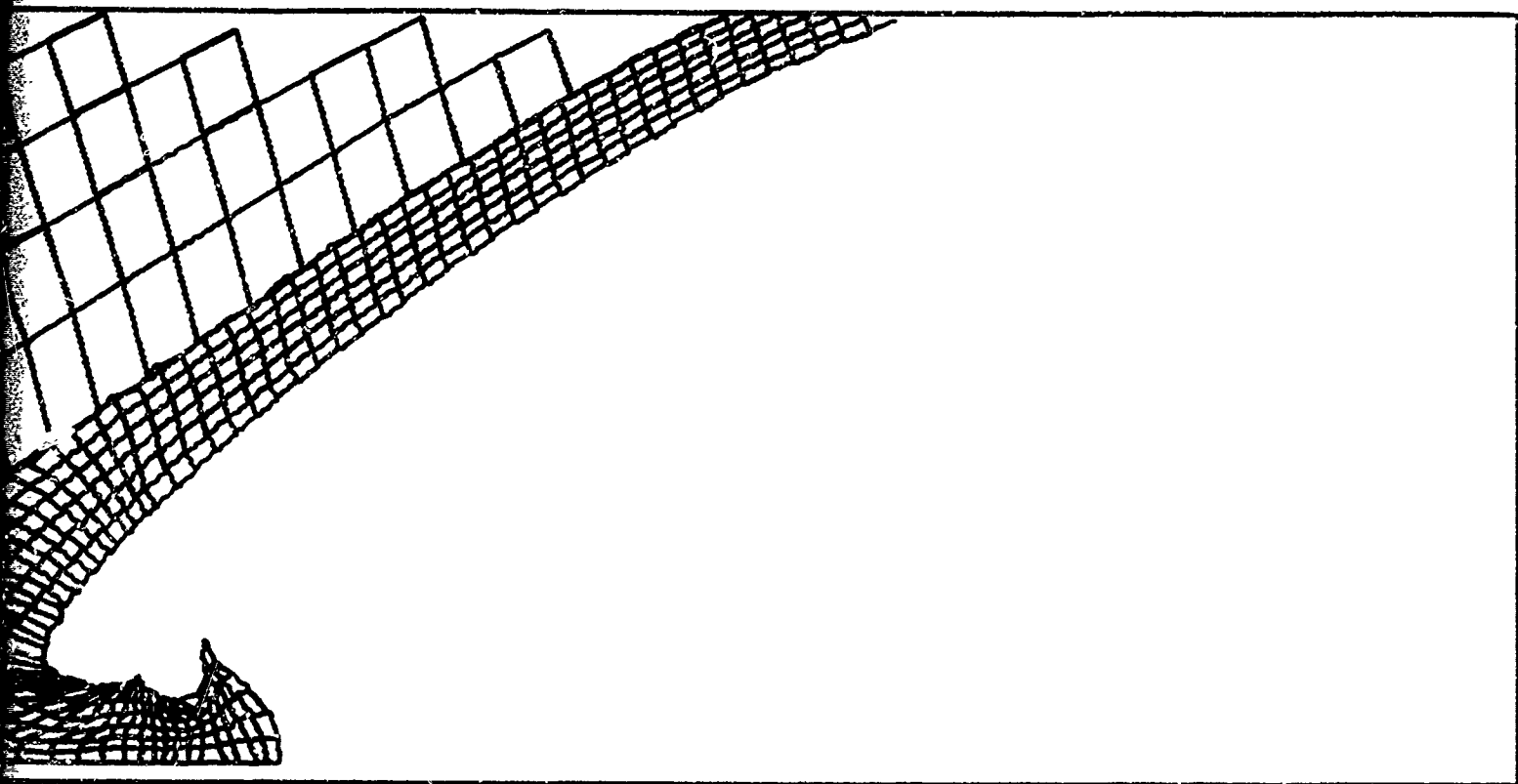
Figure A-10. Snapshot Velocity Vector Plot
at Time = 11.0 μ sec

1



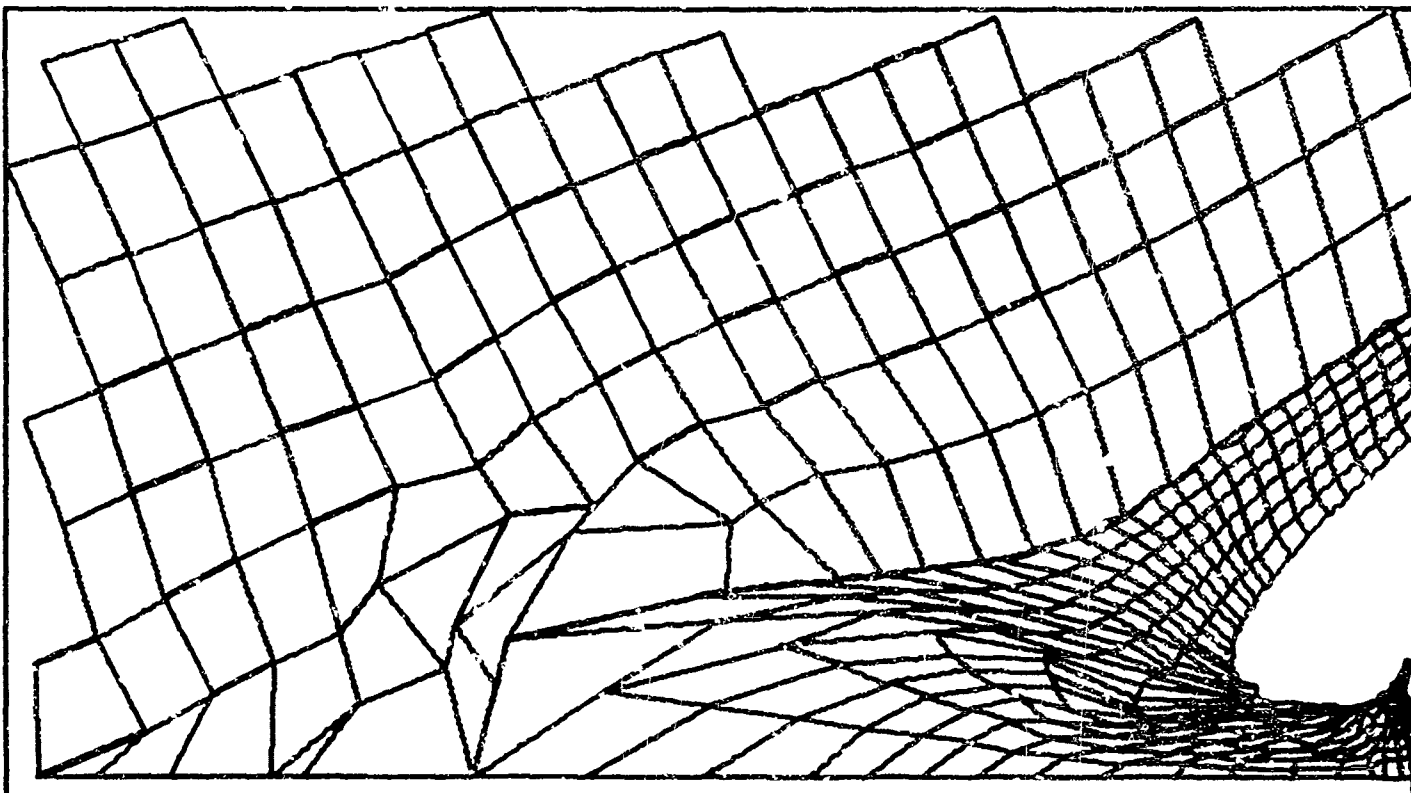
Scale: 1 inch (plotter un

2



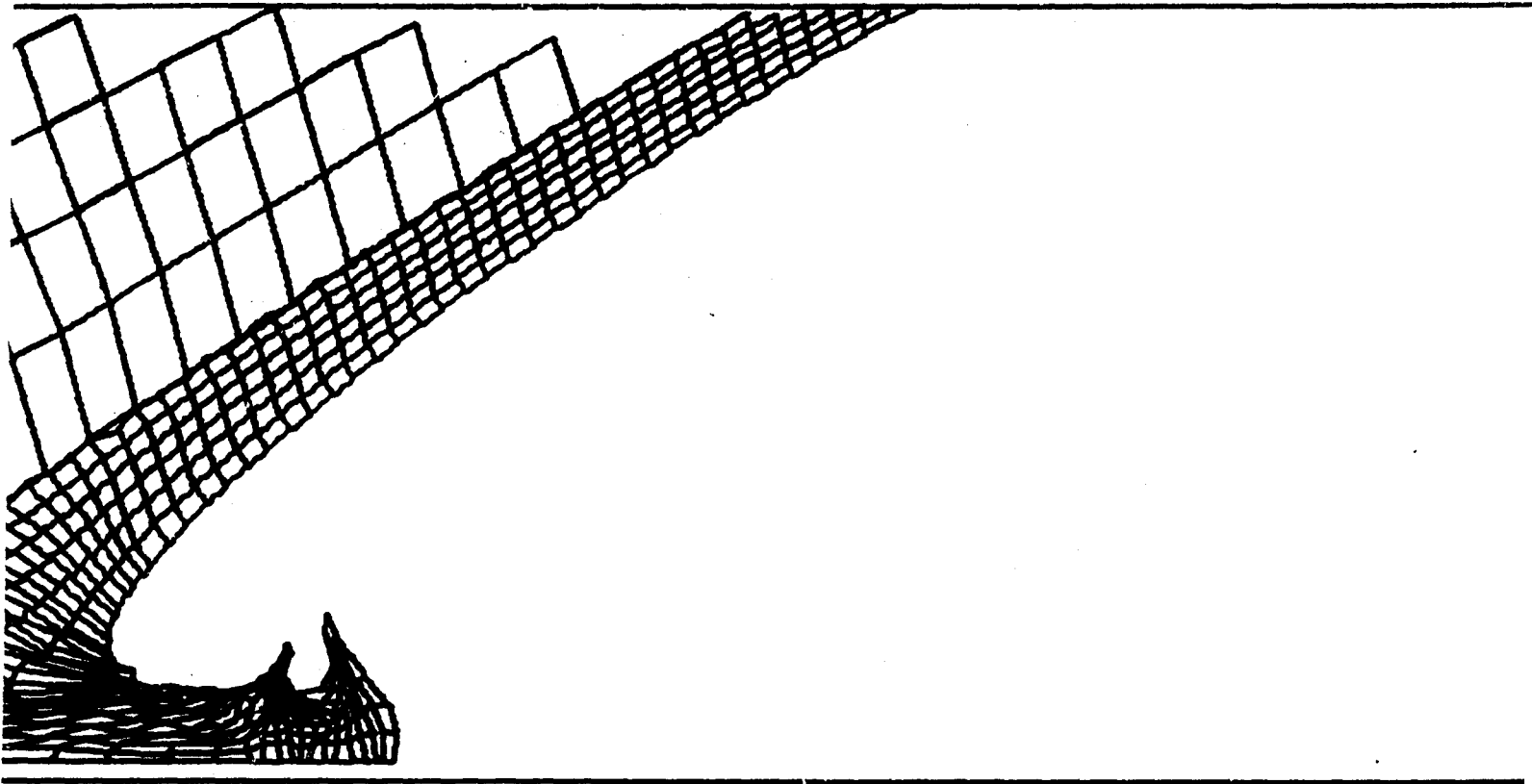
1 inch (plotter units) = 0.5 cm

Figure A-11. Snapshot Velocity Vector Plot
at Time = 12.3 μsec



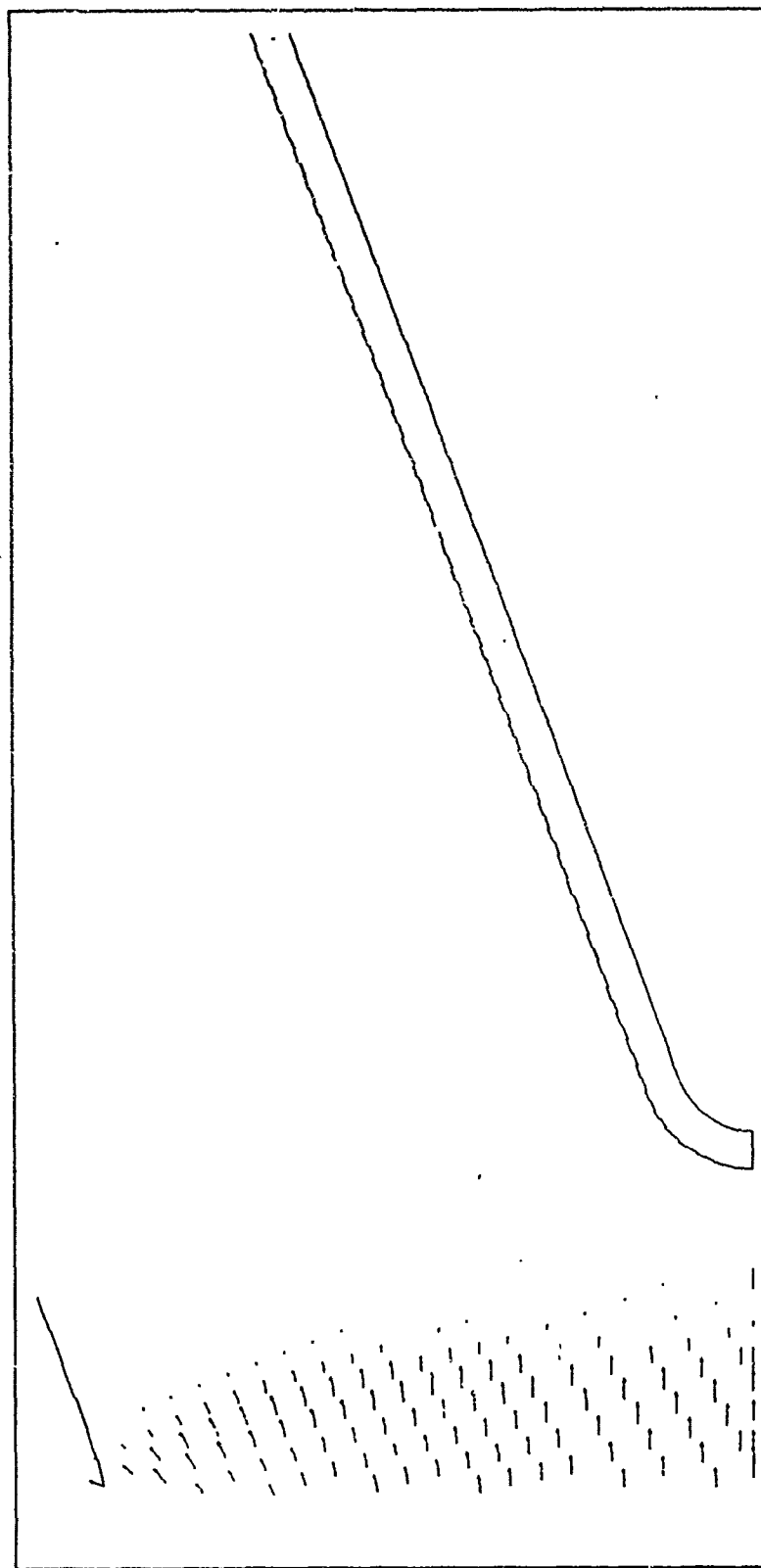
Scale: 1 inch (plotter)

2



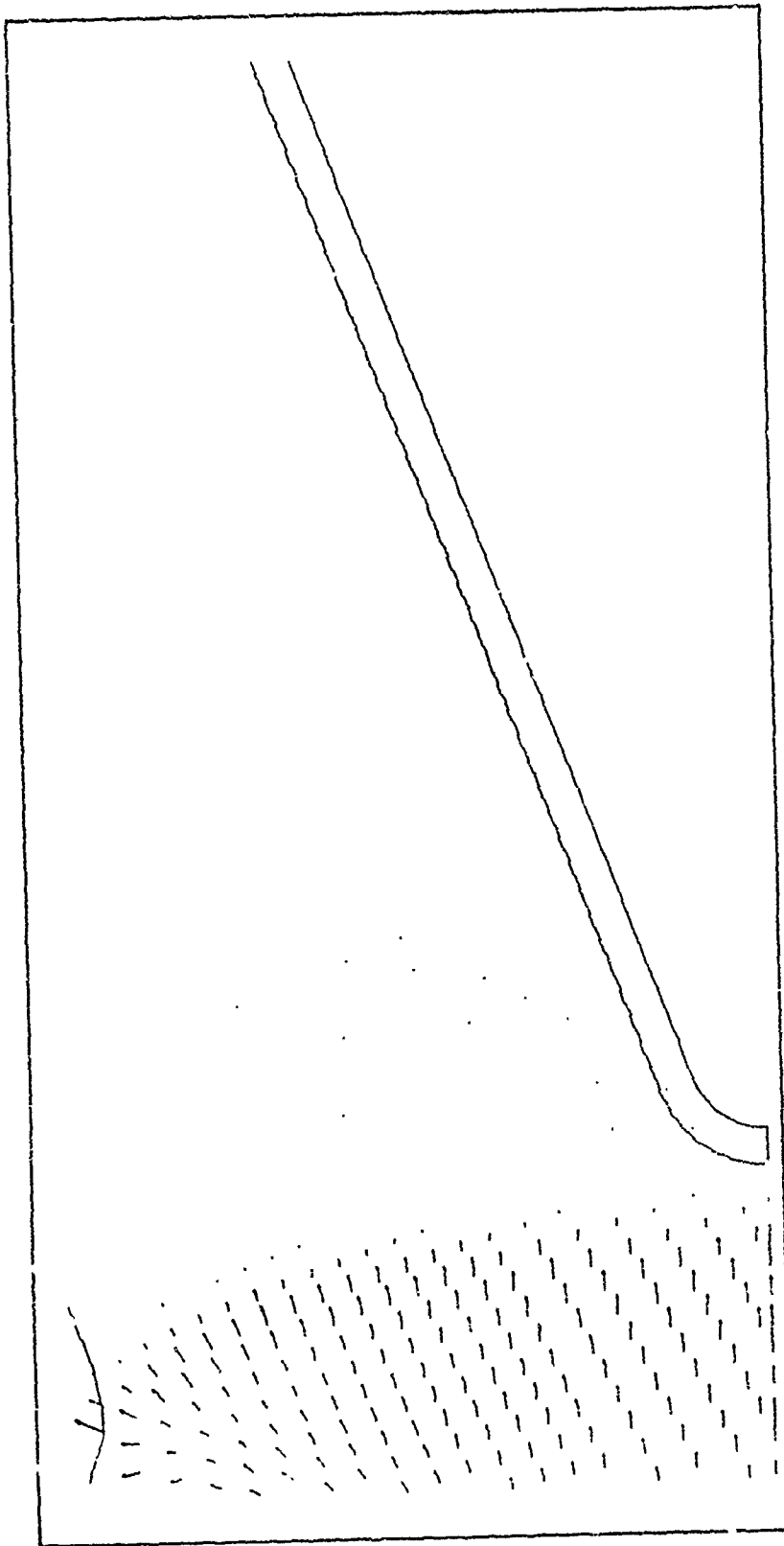
1 inch (plotter units) = 0.5 cm

Figure A-12. Snapshot Velocity Vector Plot
at Time = 13.0 μ sec



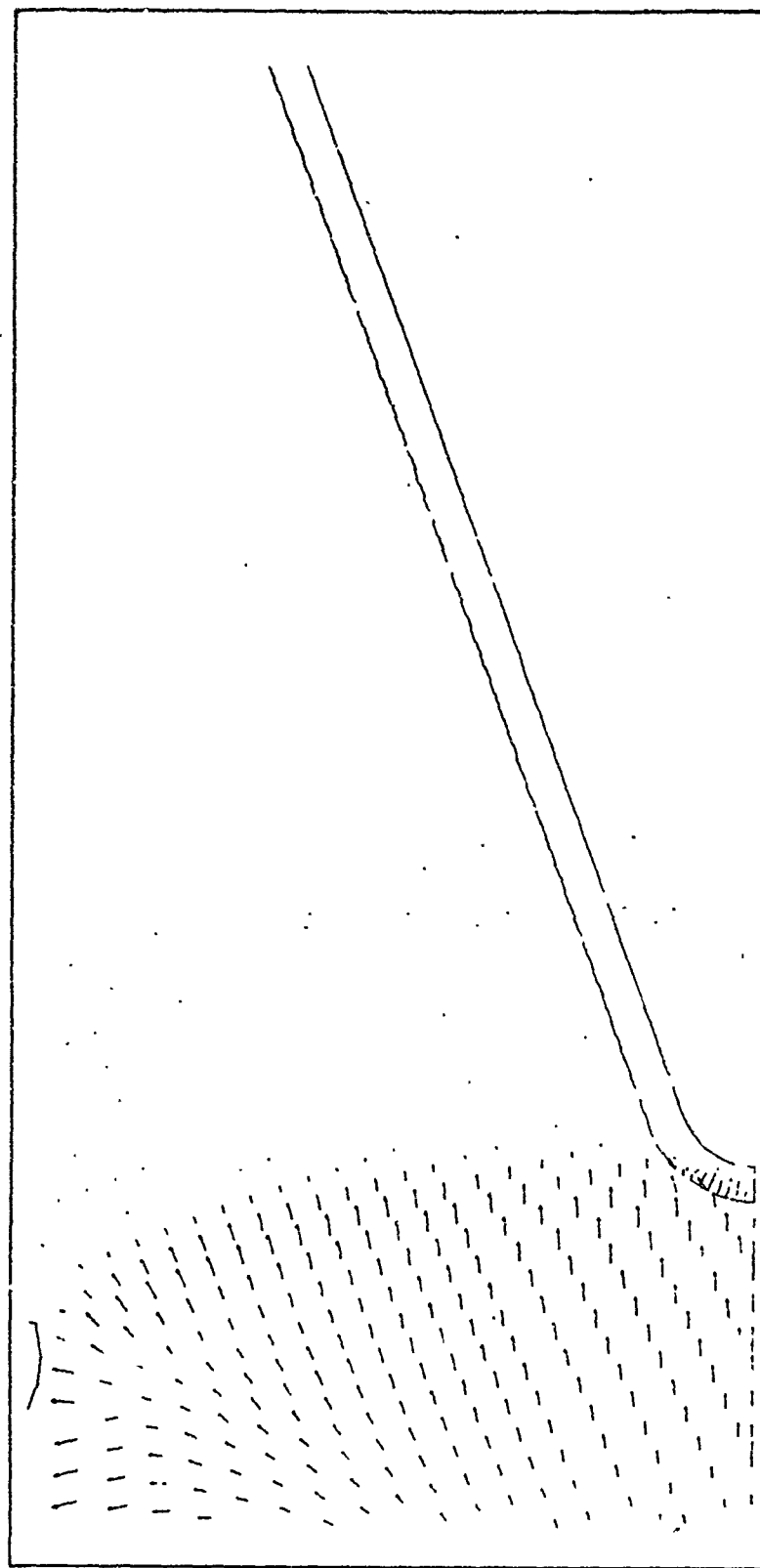
Scale: 1 inch (plotter units) = 0.5 cm
1 inch (plotter units) = 1.0 cm/ μ sec

Figure A-13. Snapshot Velocity Vector Plot at Time = 5.21 μ sec



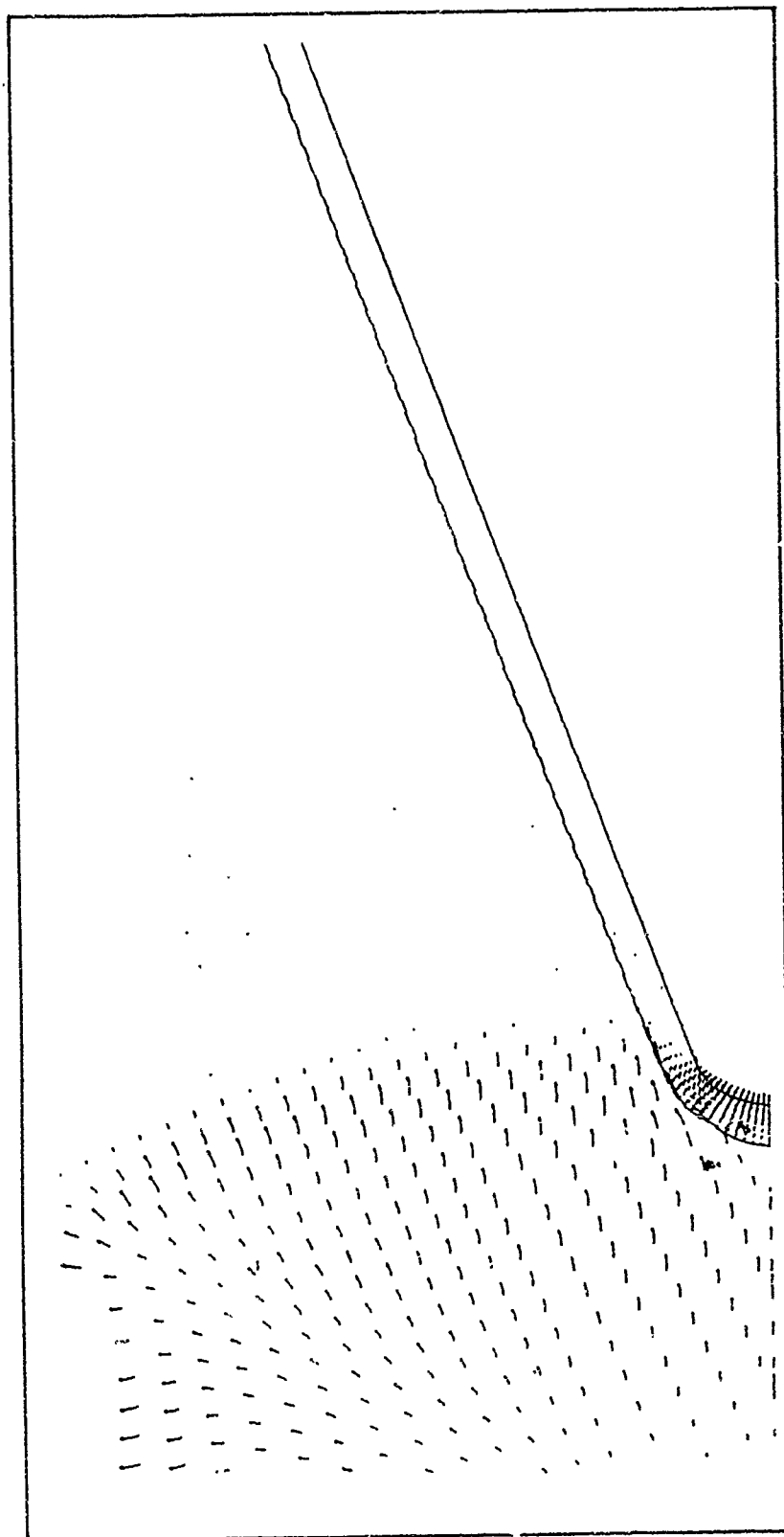
Scale: 1 inch (plotter units) \approx 0.5 cm
 1 inch (plotter units) \approx 1.0 cm/ μ sec

Figure A-14. Snapshot Velocity Vector Plot at Time \approx 5.95 μ sec



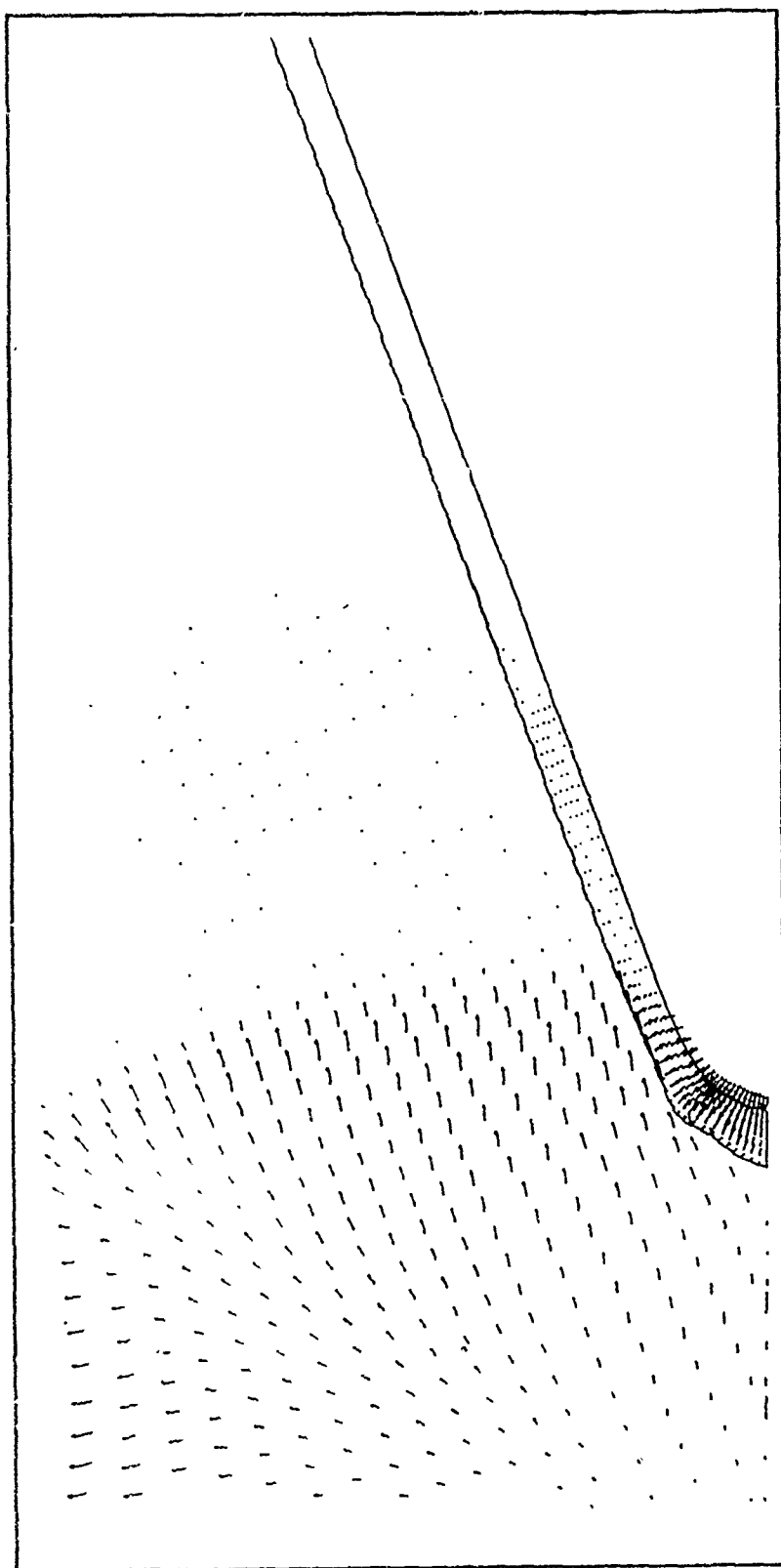
Scale: 1 inch (plotter units) = 0.5 cm
1 inch (plotter units) = 1.0 cm/ μ sec

Figure A-15. Snapshot Velocity Vector Plot at Time = 6.66 μ sec



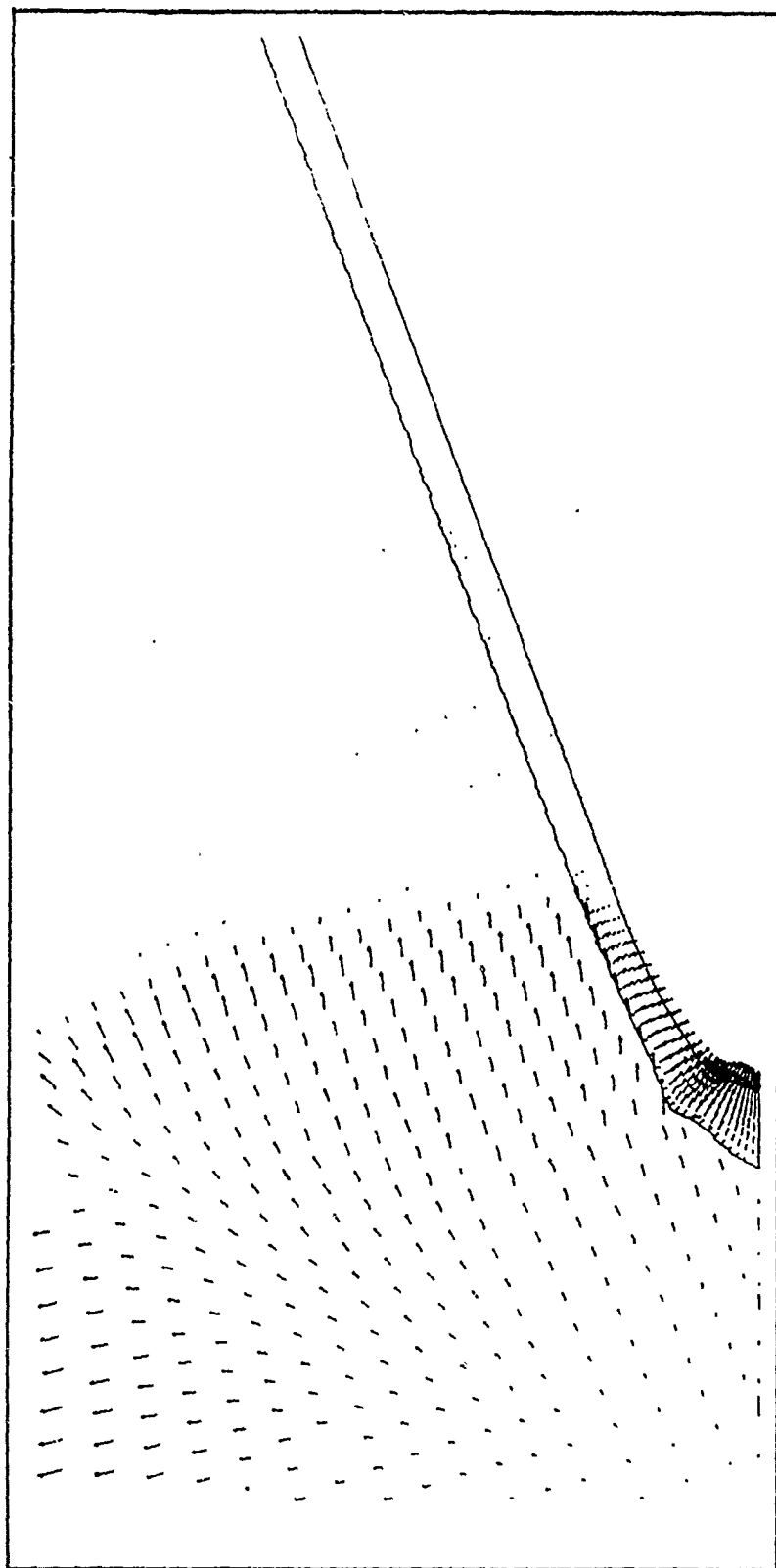
Scale: 1 inch (plotter units) = 0.5 cm
1 inch (plotter units) = 1.0 cm/ μ sec

Figure A-16. Snapshot Velocity Vector Plot at Time = 7.19 μ sec



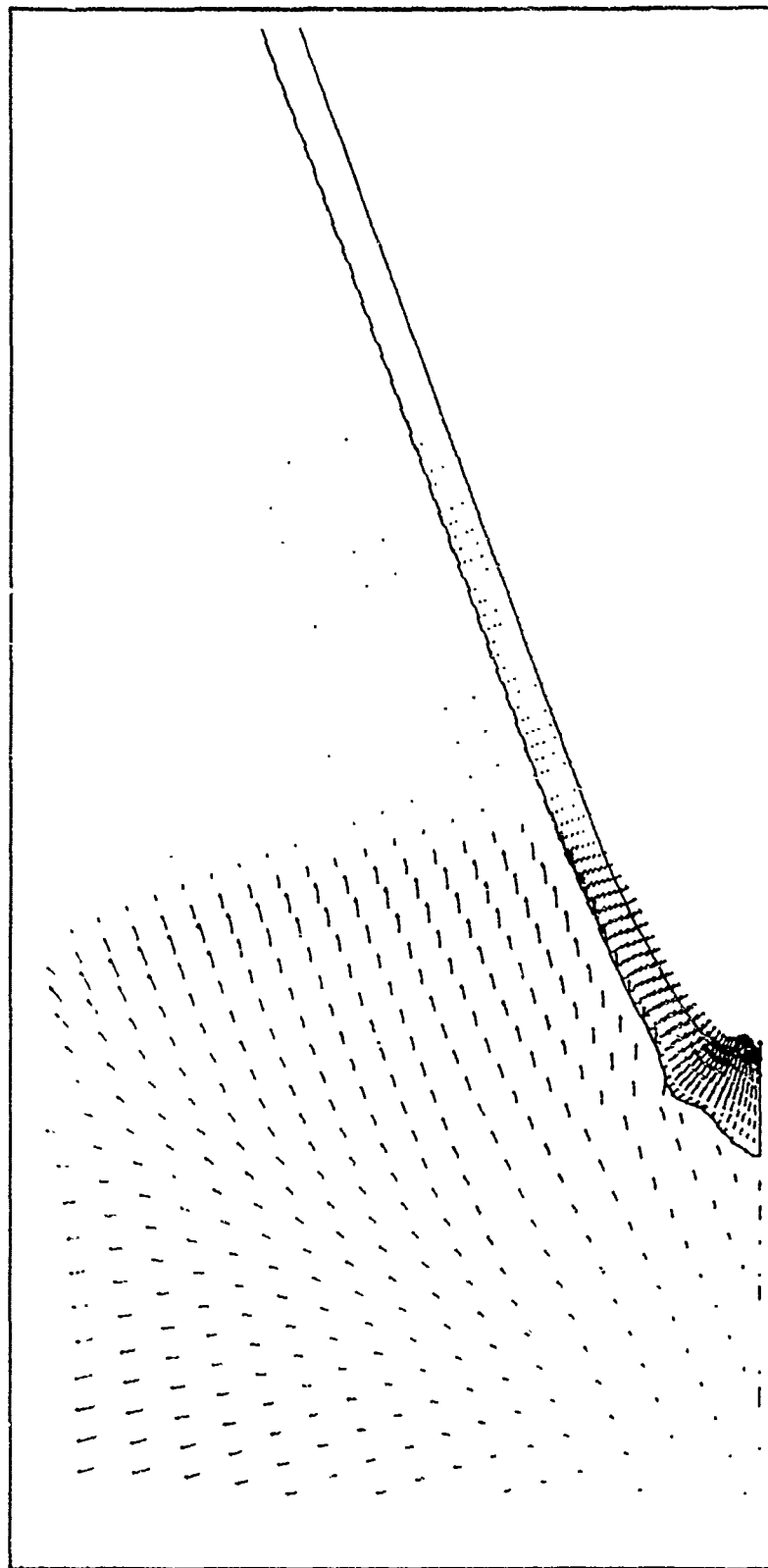
Scale: 1 inch (plotter units) = 0.5 cm
1 inch (plotter units) = 1.0 cm/ μ sec

Figure A-17. Snapshot Velocity Vector Plot at Time = 7.78 μ sec



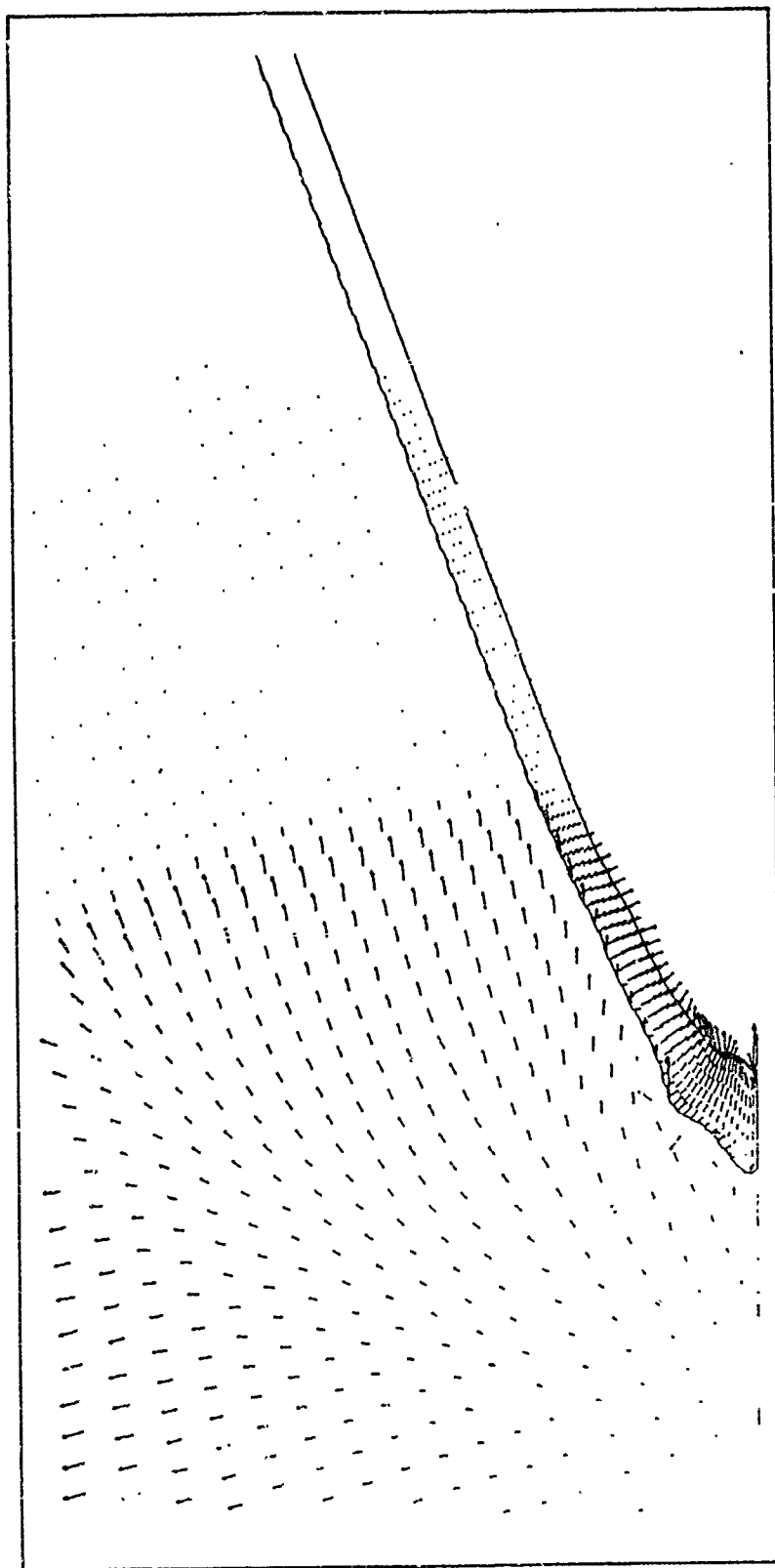
Scale: 1 inch (plotter units) = 0.5 cm
1 inch (plotter units) = 1.0 cm/ μ sec

Figure A-18. Snapshot Velocity Vector Plot at Time = 8.31 μ sec



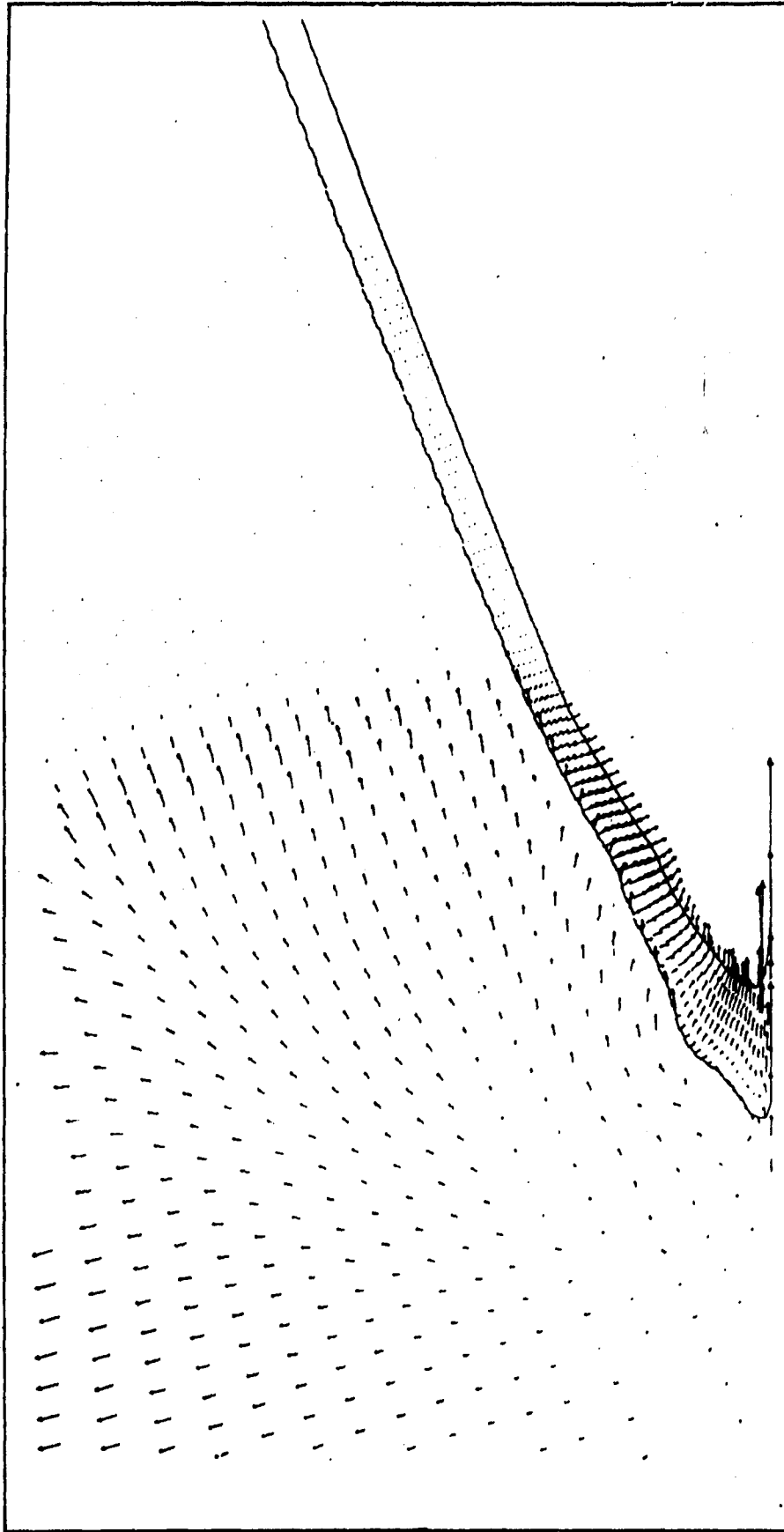
Scale: 1 inch (plotter units) = 0.5 cm
1 inch (plotter units) = 1.0 cm/ μ sec

Figure A-19. Snapshot Velocity Vector Plot at Time = 8.71 μ sec



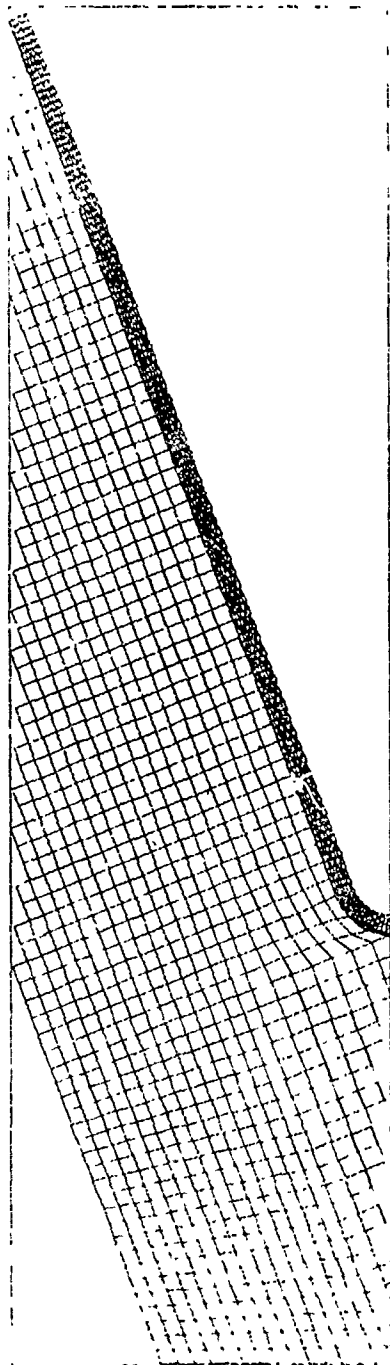
Scale: 1 inch (plotter units) = 0.5 cm
1 inch (plotter units) = 1.0 cm/ μ sec

Figure A-20. Snapshot Velocity Vector Plot at Time = 9.14 μ sec



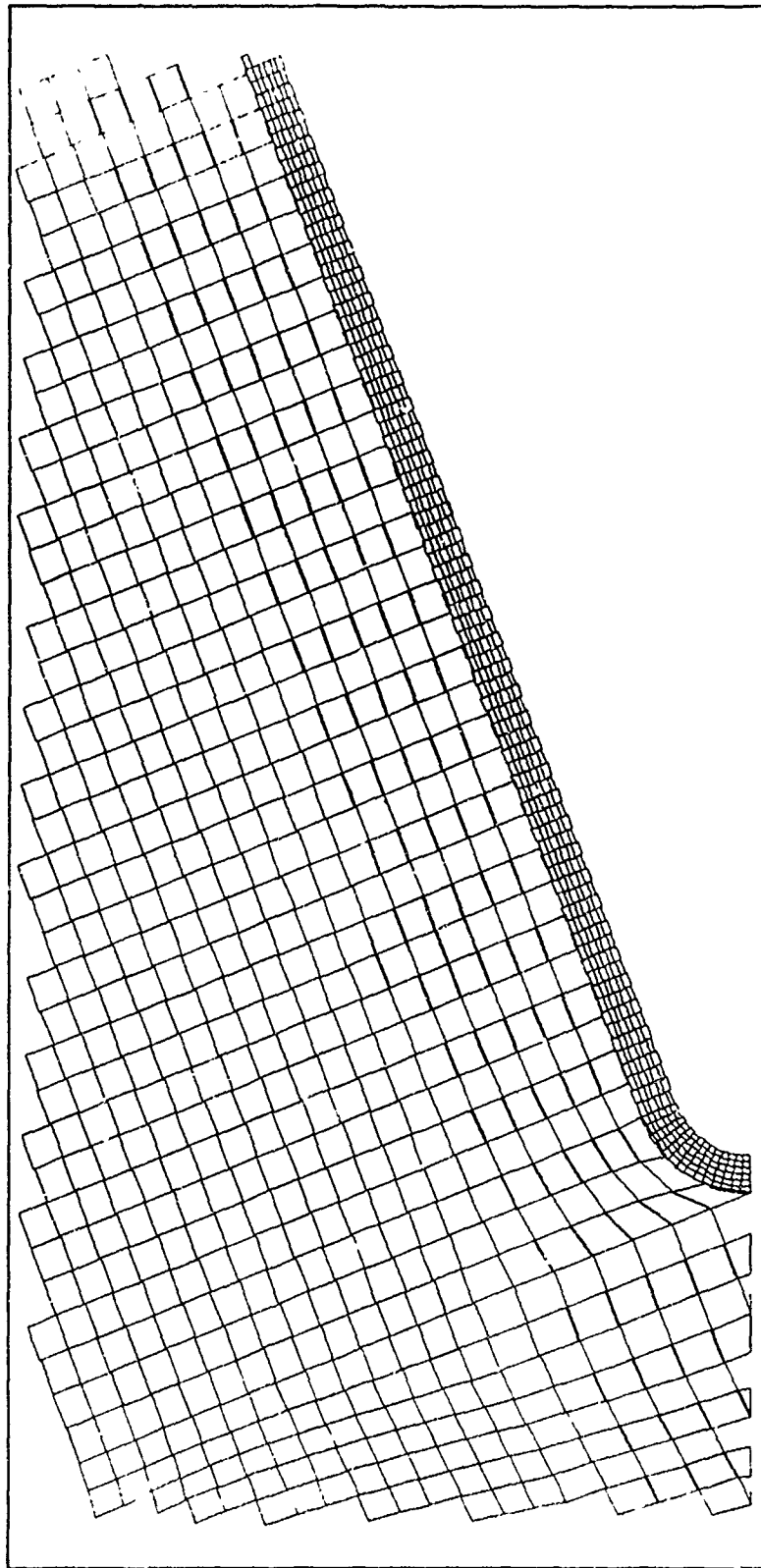
Scale: 1 inch (plotter units) = 0.5 cm
 1 inch (plotter units) = 1.0 cm/ μ sec

Figure A-21. Snapshot Velocity Vector Plot at Time = 9.68 μ sec

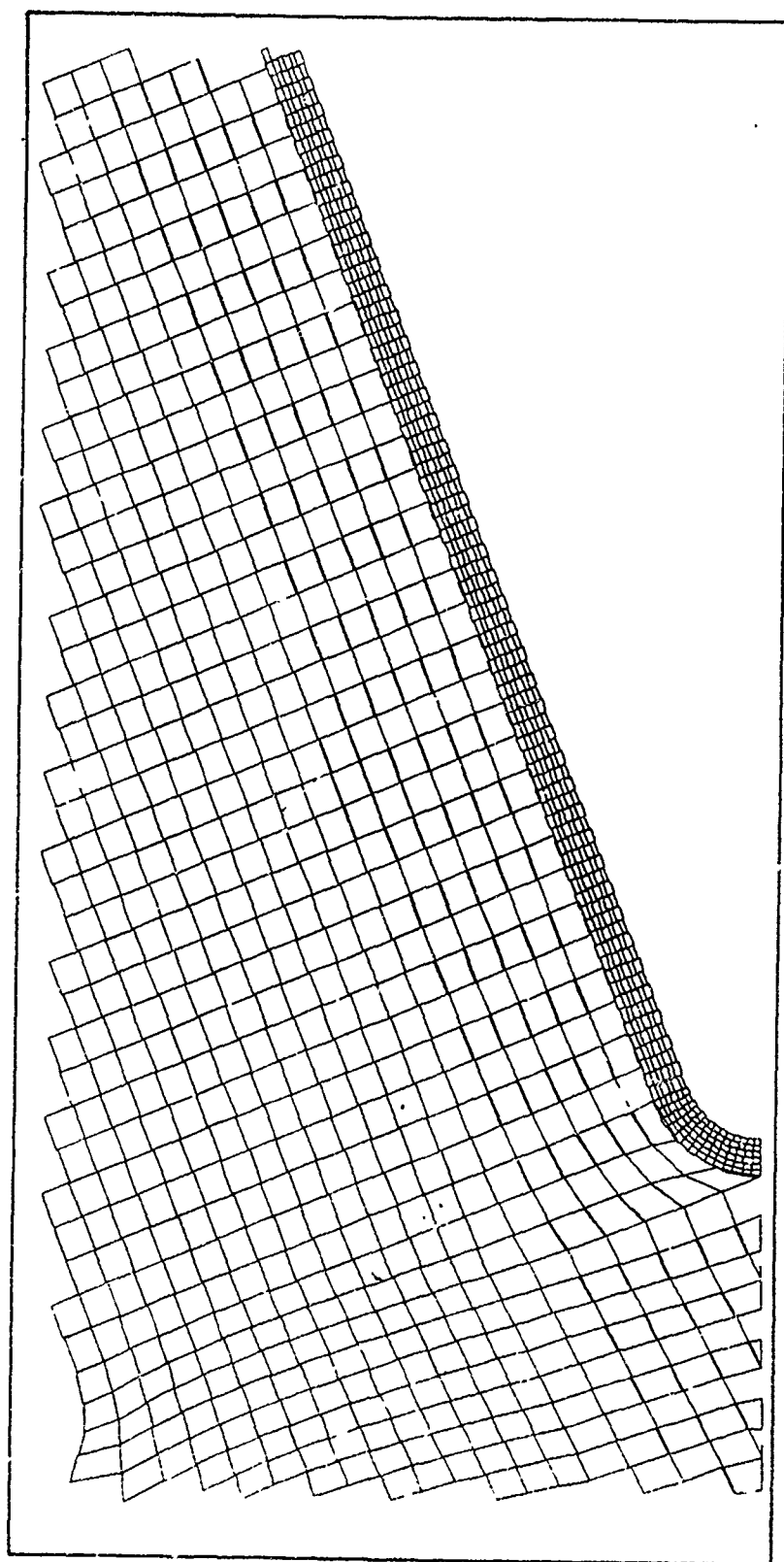


Scale: 1 inch (plotter units) = 1.0 cm

Figure A-22. Snapshot Grid Plot at Time = 0.321 μ sec

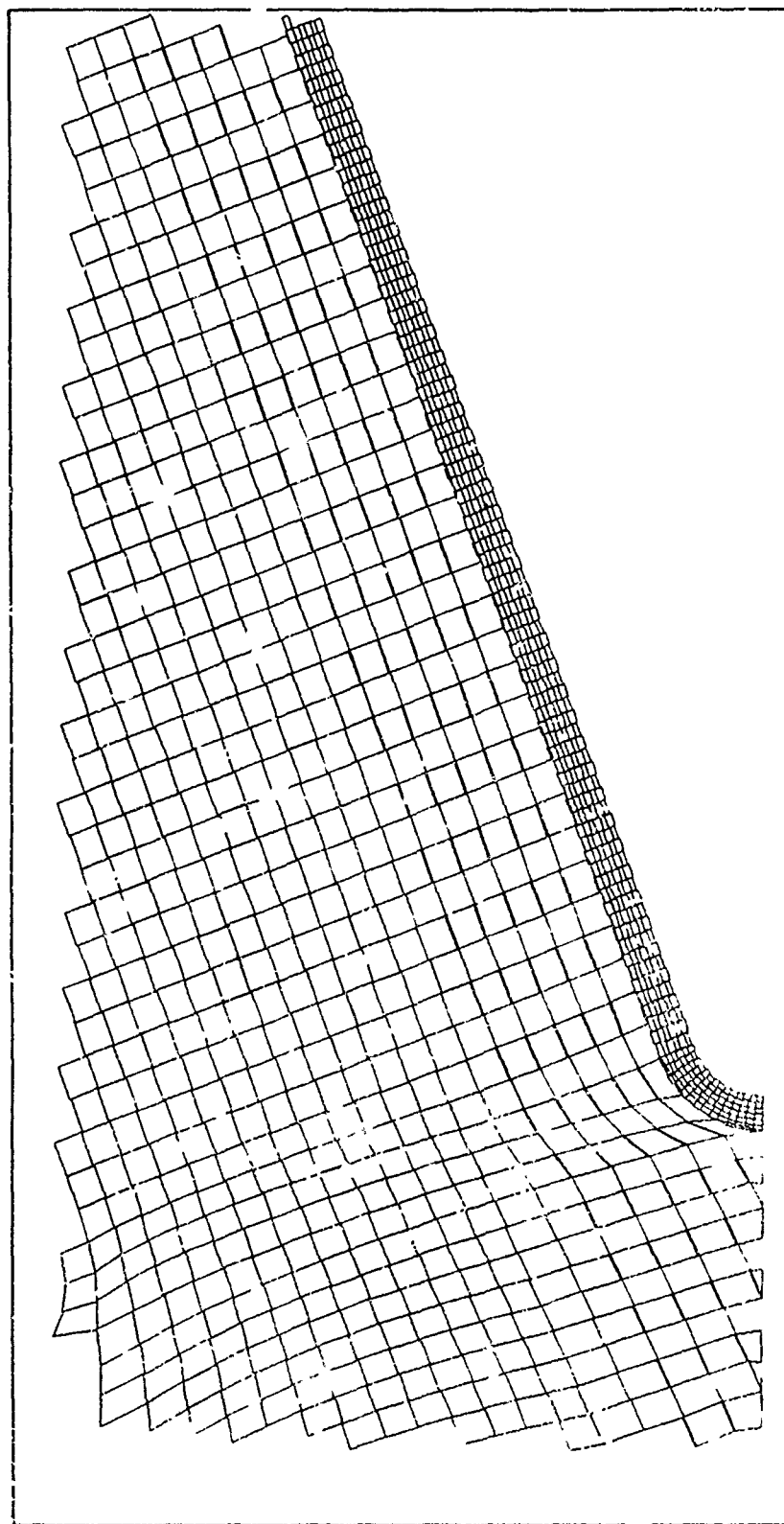


Scale: 1 inch (plotter units) = 0.5 cm



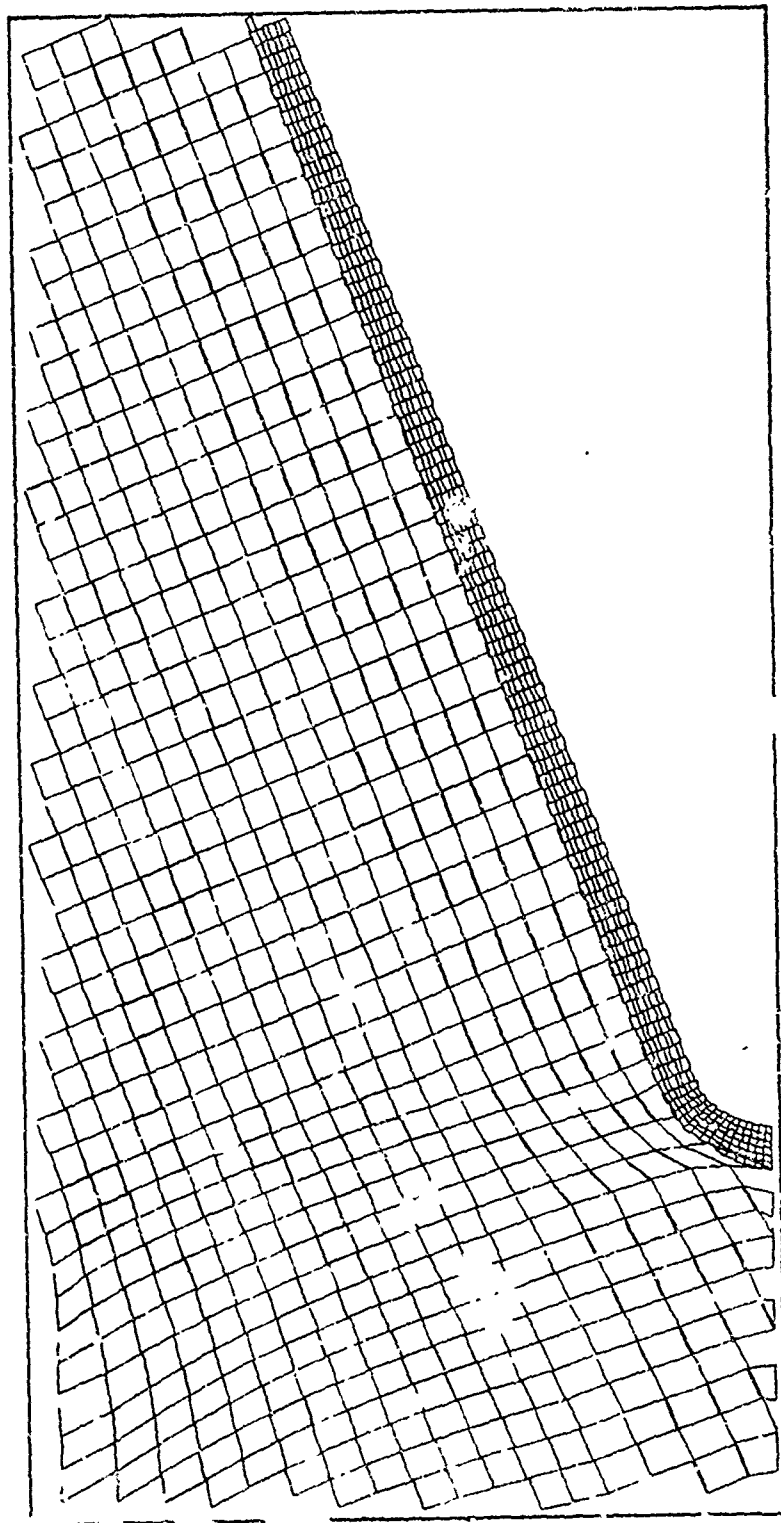
Scale: 1 inch (plotter units) = 0.5 cm

Figure A-24. Snapshot Grid Plot at Time = 5.95 μ sec



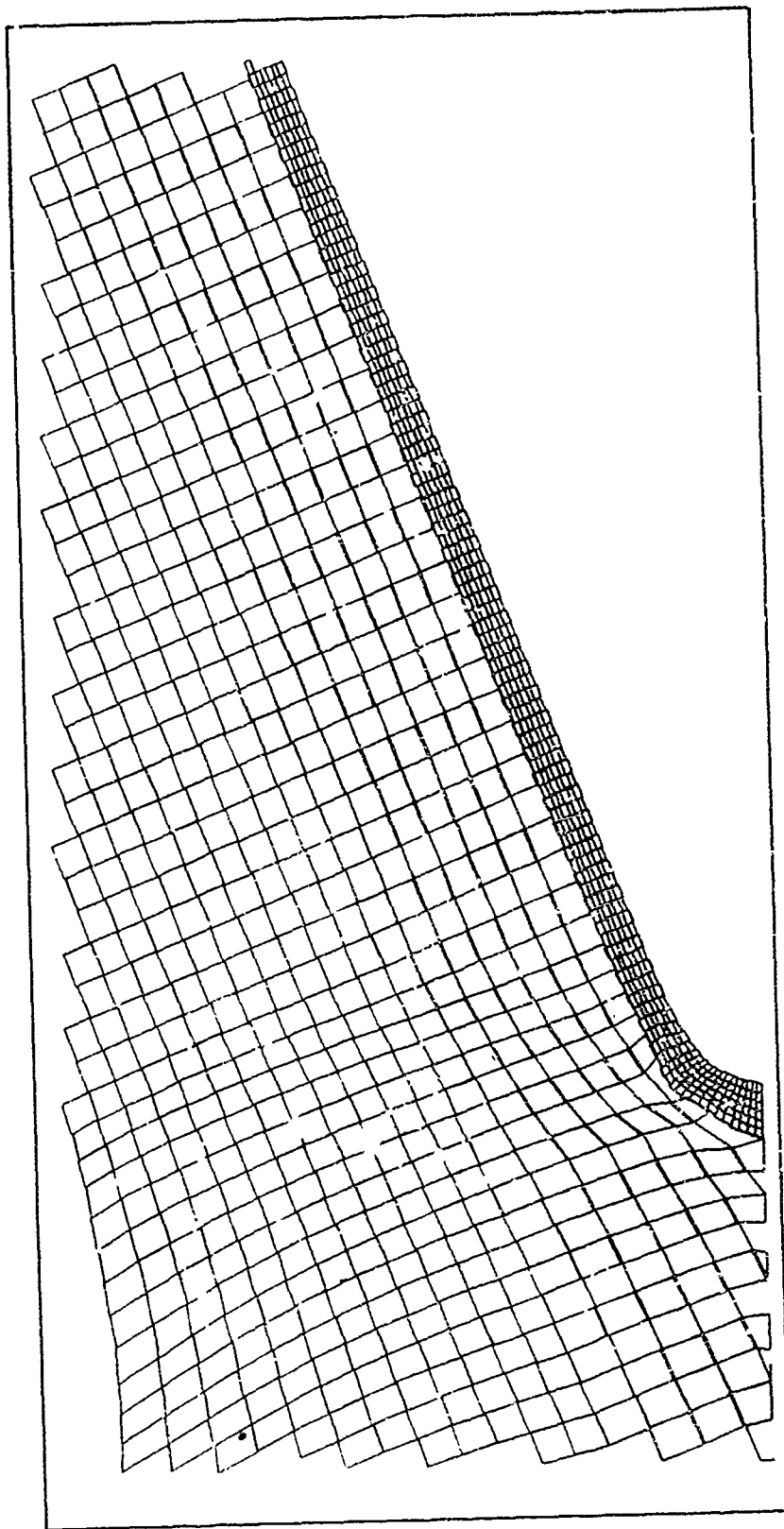
Scale: 1 inch (plotter units) = 0.5 cm

Figure 4. Snapshot Grid Plot at Time = 6.66 μ sec



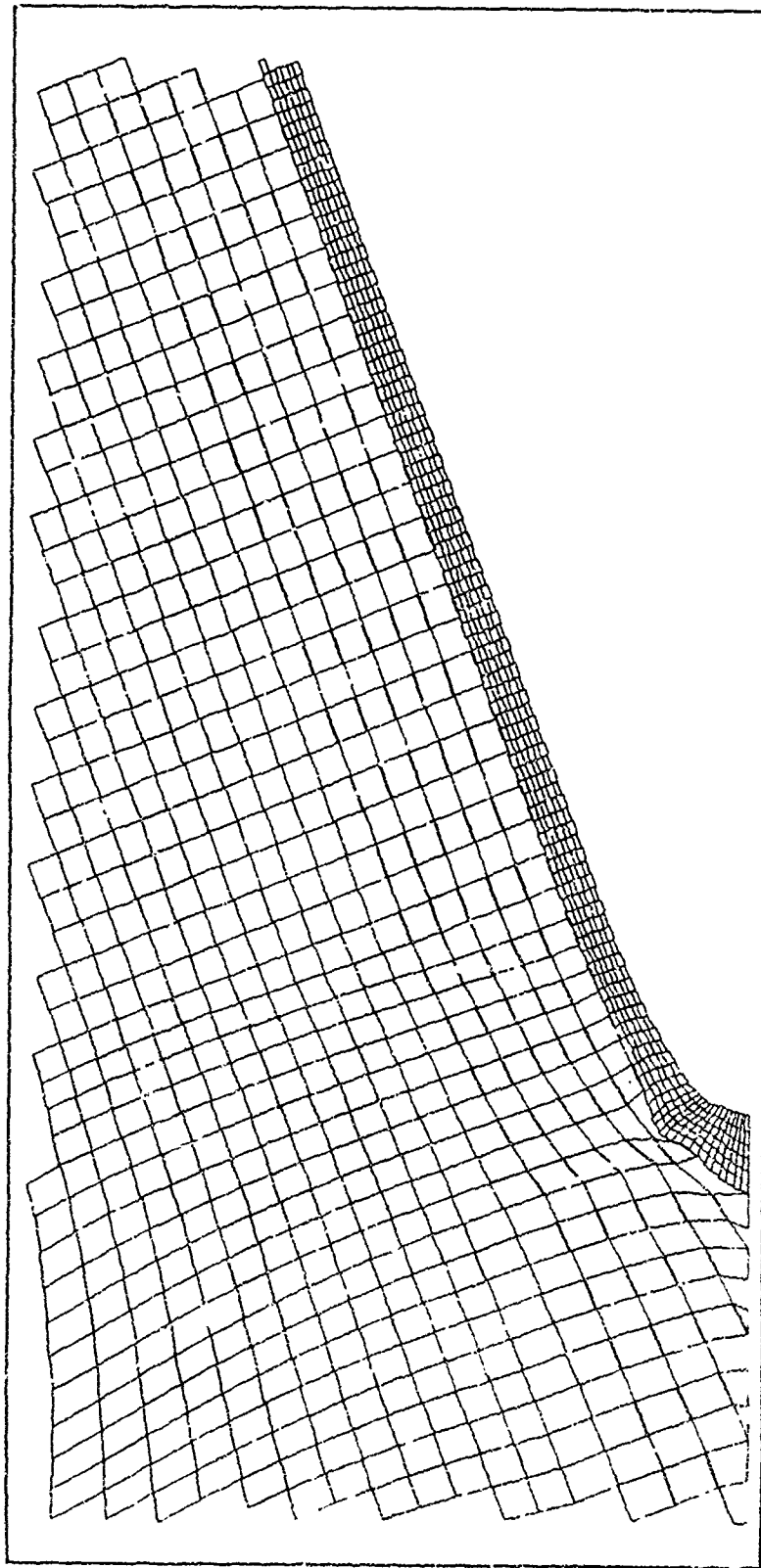
Scale: 1 inch (plotter units) = 0.5 cm

Figure A-26. Snapshot Grid Plot at Time = 7.19 μ sec



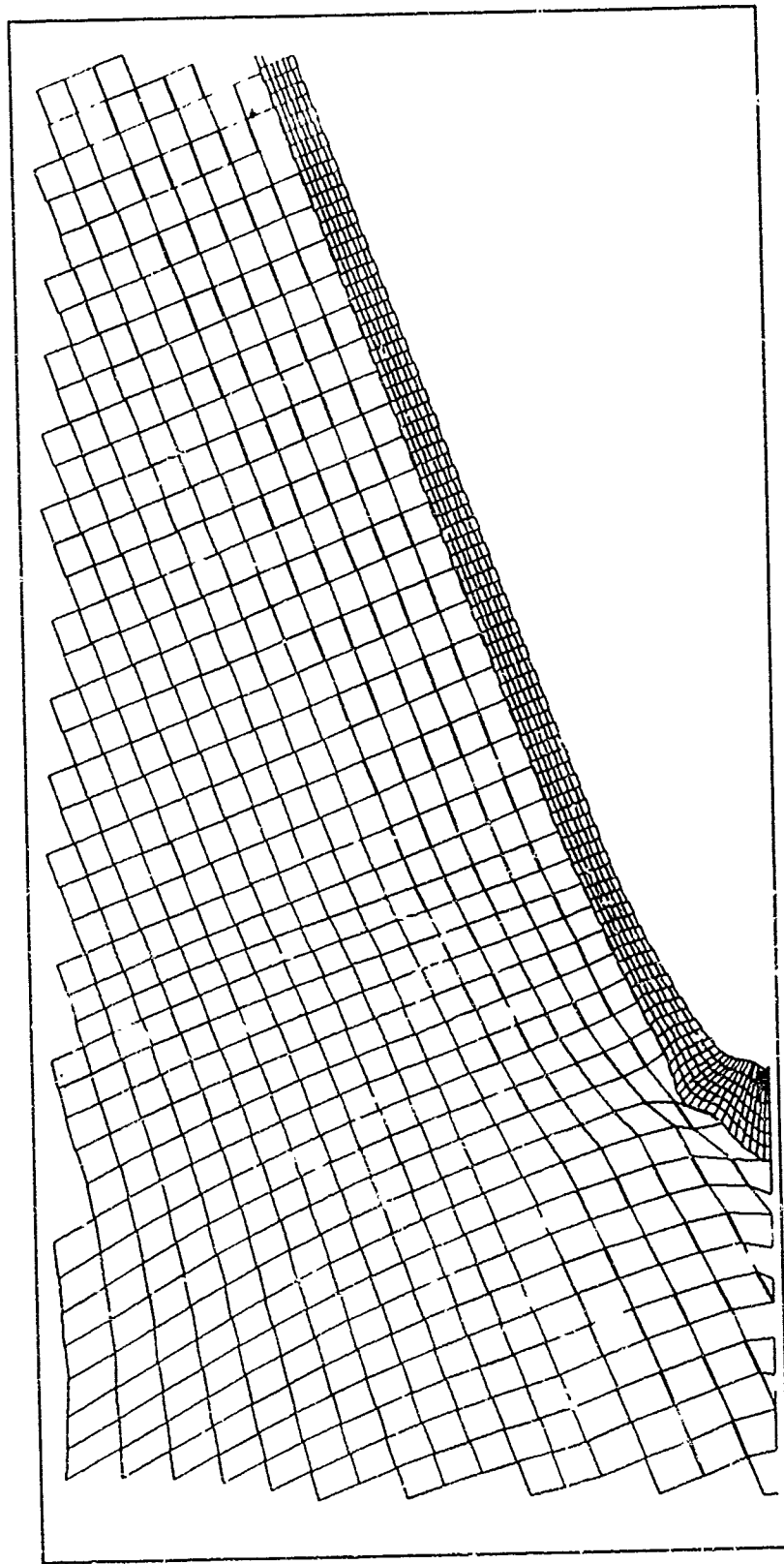
Scale: 1 inch (plotter units) = 0.5 cm

Figure A-27. Snapshot Grid Plot at Time = 7.78 μ sec



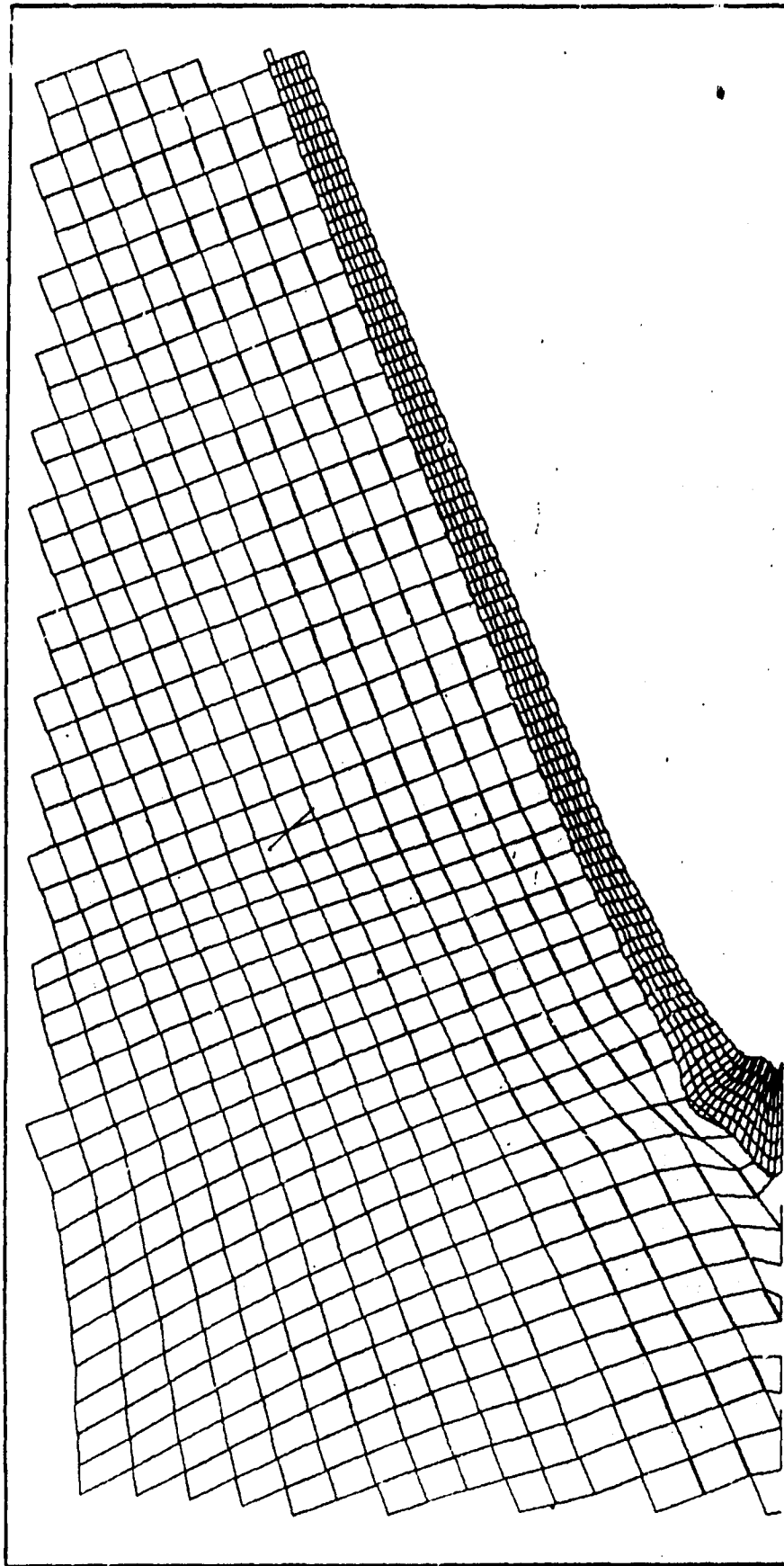
Scale: 1 inch (plotted units) = 0.5 cm

Figure A-28. Snapshot Grid Plot at Time = 8.31 μ sec



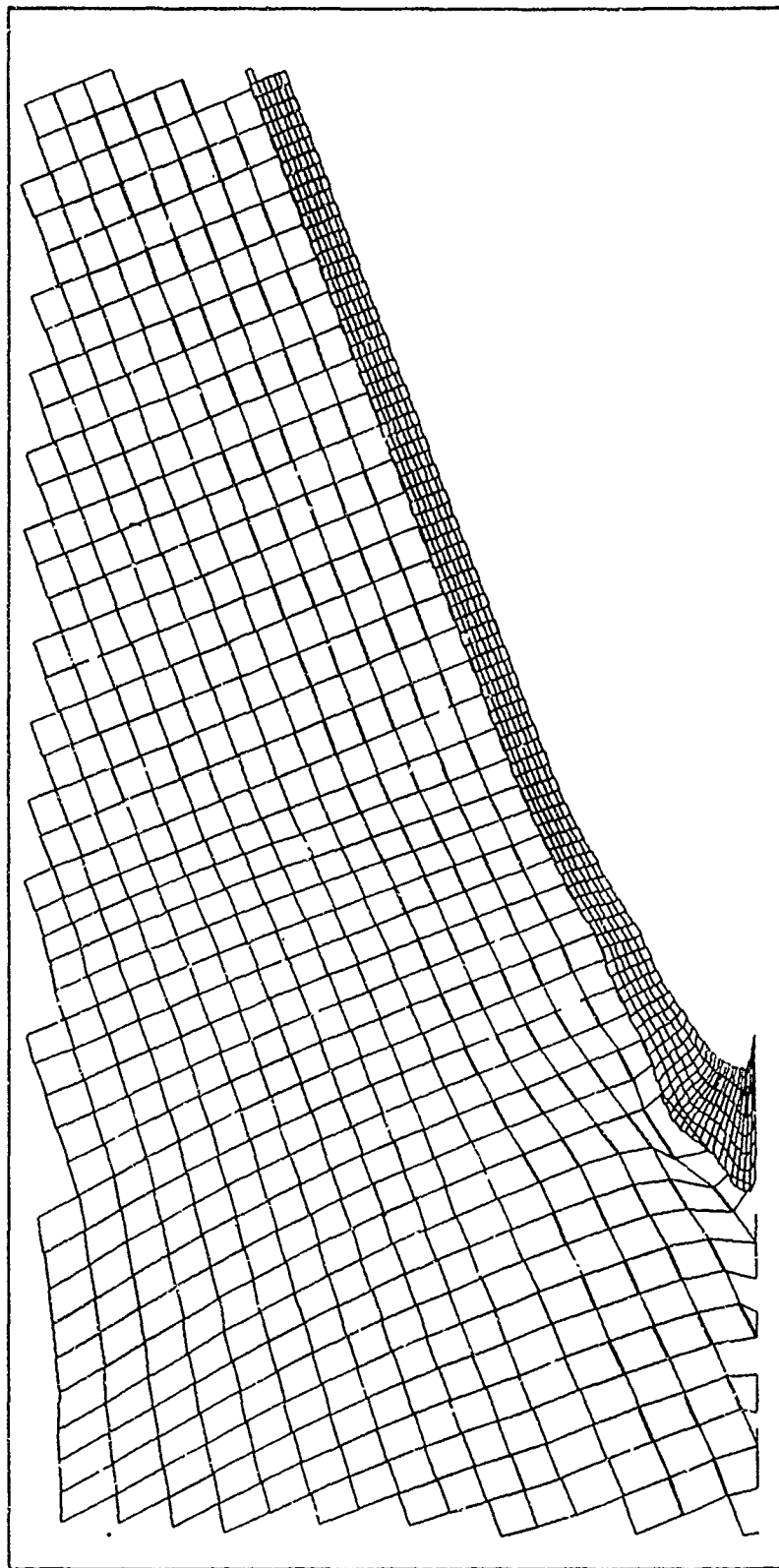
Scale: 1 inch (plotter units) = 0.5 cm

Figure A-29. Snapshot Grid Plot at Time = 8.71 μsec



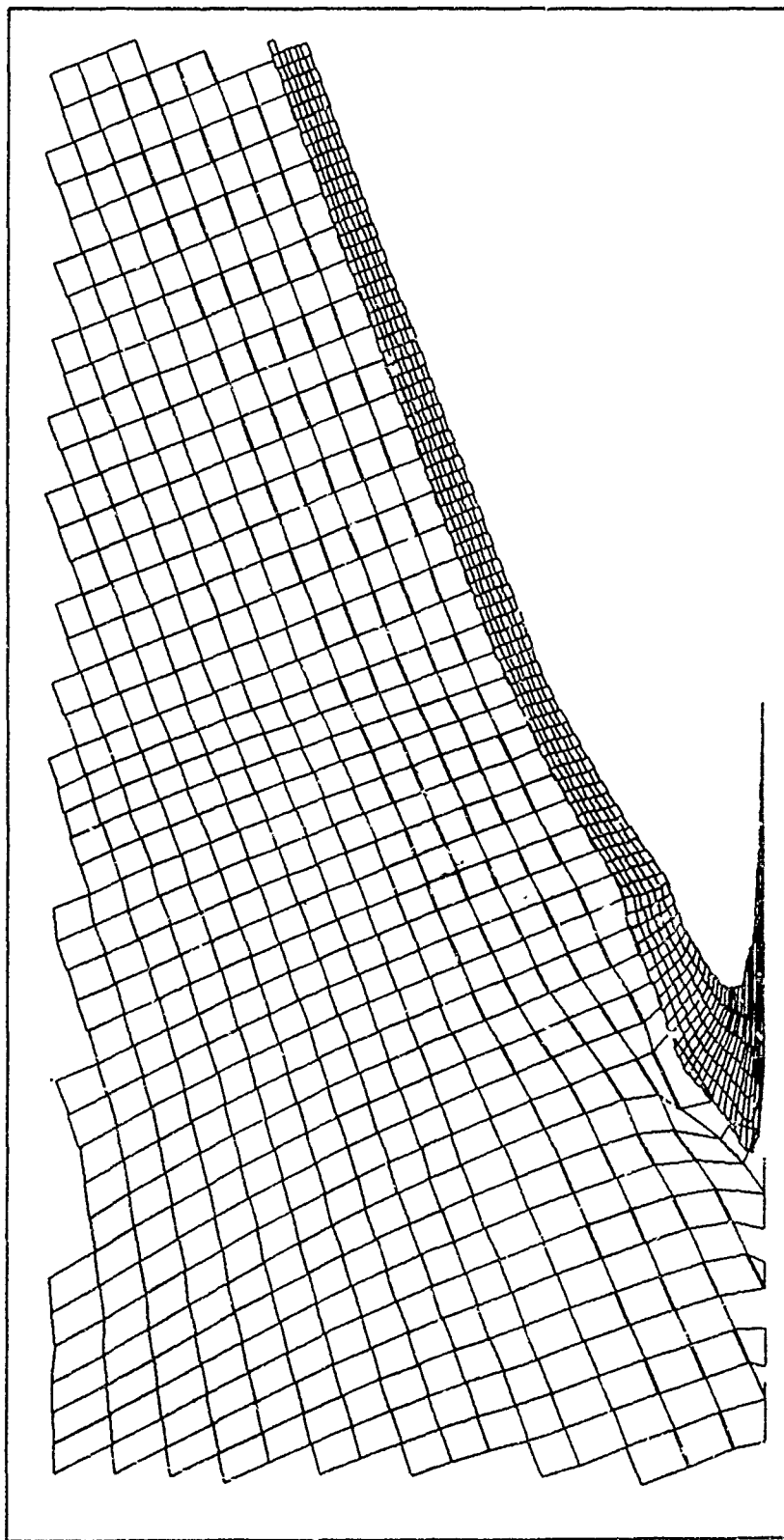
Scale: 1 inch (plotter units) = 0.5 cm

Figure A-30. Snapshot Grid Plot at Time = 0.14 μsec



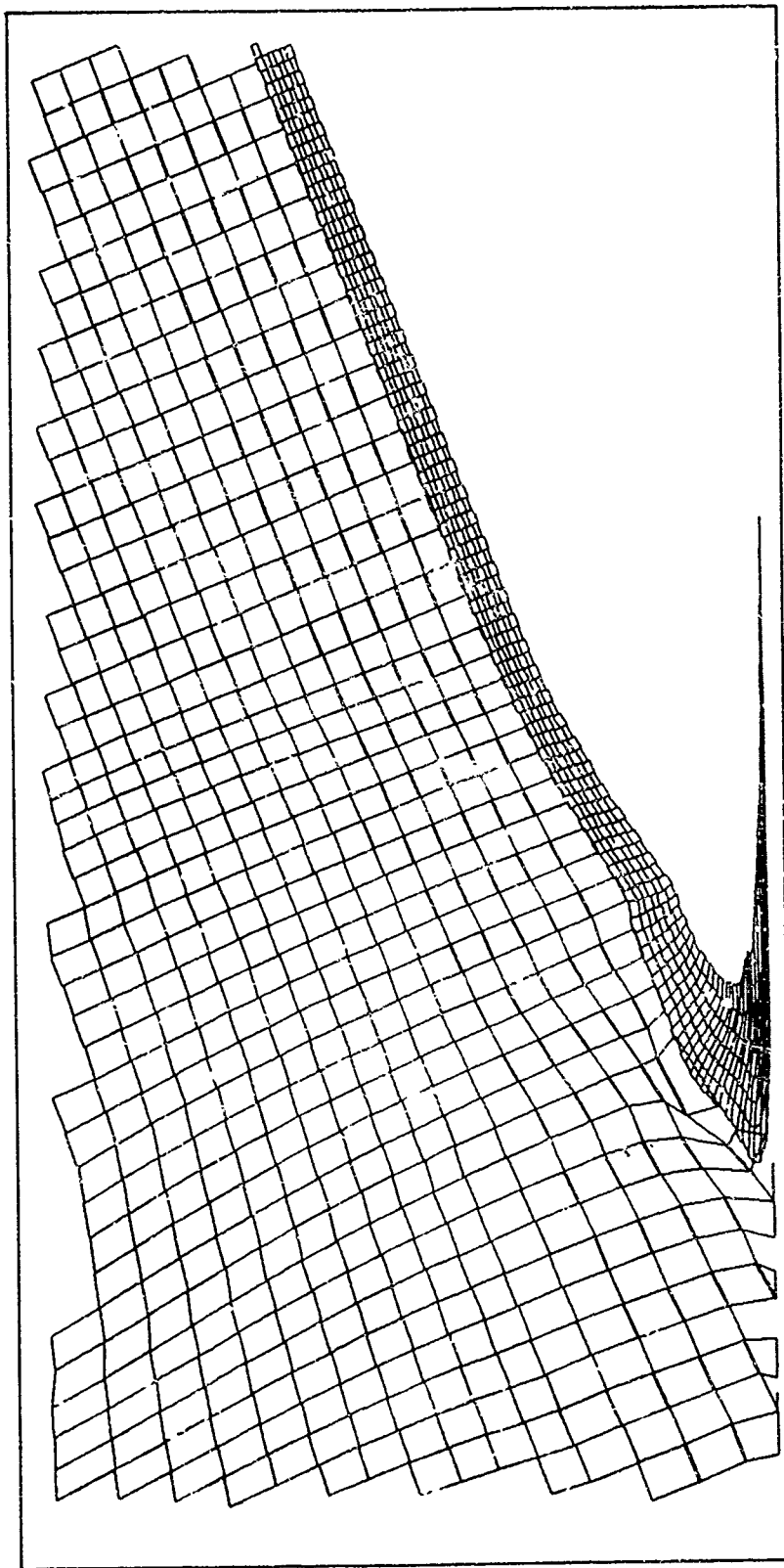
Scale: 1 inch (plotter units) = 0.5 cm

Figure A-31. Snapshot Grid Plot at Time = 9.53 μ sec



Scale: 1 inch (plotter units) = 0.5 cm

Figure A-32. Snapshot Grid Plot at Time = 10.1 μ sec



Scale: 1 inch (plotter units) = 0.5 cm

Figure A-33. Snapshot Grid Plot at Time = 10.58 μ sec

APPENDIX B
GENERALIZED BOUNDARY POINT MOTION

A boundary point is defined as any non-interior point in the grid i.e., a point which is not surrounded by four zones. The set of boundary points is comprised of all slavepoints, masterpoints, and points on the perimeter of the grid.

Possible void opening, void closing, sliding along pistons, or masterlines, and the various combinations of these options are controlled by the logic shown in Figure B-1 within subroutine MOTION.

B.1 SUBROUTINE OPEN (Figure B-2)

OPEN performs the function of determining if a point has lifted off a particular segment. The calculation is a simple one:

- (a) Determine the distance from the updated position of the point, P.
- (b) Determine if this distance is greater than the user-specified distance TOL. If it is not, the point does not lift off; return to subroutine MOTION. If it is greater, the point may possibly lift off.
- (c) Determine for the case where the distance is greater than TOL if the point moved into (crossed over) the segment or moved away from the segment. If the point moved into the segment, the void does not open. If the point moved away from the segment, the void does open.

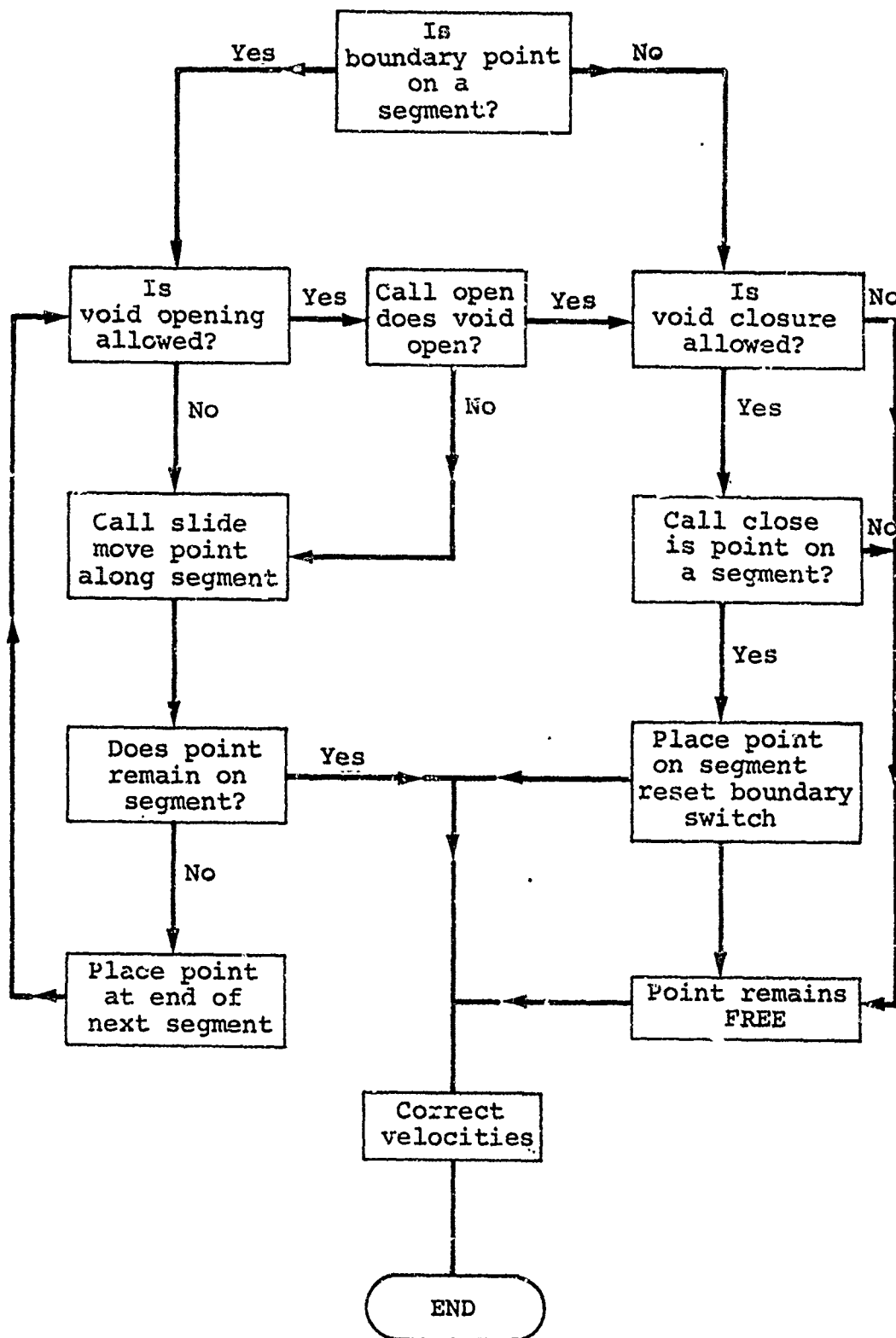


Figure B-1. Logic Controlling Subroutine MOTION

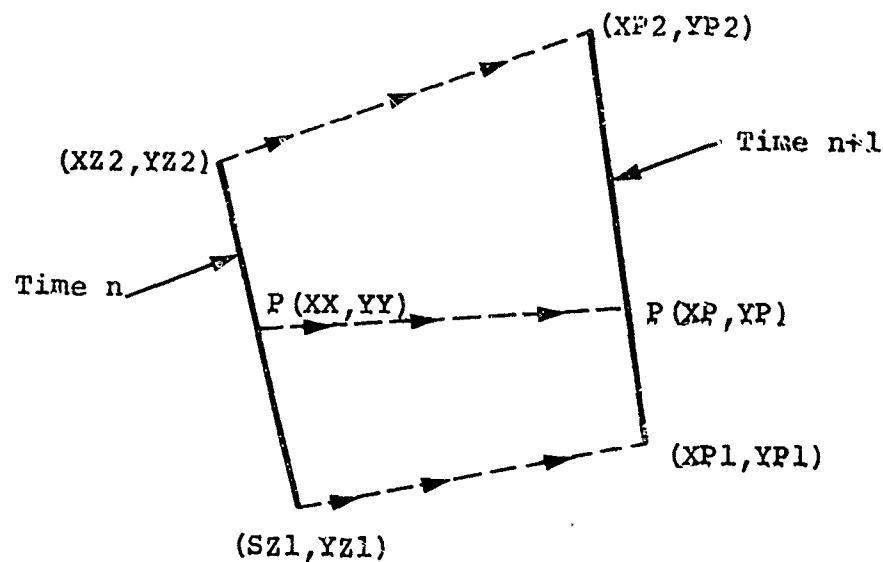


Figure B-2 Subroutine OPEN.

B.2 SUBROUTINE SLIDE

SLIDE performs the function of moving a point along the geometric constraint of a piston or masterline segment. Friction may or may not be present.

The flow of the calculation is as follows:

- a. The following values are supplied to subroutine SLIDE:

XX, YY position of point before sliding
 XD, YD velocity of point before sliding
 XDD, YDD acceleration of point before sliding

- b. Locate the coordinates and velocities for the line segment (on which the point is sliding). The segment may be defined by two points in space (a piston segment) or by two masterline points (a master segment). Slavepoints may slide on both pistons and masterline. Other points may only slide on pistons.

Component velocities for endpoints 1 and 2 are:

$$XD1 = (XP1 - XZ1)/DLTH$$

$$YD1 = (YP1 - YZ1)/DLTH$$

$$XD2 = (XP2 - XZ2)/DLTH$$

$$YD2 = (YP2 - YZ2)/DLTH$$

where $DLTH \equiv \Delta t^{n+\frac{1}{2}}$.

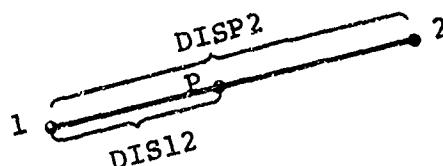
c. Resolve the point acceleration vector into normal and tangential components with respect to the segment position at $n + 1$, PNDD, and PTDD.

d. Find the velocity of the segment at point P as a linear weighted average of the velocities at each end of the segment. If first call to SLIDE, use position at time n and velocities at $n+\frac{1}{2}$. If not the first call, use positions at $n + 1$ and velocities at $n+\frac{1}{2}$. This difference between the first and subsequent calls is to allow for the point to slide over more than one segment.

Segment velocities at point $P(n+\frac{1}{2})$:

$$SXDH = FRAC * XD1 + (1.- FRAC) * XD2$$

$$SYDH = FRAC * YD1 + (1.- FRAC) * YD2$$



Resolve velocities into normal and tangential components, SNDH and STDH. If this is not the first call, set SNDH = 0.0.

e. Resolve point P velocity into normal and tangential components, PND and PTD.

f. Compute a tentative relative sliding velocity of the point on the segment at $n+\frac{1}{2}$. This velocity is for use in calculating a possible resisting tangential force due to friction. Compute resisting tangential acceleration, TDDRES.

g. Total tangential acceleration of point P is the sum of its free and resistive components:

$$TDD = PTDD + TDDRES$$

h. Update normal and tangential velocities of the point $n+\frac{1}{2}$

$$TDH = PTD + \Delta t^n * TDD$$

$$NDH = SNDH$$

Note the normal velocity of the point is identical to the normal velocity of the segment at point P.

i. Find new position of the point P:

$$XP = XX + \Delta t^{n+\frac{1}{2}} * XD$$

$$YP = YY + \Delta t^{n+\frac{1}{2}} * YD$$

j. The point must be checked to see if it still lies on the segment or has slid off one of the ends. The following possibilities exist:

(1) The point remains on the segment, the motion calculation is finished.

(2) Point goes off an end of the segment

- o If there is not another segment connected to the end, the point may
 - (a) be forced to stay at the end or
 - (b) be allowed to become a free unconstrained point. The user specifies the desired option.

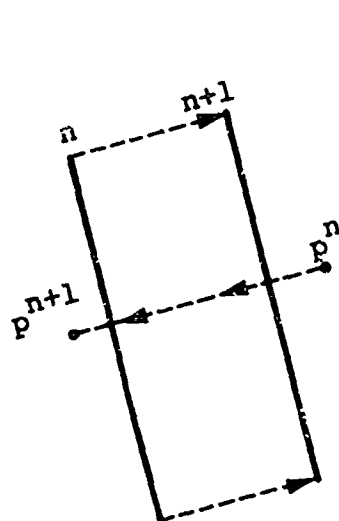
- If there is another segment connected to the end, place the point at the end of the segment and scale the acceleration by the tangential distance moved. Return control to subroutine MOTION where the point can again be checked for void opening if desired. If no void opens, call SLIDE again with the resultant acceleration and move the point along the next segment.

This method of sequentially moving a point along adjacent segments defines a unique and accurate updated position for the point. Previous methods of utilizing perpendicular projections could lead to non-unique solutions for the point position and possibly large anomalous velocities.

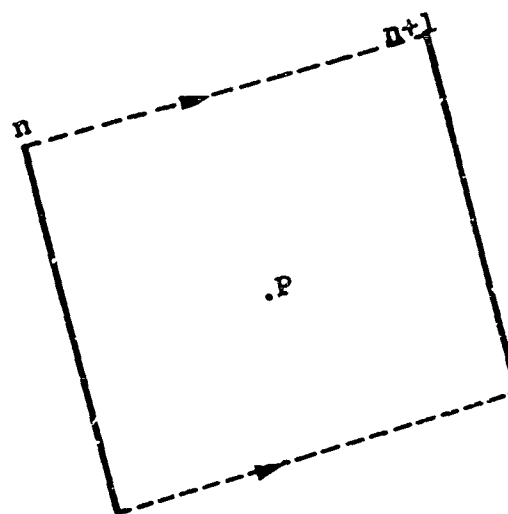
B.3 SUBROUTINE CLOSE

CLOSE performs the function of determining if a free point has impacted a particular segment. All the possible segments are checked to see if an intersection has occurred. For slave-points, both masterline segments and piston segments must be checked. Where an ambiguity exists, the masterline segments take precedence over the piston segments. For a regular boundary point including a masterpoint, only piston segments are checked. The loop through the possible segments utilizes the following algorithm.

A quadrilateral is constructed of the two endpoints of the segment at times n and $n + 1$ in a frame of reference where the point P is stationary.



a. Lab System



b. P Stationary System

Figure B-3. Subroutine CLOSE

If the point P is found within the quadrilateral as shown in Figure B-3b, then the point has impacted the segment. The position of the point is found by projecting P at $n + 1$ onto the segment at $n + 1$.

APPENDIX C
AUTOMATIC REZONER

An automatic rezone package has been developed to provide various kinds of rezones during the normal processing of a Lagrange 2D code. The unique feature of the system is that it is not necessary to stop the problem and map the old grid onto the new grid and then restart the calculation. The automatic rezoner performs its rezoning as each zone is calculated, according to the options desired.

The user specifications for automatic rezoning are as follows:

- (a) Number of rezone regions
- (b) Indices of each rezone region, IMNRZ to IMXRZ and JMNZRZ to JMXRZ

For every rezone region:

- (c) NSTART cycle at which to start rezoning
- (d) NEND cycle at which to stop rezoning
- (e) NFREQ frequency of cycles at which rezones are to be performed
- (f) N5OPT rezone options
- (g) NPO printout switch for rezone check quantities

Up to ten rezone regions in the Lagrange grid can be specified. This number is not an absolute restriction and could be easily extended. Various rezone regions may overlap in time and space.

The rezone options specified in the packed integer
N5OPT = $N_1 N_2 N_3 N_4 N_5$ are described as follows:

N_1 = NREZ, rezone control

NREZ = 0 bypass system

NREZ = 1 perform rezone of zone (JZ, IZ)

NREZ > 1 perform NREZ sweeps ($J = 1, JMAX$) on column IZ

N_2 = NXY, coordinate rezoning

NXY = 0 No coordinate rezoning

NXY = 1 Changes the old coordinates x_o, y_o of the point being rezoned to a new position x_p and y_p where x_p and y_p are constructed by a mean parallelogram method using neighbor point positions.

NXY = 2 Performs half the change corresponding to NXY = 1. That is, $x_{new} = 0.5(x_o + x_p)$ and $y_{new} = 0.5(y_o + y_p)$. This option is recommended if the rezone is applied recurrently.

NXY = 3 Changes the old coordinates x_o, y_o of the point being rezoned to a new position x_p and y_p where x_p and y_p are constructed by a centroid method using neighbor point positions.

NXY = 4 Performs half the change corresponding to NXY = 3. That is, $x_{new} = 0.5(x_o + x_p)$ and $y_{new} = 0.5(y_o + y_p)$. This option is recommended if the rezone is applied recurrently.

N_3 = NMAP, Interior Map Option

The rezoning of the coordinates of a point will result in a volume change of up to four zone interiors. Thus, $NXY \neq 0$ should be accompanied by $NMAP \neq 0$. The interior map logic conserves mass density and energy density for all new zones whose volumes have been reduced. The remaining total mass and internal energy are included in the zones that are expanded according to the method prescribed by the value of $NMAP$. If the total volume of the rezoned region is conserved, then $NMAP = 1$ and 2 give identical results. Differences result when a material interface or free surface coordinate rezone has resulted in changed volumes.

$NMAP = 1$ Conserves mass and internal energy; stresses can be unrealistic.

$NMAP = 2$ Adds or subtracts mass and internal energy to conserve mean stress.

$N_4 = NVEL$, velocity rezoning

$NVEL = 0-9$ Indicates the weighting factor used to weight the contribution to the point's velocity from its unrezoned velocity and the velocities of its neighbors. The weighting is performed according to the following prescription: neighbor velocities are weighted by:

$$\frac{1}{R_N - R_O} / \sum_{N=1}^{NN} \frac{1}{R_N - R_O} * \frac{NVEL}{10}$$

where

R_O is coordinate position of point being rezoned

R_N is coordinate position of neighboring points

NN is the number of neighboring points up to 8

The original velocity is weighted by the factor

$$\left(1 - \frac{NVEL}{10}\right)$$

Thus, $NVEL = 0$ applies no velocity rezoning, whereas $NVEL = 9$ takes 90 percent of the point's velocity from surrounding values.

$N_5 = NMOM$, momentum conservation

Use of $NMOM > 0$ will provide for momentum conservation by remapping of the velocity of the rezoned point and its neighbors.

$NMOM = 0$ No momentum conservation.

$NMOM = 1$ Rigorous conservation of momentum independent of mass conservation, analogous to $NMAP = 1$. Unrealistic velocities may result.

$NMOM = 2$ Conservation of momentum density, analogous to $NMAP = 2$.

Certain combinations of the five above options can obviously lead to disaster. An intelligent assessment of the objectives of a calculation should be made when applying the automatic rezoner because of the various tradeoffs of a particular option. Reference C.1 discusses further details of the automatic rezoning method.

C.1 D. E. Maxwell, An Existing Automatic 2D Rezoners, TCAM Technical Note, Physics International Company, San Leandro, California, 1973.

INITIAL DISTRIBUTION

BRL (Mr. Eichelberger)	1
(C. Grabarek)	1
(Dr. Kulcher)	1
Physics Intl (Mr. Behrmann)	10
System, Science & Software	
(Dr. R.T. Sedgwick)	1
ASD/ENYS	1
AVL/LSE-70-239	1
DDC-	2
Hq PACAF (IGY)	1
TRADOC/ADTC/DO	1
AFATL/DL	1
AFATL/DLB	1
AFATL/DLKS	1
AFATL/DLOSL	1
AFATL/DLRD	1
AFATL/DLRV	1
AFATL/DLYD	1
AFATL/DLYA	10
AFATL/DLJM	1
AFATL/DLIW	1

REPORT DOCUMENTATION PAGE		READ INSTRUCTIONS BEFORE COMPLETING FORM
1. REPORT NUMBER AFATL-TR-73-160, Volume II	2. GOVT ACCESSION NO.	3. RECIPIENT'S CATALOG NUMBER
4. TITLE (and Subtitle) Calculation of Shaped-Charge Jets Using Engineering Approximations and Finite Difference Computer Codes. Volume II. Modification and Utilization of a Two-Dimensional Finite Difference Continuum Mechanics Code to Calculate the Jet Formation Parameters for Any Generalized Axisymmetric Shaped Charge		5. TYPE OF REPORT & PERIOD COVERED Final Report - June 1972 to August 1973
7. AUTHOR(s) L. Behrmann N. Birnbaum		6. PERFORMING ORG. REPORT NUMBER PIFR-430
9. PERFORMING ORGANIZATION NAME AND ADDRESS Physics International Company 2700 Merced Street San Leandro, California 94577		8. CONTRACT OR GRANT NUMBER(s) F08635-72-C-0229
11. CONTROLLING OFFICE NAME AND ADDRESS Air Force Armament Laboratory Air Force Systems Command Eglin Air Force Base, Florida 32542		10. PROGRAM ELEMENT, PROJECT, TASK AREA & WORK UNIT NUMBERS Project No. 670B Task No. 10 Work Unit No. 02
14. MONITORING AGENCY NAME & ADDRESS (if different from Controlling Office)		12. REPORT DATE September 1973
		13. NUMBER OF PAGES 94
		15. SECURITY CLASS. (of this report) Unclassified
		16a. DECLASSIFICATION/DOWNGRADING SCHEDULE
16. DISTRIBUTION STATEMENT (of this Report) Distribution limited to U. S. Government agencies only; this report documents test and evaluation; distribution limitation applied August 1973. Other requests for this document must be referred to the Air Force Armament Laboratory (DLYA), Eglin Air Force Base, Florida 32542.		
17. DISTRIBUTION STATEMENT (of the abstract entered in Block 20, if different from Report)		
18. SUPPLEMENTARY NOTES Available in DDC		
19. KEY WORDS (Continue on reverse side if necessary and identify by block number) One-Dimensional Finite Shaped-Charge Design Procedure Difference Continuum Mechanics Jet Penetration Characteristics Calculations Shaped-Charge Launcher Two-Dimensional Finite Difference Mechanisms of Jet Formation Continuum Mechanics Code Non-Steady State Theory of Jet Formation Jet Stability		
20. ABSTRACT (Continue on reverse side if necessary and identify by block number) This report describes a technique to optimize the current shaped-charge design procedure as follows. Starting with the desired target to be defeated, a determination of the desired penetration characteristics of the jet would be made. Existing jet penetration theory would then be used to estimate the ideal characteristics of the jet to defeat the given target. A shaped charge launcher would then be designed to give these		

DD Form 1473: Report Documentation Page
UNCLASSIFIED

SECURITY CLASSIFICATION OF THIS PAGE(When Data Entered)

ideal jet characteristics. However, a suitable design procedure requires (1) a viable analytical or empirical design approach to obtain a first cut shaped charge design, (2) a better understanding than now exists of the detailed mechanisms of jet formation, and (3) a better understanding of the phenomenon of jet penetration. This report, which is contained in two volumes, addresses the first two of these requirements. Volume I describes the use of the existing non-steady state theory of jet formation with experimental data and one-dimensional finite difference continuum mechanics calculations to obtain the linear collapse velocity for generalized axisymmetric shaped charges. The results of this work are then used to obtain non-unique shaped charge designs which give the required idealized jet parameters. Volume II describes the modification and utilization of a two-dimensional finite difference continuum mechanics code utilizing the Lagrangian coordinate system to calculate the complete jet formation parameters for any generalized axisymmetric shaped charge. The utilization of this code allows a more detailed study of such phenomena as jet stability, bifurcation on the axis, shear gradients, viscosity, shocks, incipient vaporization, surface tension, and possible other effects. The combined use of both the engineering formulations along with the sophisticated two-dimensional code calculation allows design engineers the versatility to design the most optimum shaped charge for their particular application.

UNCLASSIFIED

SECURITY CLASSIFICATION OF THIS PAGE(When Data Entered)